CYCLIC BEHAVIOR OF HIGH STRENGTH CONCRETE BEAMS

by

David L. Hanks

David Darwin

A Report on Research Sponsored by

THE NATIONAL SCIENCE FOUNDATION

Research Grant

PFR 79-24696

AND

THE UNIVERSITY OF KANSAS

General Research Fund Allocations

3464-XO-0038

3064-XO-0038

UNIVERSITY OF KANSAS

LAWRENCE, KANSAS

August 1988

50272-101

REPORT DOCUMENTATION PAGE	1. REPORT NO.	2.	3. Recipient's Accession No.

4. Title and Subtitle

Cyclic Behavior of High Strength Concrete Beams

5. Report Date August 1988

6.

7. Author(s)

David L. Hanks and David Darwin

8. Performing Organization Rept. No. SM Report No. 21

9. Performing Organization Name and Address

University of Kansas Center for Research, Inc.
2291 Irving Hill Drive, West Campus
Lawrence, KS 66045

10. Project/Task/Work Unit No.

11. Contract(C) or Grant(G) No.

NSF PFR 79-24696
(G) GRF 3464-XO-0038
(G) GRF 3064-XO-0038

12. Sponsoring Organization Name and Address

National Science Foundation
Washington, D.C. 20550

University of Kansas
Lawrence, KS 66045

13. Type of Report & Period Covered

14.

15. Supplementary Notes

16. Abstract (Limit: 200 words)

Four high strength, lightly reinforced concrete beams were fabricated and tested to evaluate member response under severe cyclic loading. Concrete strengths varied from 11,310 to 12,860 psi with reinforcement ratios of 0.68 and 1.02%. Nominal stirrup strength was approximately 170 psi for all specimens. The applied shear stress ranged from 145 to 210 psi.

The measured energy dissipation capacity for the beams investigated in this study was compared to specimens fabricated with concrete strengths between 4000 and 6000 psi. Based on a statistical analysis of research representing five major studies, recommendations are made to improve the cyclic performance of reinforced concrete beams.

The findings show that for beams with similar geometry, strength and load history, an increase in concrete strength improves cyclic performance. The primary factor influencing cyclic behavior is the applied shear stress. Results also indicate that the use of reduced stirrup spacing and increased beam widths provide improved cyclic performance. Increases in beam width appear to be the most effective means to improve the cyclic performance of beams subjected to severe seismic loading.

17. Document Analysis a. Descriptors

beams (supports), concrete (reinforced), design, ductility, earthquakes, high-strength concretes, hinges (structural), loads (forces), reinforcement, shear, shear strength, stirrups, strains, stresses, structural engineering

b. Identifiers/Open-Ended Terms

c. COSATI Field/Group

18. Availability Statement

Release unlimited

19. Security Class (This Report) Unclassified

20. Security Class (This Page) Unclassified

21. No. of Pages

22. Price

(See ANSI-Z39.18) *See Instructions on Reverse*

OPTIONAL FORM 272 (4-77)
(Formerly NTIS-35)
Department of Commerce

ACKNOWLEDGEMENTS

This report is based on a thesis submitted by David L. Hanks to the Civil Engineering Department of the University of Kansas in partial fulfillment of the requirements for the MSCE degree.

The research was supported by the National Science Foundation under NSF Grant No. PFR 79-24696 and the University of Kansas under General Research allocations No. 3464-XO-0038 and No. 3064-XO-0038. Sheffield Steel Corporation and Armco, Inc., donated the deformed bars and wire reinforcing steel, respectively. Monarch Cement Company donated the portland cement, and Elkem Chemicals, Inc. donated the silica fume slurry. Penny's Concrete of Lawrence, Kansas furnished the concrete gratuitously. Nox-crete Chemicals donated the form release agent.

Numerical calculations were performed on a Harris H-1000 computer maintained by the Computer Aided Engineering Laboratory, School of Engineering, at the University of Kansas.

TABLE OF CONTENTS

TABLE OF CONTENTS (con't)

LIST OF TABLES

LIST OF FIGURES

LIST OF FIGURES (con't)

LIST OF FIGURES (con't)

LIST OF FIGURES (con't)

CHAPTER 1

INTRODUCTION

1.1 GENERAL

The response of reinforced concrete structures to severe seismic activity is highly dependent upon the nonlinear material response of elements within the system. Both the magnitude and cyclic nature of the displacements contribute to significant reductions in the overall strength and stiffness of the structure. A fundamental understanding of the hysteretic relationship between force and displacement is an essential requirement for the proper design of earthquake resistant structures.

Current practice for the design of reinforced concrete frames resisting seismic loading reflects the "strong column-weak beam" philosophy. Lateral-force resisting systems which adopt this design principle have increased structural stability and are less susceptible to catastrophic failures. A safe, economical structure, is designed so that seismic energy is dissipated through the formation and rotation of plastic hinges within the beam elements of the system. However, when beam hinges are subjected to several cycles of severe inelastic loading, the successive loss in energy dissipation capacity becomes a dominant factor in both member and structure response. The functional

design of earthquake resistant beam elements must therefore reflect both adequate hinge ductility and an acceptable level of strength.

Research concerning hinge degradation in moment resistant frames has traditionally been performed on prototype specimens representing beam-to-column subassemblies (Popov, Bertero & Krawinkler 1972, Wight & Sozen 1973 and 1975, Bertero, Popov & Wang 1974, Ma, Bertero & Popov 1976, Scribner & Wight 1978 and 1980, Hwang 1982, Ehsani & Wight 1982 and 1985, Hwang & Scribner 1984, Nmai & Darwin 1984 and 1986, Abdel-Fattah & Wight 1985 and 1987, and Ehsani, Moussa & Vallenilla 1987). Since lateral displacements induced by earthquakes produce zero moments near the mid-span of beam elements, laboratory tests reflecting member response have been readily obtained through the application of cyclic loads to the free end of cantilevered beams within the subassemblies. A cumulative evaluation of the results from these tests has been complicated due to variations in specimen geometry and strength, and differences in the magnitude of the beam tip displacements applied in the tests.

In recent years, a number of normalized measures relating cyclic loading to hinge performance have been developed. These measures include the "work index", I_w, and "modified work index", I'_w, (Gosain, Brown & Jirsa 1977) and the "energy dissipation index", D_i, (Nmai & Darwin 1984, Darwin & Nmai 1986). Even though there is, as yet, no direct design application for these

indices, they do provide a means to indirectly evaluate hinge response as a function of variations in beam geometry, strength and severity of cyclic loading.

D_i proved to be more effective than I_w or I'_w in providing a quantitative evaluation of beam parameters that significantly affect hinge performance. However, the development of D_i and the subsequent evaluation of parameters influencing cyclic response was based upon test results representing a relatively narrow range of concrete strengths. The increasing use of high strength concrete to reduce element size and structure weight not only affects strength and stiffness but also potentially influences cyclic response. Additional research on beams fabricated with high strength concrete and subjected to severe inelastic loading is necessary to determine and evaluate the relationship between element size, material behavior and hinge performance.

1.2 PREVIOUS WORK

Experimental investigations concerning the response of reinforced concrete beams subjected to cyclic loading have predominantly used test specimens fabricated with concrete with a compressive strength of 4000 to 6000 psi.

Wight & Sozen (1973, 1975) studied the affect of severe cyclic loading on the reduction in shear strength and energy dissipation capacity of twelve reinforced concrete columns. The

primary test variables were the magnitude of the axial compressive load (zero to one-half of the balanced load), the transverse reinforcement ratio (0.33 to 1.47%) and the displacement ductility factor, μ (defined as the ratio of the maximum lateral displacement to the initial yield displacement) ($2 \leq \mu \leq 4$). Concrete strengths ranged from 3750 to 5150 psi. Although the specimens represented reinforced concrete columns, the test results for members without axial load have been used to study beam hinge response (Nmai & Darwin 1984, Darwin & Nmai 1986). Wight & Sozen found that improvements in cyclic performance are directly related to the integrity of the concrete core, which ultimately transfers the applied shear to the transverse reinforcement. Parameters that facilitate the transfer of shear through the concrete, such as increased axial load or reduced stirrup spacing to improve confinement of the core, influence cyclic behavior by decreasing the rate of strength and stiffness decay. A maximum tie spacing of one-fourth of the effective depth was suggested as a means to increase energy dissipation capacity. They found that hinge performance also depends upon the displacement ductility factor. Specimens subjected to a displacement ductility factor of 2 did not exhibit a significant reduction in strength. However at a displacement ductility factor of 4, member strength was substantially reduced due to the increase in cyclic degradation of the concrete core.

Scribner & Wight (1978, 1980) studied the effect of intermediate longitudinal reinforcement on reducing beam shear strength decay in specimens fabricated with concrete strengths ranging from 3980 to 4970 psi. The area of intermediate reinforcement, A_i, varied from zero to approximately one-half of the area of the main tension reinforcement, A_s. They found that intermediate reinforcement restrains crack growth and results in more uniformly distributed cracking, which decreases the rate of hinge degradation and increases total energy dissipation compared to specimens without intermediate reinforcement. In their tests, the dominant factor influencing hinge performance was the maximum applied shear stress, expressed in multiples of $\sqrt{f'_c}$. Beams subjected to an applied shear stress of less than $3\sqrt{f'_c}$ did not exhibit shear deterioration and responded in a ductile-flexure mode, while applied shear stresses in excess of $6\sqrt{f'_c}$ resulted in substantial reductions in beam strength and relatively rapid degradation of the hinging zone. For specimens with an applied shear stress between $3\sqrt{f'_c}$ and $6\sqrt{f'_c}$, the inclusion of nominal amounts of intermediate reinforcement ($A_i/A_s \approx 0.25$) provided additional confinement for the concrete core and subsequently increased energy dissipation capacity. A large amount of intermediate reinforcement ($A_i/A_s = 0.52$) did not contribute to improved cyclic performance because this added reinforcement increased the concrete compressive stresses which offset the beneficial effect of additional confinement. Scribner & Wight

also observed that at advanced stages of cyclic loading, buckling of the compression reinforcement resulted in a substantial loss in flexural strength. An increase in the size of vertical stirrups decreased buckling by increasing the lateral stability of the flexural reinforcement. Specimens with larger ties also had an increase in the total dissipated energy due to improved concrete confinement provided by the increased stirrup size.

Hwang (1982) and Hwang & Scribner (1984) investigated the effects of variations in load history on the total energy dissipation capacity of reinforced concrete beams with concrete strengths ranging from 4710 to 5900 psi. Not only were the effects of changes in the maximum beam tip displacement studied, but the sequence in which the displacement amplitudes were applied was studied as well. Beam tip displacements, represented as a multiple of the shear span, were compared to story drift, expressed as an equivalent percentage of floor height. Specimens were subjected to displacements representing story drifts of 2% ($\mu \approx 2$) and 4% ($\mu \approx 4$). The applied shear stresses corresponding to the maximum story drifts were $3.3\sqrt{f'_c}$ and $7.4\sqrt{f'_c}$, respectively. Beam response was dependent upon the magnitude of the maximum applied shear stress and was largely independent of the sequence in which the beam tip displacements were applied. For members subjected to similar load histories, an increase in the magnitude of the applied shear stress resulted in a reduction in the total energy dissipated as compared to specimens with lower values of

applied shear stress. Hwang also concluded that increases in energy dissipation capacity were possible with increases in the shear span-to-effective depth ratio, a/d, which decreases the maximum applied shear stress.

The tests by Nmai & Darwin (1984, 1986) using beams with nearly equal concrete strengths (4260 to 4370 psi) show that beams fabricated with low reinforcement ratios (ρ = 0.69 versus ρ = 1.02) have a reduced rate of cyclic degradation due to a reduction in compressive and shear stresses. Total energy dissipation for beams subjected to displacement ductilities in the range $3.9 \leq \mu \leq 5.1$ was increased with reduced values of μ and decreased stirrup spacing. Improvements in energy dissipation capacity were also obtained with an increase in the ratio of positive (bottom) to negative (top) flexural reinforcement, (A_s'/A_s), which decreased both spalling of the compressed concrete and buckling of the longitudinal reinforcement as the beam underwent negative bending.

In an effort to obtain a comprehensive understanding of the experimental results reflecting multiple beam parameters and testing variables on hinge response, some researchers have developed normalized "indexes" to quantitatively measure cyclic behavior. The work index, I_w, and modified work index, I_w', (Gosain et al. 1977) were developed as a means to make comparisons of the overall energy absorption capacity for specimens subjected to variations in load histories. Energy absorption, or

work done, is calculated by summing the areas under the load-deflection hysteresis loops. For a member subjected to cyclic loading, the product of the peak load, P_n, and peak deflection, Δ_n, may be used as an approximation of the work done during the n'th cycle of loading. When the work done is normalized with respect to the product of the longitudinal reinforcement's yield load and deflection (P_y and Δ_y, respectively), the expression for the work index becomes

$$I_w = \sum \frac{P_n \Delta_n}{P_y \Delta_y} \tag{1.1}$$

The summation is over all cycles in which the ratio $P_n \geq 0.75P_y$. Since the load ratio, P_n/P_y, is anticipated to be in the range of 0.75 to 1.25, P_n/P_y is assumed to be unity and a simplified calculation of I_w is obtained using the number of cycles for which $P_n \geq 0.75P_y$ and the deflection ratio, Δ_n/Δ_y. The effects of shear span and axial compression on energy absorption capacity are evaluated by using the modified work index, I'_w.

$$I'_w = I_w\left(1 - \frac{d_c}{a}\right)\left(1 + \frac{0.0005N}{A_{core}}\right) \tag{1.2}$$

in which d_c = depth of concrete core measured to outside of stirrups, a = shear span, N = axial compression load and A_{core} = area of concrete core. While I_w and I'_w represent quantitative

measures of member ductility, the actual effects of shear deformation on energy dissipation (Popov et al. 1972) are neglected. Thus improvements in I_w can be attained only if the actual work or area bounded by the load-deflection hysteresis loops are utilized.

The energy dissipation index, D_i, (Nmai & Darwin 1984, Darwin & Nmai 1986) provides a means by which changes in the cyclic load-deflection relationship are incorporated into a measure of beam performance. D_i is expressed as a function of the actual work done, normalized with respect to an estimate of a beam's total elastic energy at yield.

$$D_i = \frac{E}{0.5P_y\Delta_y\left[\ 1 + \left(\frac{A'_s}{A_s}\right)^2\ \right]} \qquad (1.3)$$

in which E is the summation of energy dissipated for cycles in which $P_n \geq 0.75P_y$, A'_s = area of bottom steel and A_s = area of top steel. The normalizing term in Eq. 1.3 approximates the sum of the elastic energies at yield for negative and positive bending and is based on the experimental values of yield load, P_y, and deflection, Δ_y, (in negative bending) obtained during the first half cycle of load.

To evaluate the proposed measure of cyclic response, Nmai & Darwin performed a regression analysis on D_i versus the maximum applied shear stress, v_m, concrete strength, f'_c, and nominal

stirrup capacity expressed in terms of stress, $v_s = A_v f_{vy}/(bs)$, in which A_v = total cross-sectional area of shear reinforcement, f_{vy} = yield strength of shear reinforcement, b = beam width, s = stirrup spacing. Using the results of six experimental studies (Wight & Sozen 1973, Bertero et al. 1974, Ma et al. 1976, Scribner & Wight 1978, Hwang & Scribner 1984, and Nmai & Darwin 1984), Darwin & Nmai (1986) found that the combination of parameters providing the most consistent measure of performance for beams subjected to severe cyclic loading ($3.9 \leq \mu \leq 6.0$) was $(v_s f'_c)^{0.5}(v_m)^{-1.5}$. This expression indicates that D_i is most significantly affected by the maximum applied shear stress, v_m. Darwin & Nmai concluded, however, that v_s, f'_c and v_m did not fully account for the cyclic load response of reinforced concrete members. A plot of D_i versus $(v_s f'_c)^{0.5}(v_m)^{-1.5}$ and the relative position of the discrete data points with respect to the best fit line indicated that beam size and shape also influenced member performance. They proposed that for sections with identical areas of flexural reinforcement and effective depths, improved cyclic performance may be achieved more efficiently through the use of increased beam width than through an increase in the percentage of transverse reinforcement. Not only will an increase in beam width decrease v_m, but for width-to-depth ratios less than 1.0, it will also increase confinement of the concrete core.

The use of high strength concrete has recently been considered in experimental studies for members subjected to cyclic loading. Ehsani, Moussa & Vallenilla (1987) compared the inelastic behavior of reinforced concrete specimens fabricated with ordinary (≈ 6000 psi) and high strength (≈ 9500 psi) concretes. The load history used to test the specimens represented a continuous increase in the beam tip displacement for each cycle of loading (i.e. $0 < \mu < 9$). While this type of variable loading prevents test results from being compared with prior studies using D_i, the hysteretic response was found to be similar for specimens fabricated with ordinary and high strength concrete. Although the research by Ehsani et. al was undertaken to compare the inelastic behavior of reinforced concrete specimens fabricated with a wide range of concrete strengths, the influence of high strength concrete on cyclic performance was not well defined. However, regardless of the concrete strength, a reduction in member stiffness was observed with each cycle of inelastic loading and the effects of shear deformation produced a distinct "pinching" of the load-deflection hysteresis loops and a subsequent decrease in energy dissipation capacity.

1.3 OBJECT and SCOPE

The purpose of this investigation is to measure the cyclic performance of reinforced concrete beams fabricated with high strength concrete and to use those results, along with existing

results obtained with lower strength concretes, to determine the parameters that control the behavior of reinforced concrete beams under cyclic load.

Four specimens representing exterior beam-column subassemblies in a moment resistant frame are fabricated with concrete strengths between 11,310 and 12,860 psi and reinforcement ratios of 0.68 and 1.02%. All specimens are identical with respect to the dimensions of the formed concrete. Each specimen is subjected to a cyclic beam tip deflection representing a displacement ductility factor $\mu = 5$.

Member performance is quantitatively compared to previous research through the use of the energy dissipation index, D_i (Nmai & Darwin 1984, Darwin & Nmai 1986). Based on the resulting statistical analysis, recommendations are made concerning improvements in beam performance for members subjected to severe seismic loading.

CHAPTER 2

EXPERIMENTAL INVESTIGATION

2.1 GENERAL

Several experimental investigations have been undertaken to study the response of reinforced concrete members subjected to cyclic loading (Popov et. al 1972, Wight & Sozen 1973 and 1975, Bertero et. al 1974, Ma et. al 1976, Scribner & Wight 1978 and 1980, Hwang 1982, Ehsani & Wight 1982 and 1985, Hwang & Scribner 1984, Nmai & Darwin 1984 and 1986, and Abdel-Fattah & Wight 1985 and 1987). While a broad range of reinforcement ratios and load histories have been studied, experimental research has primarily reflected the cyclic response of members fabricated with concrete compressive strengths ranging from 4000 to 6000 psi. The purpose of this investigation is to test and evaluate the cyclic response of high strength, lightly reinforced concrete specimens.

2.2 TEST SPECIMENS

Horizontal displacements of lateral-force resisting frames result in zero moments at or near the midspan of beam elements. The application of cyclic loads at the free end of cantilevers provides a method to measure the seismic performance of flexural members without the construction of full-scale frames.

In this study, four cantilever specimens (Fig. 2.1) were fabricated in a vertical position to duplicate cast-in-place concrete. All specimens were identical with respect to the overall dimensions of the formed concrete. Nominal cross-section dimensions of the beams and columns were 7.5 x 18 in. and 15 x 28 in., respectively. Actual dimensions are given in Table 2.1. Both the beam shear span and the overall column height were 60 in. Each beam-column specimen was cast monolithically. Transverse and longitudinal reinforcement was designed and placed to conform to the requirements of ACI 318-83, Appendix A (ACI Committee 318 1983). Reinforcement ratios and spacing of the transverse beam reinforcement was selected to insure ductile behavior and a flexure-shear mode of failure. Longitudinal beam reinforcement ratios of 0.68% (Beams G-1 & G-3) and 1.02% (Beams G-2 & G-4) were used. The beam transverse reinforcement, $v_s = A_v f_{vy}/(bs)$, ($A_v = 0.077$ in.^{2}), was essentially constant, ranging from 168 to 176 psi (Table 2.1). The maximum applied shear stress, v_m, varied from $1.3\sqrt{f'_c}$ to $2.0\sqrt{f'_c}$. Concrete compressive strengths ranged from 11,310 to 12,860 psi.

Beams G-1 and G-3 contained four #4 bars (in two layers) as longitudinal negative moment reinforcement and two #4 bars as positive moment reinforcement. Beams G-2 and G-4 contained six #4 bars (in two layers) as negative moment reinforcement and three #4 bars as positive moment reinforcement. The longitudinal reinforcement extended to the far face of the column and was

welded to a 3/4 x 8 x 18 in. bearing plate to prevent anchorage failure.

Transverse reinforcement in the beam was placed 3 5/8 in. center to center, with the first stirrup positioned approximately 1 in. from the formed vertical face of the column.

2.3 MATERIALS

2.3.1 REINFORCEMENT

Transverse reinforcement in the beams consisted of 7/32 in. nominal diameter hot rolled rod. 48 in. long pieces were cut from a single coil, straightened, then preloaded to 2000 pounds so that a well-defined yield strength was obtained. After forming each stirrup, a 2 in. overlap length was welded to form a closed hoop. The welded overlap was positioned on the top of the beam reinforcing cage for all specimens.

Beam longitudinal reinforcement consisted of #4 deformed bars. Reinforcement in the column section of all specimens consisted of four #6 and four #8 deformed longitudinal bars and #3 deformed bars as column ties (Fig. 2.1).

Stress-strain relationships for the beam stirrups and #4 longitudinal reinforcement are shown in Fig. 2.2 and 2.3, respectively.

2.3.2 CONCRETE

Two different high strength concrete mixtures were utilized in the construction of the beam-column subassemblies. Mix A

concrete, made with fly ash, was used in Beam G-2. Mix B concrete, made with a commercially available silica fume/superplasticizer slurry, was used in the remaining three specimens. Both mixes were non-air-entrained and used Monarch Type I portland cement, Kansas River sand and crushed limestone. The nominal maximum size of coarse aggregate was 1/2 in. Slump of Mix A was 2 1/2 in. Slump for the three specimens using Mix B ranged from 8 1/2 to 9 3/4 in. The high slump of Mix B was attained solely with the free surface moisture on the aggregate and the silica fume slurry. No mixing water was batched. Actual mix proportions and physical properties of the aggregates and concrete are presented in Table 2.2.

The concrete was obtained from a local central-mix plant and transported in inclined axis mixing trucks. All constituents of Mix A were plant batched, except for the superplasticizer, which was added to the batch at the time of delivery to obtain the desired slump. For Mix B, the cement and aggregate (with free surface moisture) were batched and transported "dry". The addition of the silica fume/superplasticizer slurry commenced upon arrival at the test facility. A minimum of 1.5 cubic yards of concrete was batched for each specimen.

2.4 SPECIMEN FABRICATION

Fabrication procedures for all specimens were similar to those used by Nmai and Darwin (1984). Formwork was fabricated

from Class I, 3/4 in. American Plywood Association grade B-B Plyform. The plywood was supported by 2 x 4 timber studs, joists, and wales. Form ties for the column and beam sections were 1/4 and 3/8 in. diameter all-thread rods, respectively. One coat of clear lacquer was applied to the Plyform prior to the application of form oil.

1.0 and 1.5 in. nominal size bar supports were used to maintain concrete cover in the beam and column sections, respectively. Placement of the concrete was continuous, in lifts not exceeding 12 in. in the column and 9 in. in the beam. Consolidation was performed with a 1.5 in. flexible shaft internal vibrator. When the level of consolidated concrete coincided with the top of the beam, placement was temporarily halted. Concrete in the beam was then floated and covered with plywood sheathing to prevent further displacement due to addition of concrete in the remaining portion of the column. After placement was completed, the specimen was covered with polyethylene for 24 hours. Forms were then removed, and the beam-column subassembly was moist cured under polyethylene.

Prior to testing, the beam-column subassembly was post-tensioned to a reusable companion column stub (Fig. 2.4). The total post-tensioning force connecting the two column sections was 160 kips. The test specimen was then positioned beneath a hydraulic actuator (Fig. 2.5(a) and 2.5(b)). Both column sections were post-tensioned to the structural floor of the test

facility with a total force of 200 kips. The free end of the cantilever beam was supported until the time of testing. Prior to testing, a diluted mixture of latex paint was applied to the beam-column assembly. The location of the transverse and longitudinal reinforcement was marked on the vertical face of the beam.

2.5 INSTRUMENTATION

Strains in the beam transverse and longitudinal reinforcement were measured with Micro-Measurements EA-06-031DE-120 electrical resistance foil gages. A total of 12 strain gages were installed for each specimen (Fig. 2.6). To protect the strain gages during concrete placement, Micro-Measurements M-Coats B, D and G were applied to the gage and adjacent reinforcement.

Schaevitz DC-operated linear variable differential transformers (LVDT's) were used to control the displacement of the beam and measure flexural rotation of the beam, shear deformation, and rigid body rotation of the subassembly relative to the floor (Fig. 2.7). A standard dial gage was positioned on the vertical face of the beam tip to measure changes in beam length (Fig. 2.7).

An MTS 110 kip, 10 in. stroke actuator and closed-loop servohydraulic control system applied the load at the end of the

cantilever. LVDT #1 provided the feedback signal to the MTS control unit.

A continuous graph of load versus displacement was recorded with a potentiometric X-Y recorder. Voltage outputs from the strain gages, LVDT's and load cell were recorded using a Hewlett-Packard 3054 Data Acquisition System, consisting of a 3456A Voltmeter, 3497A Control Unit, and 9825T calculator.

2.6 TEST PROCEDURES

After connection of the electrical circuitry, the hydraulic actuator load head was attached to the end of the beam. Beams G-1 thru G-3 were subjected to a 1 kip preload to verify the instrumentation output, then returned to a position of zero displacement. Downward displacement of these three specimens proceeded until a well-defined yield point was established, as depicted by the X-Y recorder output. The beam was then returned to a position of zero displacement, and the control system was set to produce a maximum displacement of five times the yield displacement (displacement ductility factor $\mu = 5$) to insure severe cyclic loading. A typical loading schedule is shown in Fig. 2.8.

As the result of an electrical offset in the servohydraulic control unit, Beam G-4 was inadvertently subjected to an initial downward load of 9.8 kips prior to the start of cyclic loading. The first displacement cycle subsequently began at the point of

initial load and displacement. For the purposes of determining maximum displacement, the yield load and yield displacement were chosen to coincide with those of Beam G-2, based on the similarity of the two specimens. For comparison purposes, the first quarter cycle of Beam G-2 has been superimposed on the applicable plots for Beam G-4.

Termination of the tests occurred when a positive moment reinforcing bar(s) (bottom steel) fractured during a cycle in which the maximum load had dropped below one-half of the yield load. When the positive moment reinforcement fractured and the maximum load within the cycle was greater than one-half of the yield load, termination took place at the end of the cycle.

At periodic intervals, the beam displacement was held constant and recordings of strain, displacement, and load were made. Data was recorded approximately 30 times per cycle. Each of the first three cycles took about 30 minutes to complete. After the third cycle, the hinge within the beam was well-defined and the rate of loading was doubled. The total elapsed time for the remaining cycles was about 15 minutes.

Cracks were marked on the beam and column section during each cycle at points of zero load. Cracks were also marked at the yield and maximum loads within the first quarter cycle. Photographs of the hinging zone were taken at the completion of each cycle.

2.7 EXPERIMENTAL RESULTS

The area enclosed by the load-displacement hysteresis loops is equal to the energy dissipated by the beam and is a principal means by which a beam's performance can be evaluated under cyclic loading. A shallow slope of the load-displacement plot indicates that the specimen has a reduced ability to carry increased load. Reduced resistance to applied loads, which reflects the loss in member stiffness, results in increased deflections for small changes in load and decreased energy dissipated for specimens subjected to constant displacements. Plots of load versus displacement are presented in Fig. 2.9(a) - 2.9(d). The peak load-displacement value for Beam G-1 was not recorded immediately after determination of the yield displacement. This resulted in an apparent reduction in energy dissipated, as depicted in Fig. 2.9(a).

Total deflection of the cantilever beam tip may be expressed as the summation of the flexural and shear deformations of the beam and rigid body rotation of the column. Expressions for the calculation of specimen deformation and rotation are presented in Appendix B. Flexural rotation of the beam element (LVDT's #7 and #8) is presented in Fig. 2.10(a) - 2.10(d). Load versus shear deformation, in the area extending a distance d from the column face (LVDT's #3 and #4), is shown in Fig. 2.11(a) - 2.11(d). Similarly, shear deformation for the area extending a distance d to 2d from the column face (LVDT's #5 and #6) is presented in

Fig. 2.12(a) - 2.12(d). Flexural rotation of the beam element accounted for the majority of the beam tip deflection as seen by comparing Fig. 2.10 and 2.11. Rotation of the column stub relative to the structural floor (LVDT's #9 and #10) was, at most, 0.000135 radians and accounted for less than 0.5% of the total beam tip deflection.

Anchorage of the #4 longitudinal beam reinforcement, within the column core, was maintained throughout the test as seen by the load versus strain relationships (gage's #5 and #6) in Fig. 2.13(a) and 2.13(b). Strain gages located on the transverse reinforcement were installed in the same relative position for each specimen. Representative plots of load versus strain for the beam transverse reinforcement are shown in Fig. 2.14(a) and 2.14(b).

The principal experimental results, including calculated and measured shears, are summarized in Tables 2.3 and 2.4.

2.8 SPECIMEN BEHAVIOR

2.8.1 GENERAL

During the first inelastic load cycle, well defined flexure cracks developed in the top of a beam prior to the load reaching the initial yield value. As the load increased, inclined flexure-shear cracks progressed towards the beam mid-depth. At the completion of the first quarter cycle of downward displacement, flexure-shear cracks projected diagonally towards the

column and were terminated by the compression reinforcement (Fig. 2.15(a)).

At the end of the first complete cycle, all specimens had developed at least two distinct "X" shaped cracks throughout the entire depth of the hinging zone. The inclined cracks intersected below the mid-depth of the section as a result of the unsymmetrical flexural reinforcement. Large uncracked blocks of concrete remained intact near the center of the beam, while a closer grid of smaller cracks was present on the vertical face of the beam near the flexural reinforcement. Minor cracking also occurred in the column face adjacent to the beam. Initial spalling of the concrete, around the lower flexural reinforcement, took place during the second or third cycle and was adjacent to, and within a distance 0.25d, of the column face, where d is the effective beam depth in negative bending.

Continued cyclic loading produced additional cracks within the hinging zone, increased spalling, and buckling of the lower reinforcement. As the specimen approached zero load during each remaining cycle, flexure-shear cracks remained open, and resulted in relatively large displacements for small changes in load. Subsequently, the load-shear deformation plots took on a "pinched" shape near zero load, as seen in Fig. 2.11. At the maximum downward load, the peaks shown on the load-shear deformation plots (Fig. 2.11(a) - 2.11(d)) occurred as the flexure-shear cracks closed and the shear force resisted by the concrete

increased. As a result of the initial inelastic load in the downward direction and the subsequent permanent yielding of the top longitudinal beam reinforcement, flexure-shear cracks did not completely close at the maximum upward load and the shear capacity of the concrete was not entirely developed.

By the end of the sixth load cycle, spalling of the bottom concrete cover had extended 0.5d from the column face and progressed upward a distance of 0.25d. The loss of cover adjacent to the lower flexural reinforcement was more severe in the area of the second or third stirrup, as measured from the column face. Buckling of the compression reinforcement became more pronounced as deterioration of the concrete cover progressed.

Abrading of the concrete along the flexure-shear cracks and buckling of the lower flexural reinforcement resulted in additional spalling of the concrete. By the completion of the seventh inelastic load cycle, deterioration of the concrete had progressed upward to 0.3d from the bottom of the beam. Repeated load reversals, coupled with inelastic buckling of the compression reinforcement, continued until the reinforcement fatigued and fractured.

At the termination of a test, a fine grid of cracks was present on the vertical face of the beam adjacent to the positive and negative moment reinforcement. Somewhat larger uncracked sections of concrete remained clustered near mid-depth, well within the hinging zone (Fig. 2.15(b)).

The following sections describe the behavior of individual test specimens.

2.8.2 BEAM G-1 ($\rho = 0.68\%$, $f'_c = 11{,}610$ psi, $A_s = 0.80$ in.^{2}, $A'_s = 0.40$ in.^{2}, $v_s/v_m = 1.16$, $v_m/\sqrt{f'_c} = 1.35$)

As compared to the other specimens, Beam G-1 lost the least amount of concrete cover. Virtually all of the visible flexure-shear cracks were confined to the hinging zone.

At the completion of the first quarter cycle, several flexure-shear cracks had progressed to a depth of 0.5d, as measured from the top of the beam. Two primary flexure-shear cracks traversed the entire depth of the section (Fig. 2.15(a)).

Initial spalling of the concrete cover took place during the first half of the second inelastic load cycle. The spalled concrete was located on the bottom of the beam, between the column face and first stirrup.

Continued application of the load cycles resulted in grinding and abrading of concrete adjacent to the flexure-shear cracks. Yielding of the lower flexural reinforcement, coupled with the pronounced effect of spalling concrete contributed to the reduction in flexural strength of the section. By the end of the fifth load cycle, the loss of concrete cover exposed the lower flexural reinforcement. The exposed reinforcement extended a distance 0.5d from the column face.

Subsequent load cycles resulted in buckling of the lower flexural reinforcement and a continued loss in concrete cover.

Spalling progressed up to 0.25d from the bottom of the beam and was primarily concentrated in the area adjacent to the second stirrup (Fig. 2.15(b)).

The lower flexural reinforcement fractured after 8 1/2 inelastic load cycles, and the test was terminated after completion of the cycle. Fracture of the reinforcement occurred between the first and second stirrups.

2.8.3 BEAM G-2 (ρ = 1.02%, f'_c = 11,310 psi, A_s = 1.20 in.^{2}, A'_s = 0.60 in.^{2}, v_s/v_m = 0.80, $v_m/\sqrt{f'_c}$ = 1.97)

Beam G-2 had 50% more positive and negative moment reinforcement than Beam G-1 and a 2 1/2% reduction in the concrete compressive strength.

By the end of the first quarter cycle, flexure-shear cracks extended to a distance 2.5d beyond the face of the column (Fig. 2.16(a)). Within the hinging zone, two primary flexure-shear cracks traversed the entire depth of the section. Beyond the hinging zone, cracks projected downward from the top of the beam to a depth of 0.75d. Tension cracks, perpendicular to the longitudinal axis of the beam, were present at the column face around the upper one half of the beam.

Initial spalling of the lower flexural reinforcement concrete cover took place during the first full cycle. Spalling occurred adjacent to the column face and extended 0.25d towards the beam tip. Flexure-shear cracks beyond the hinging zone

projected diagonally away from the top and bottom of the beam towards the column face.

By the end of the third cycle, the spalled concrete cover extended across the entire width of the beam, exposing the lower flexural reinforcement. Movement of the concrete along the interface of the primary flexure-shear cracks resulted in a further loss of concrete cover during subsequent load cycles.

By the end of the fifth cycle, spalling of the cover, adjacent to the lower flexural reinforcement, extended 0.75d from the column face. Buckling of the reinforcement was more pronounced as the loss of cover progressed (Fig. 2.16(b)).

Spalling of the concrete on the vertical beam face, within the hinging zone, occurred during the sixth cycle. The majority of the displaced concrete was centered between the first and second stirrups and projected 0.5d upward from the bottom of the beam.

During the seventh load cycle, additional concrete cover spalled adjacent to the lower flexural reinforcement and extended 0.25d above the bottom of the beam in the area next to the third stirrup. Buckling of the lower reinforcement continued until termination of the test, which occurred after 7 1/4 cycles. Fracturing took place in the lower flexural reinforcement between the first and second stirrups. At termination of the test, the loss in concrete cover was at least twice as extensive as Beam G-1 for the same cycle.

2.8.4 BEAM G-3 (ρ = 0.68%, f'_c = 12,860 psi, A_s = 0.80 in.^{2}, A'_s = 0.40 in.^{2}, v_s/v_m = 1.16, $v_m/\sqrt{f'_c}$ = 1.33)

The longitudinal flexural reinforcement for Beam G-3 was identical to Beam G-1. However, the concrete compressive strength was about 11% greater.

Two primary flexure-shear cracks traversed the entire depth of the hinging zone prior to the completion of the first quarter cycle. Cracking of the concrete also occurred on the vertical face of the column around the upper 0.75 of the beam perimeter. Similar to Beam G-1, the majority of flexure-shear cracks in the beam were located within a distance d from the column face.

After completion of the first full inelastic load cycle, several flexure-shear cracks extended 0.25d to 0.5d upward from the bottom of the beam towards mid-depth of the section. Web-shear cracks were present beyond the hinging zone (Fig. 2.17(a)).

During the third inelastic load cycle, minor spalling of the concrete cover took place on the vertical sides of the hinging zone, adjacent to the column face and lower flexural reinforcement.

By the end of the sixth load cycle, complete spalling of the concrete cover for the lower flexural reinforcement extended 0.5d from the column face (Fig. 2.17(b)).

Buckling of the lower flexural reinforcement became more pronounced with additional reduction in concrete cover.

Predominant spalling of the cover and deterioration of the concrete core was in the area adjacent to the third stirrup and extended upward 0.75d from the bottom of the beam.

Failure of the section occurred after 8 1/2 cycles of inelastic loading. Fracturing of the lower flexural reinforcement occurred between the second and third stirrup and terminated the test. As compared to the other three specimens at the end of the test, Beam G-3 had the largest uncracked blocks of concrete which remained intact.

2.8.5 BEAM G-4 (ρ = 1.02%, f'_c = 12,700 psi, A_s = 1.20 in.^{2}, A'_s = 0.60 in.^{2}, v_s/v_m = 0.79, $v_m/\sqrt{f'_c}$ = 1.87)

Similar to G-2, Beam G-4 had 50% more positive and negative moment reinforcement than Beams G-1 and G-3. The concrete compressive strength was 12.3% greater than Beam G-2.

As a result of Beam G-4 being subjected to an initial downward load of 9.8 kips, several cracks were present prior to the start of cyclic loading. At the onset of the alternating load sequence, there was one primary flexure-shear crack which traversed the entire depth of the section. For the upper three-fourths of the section, this crack was located between the second and third stirrups. Below this depth, the crack was located between the first and second stirrup (Fig. 2.18(a)). Tension cracks in the column face, around the top of the beam perimeter, and flexure-shear cracks adjacent to the upper flexural reinforcement were also present.

Spalling of the concrete cover occurred near the column face and adjacent to the lower flexural reinforcement prior to the completion of the first load cycle. A small section of the concrete cover on the vertical face of the beam, near mid-depth, also spalled.

During the fourth inelastic load cycle, concrete cover, projecting outwards 0.5d from the column face, completely spalled and exposed the lower flexural reinforcement. The loss of concrete, which projected 0.25d upward from the bottom of the beam, was predominantly between the second and third stirrups.

Continued cyclic loading resulted in additional spalling of the concrete cover, buckling of the lower flexural reinforcement, and cracking of the concrete near the upper flexural reinforcement.

Fatigue and fracture of the lower flexural reinforcement terminated the test after 7 1/2 inelastic cycles (Fig. 2.18(b)). The reinforcement fractured between the second and third stirrups. At the conclusion of the test, cracks located beyond the hinging zone were predominantly web shear cracks. Within the hinging zone, the area which suffered the largest relative loss of cover was adjacent to the inclined crack which traversed the entire beam depth.

CHAPTER 3

DISCUSSION AND EVALUATION OF TEST RESULTS

3.1 GENERAL

Building codes for reinforced concrete structures (ACI Committee 318 1983, Uniform Building Code 1985) require lateral-force resisting frames in zones of moderate and high seismic risk to exhibit ductile behavior when subjected to repetitive cycles of inelastic loading. The dissipation of applied seismic energy, which ideally occurs through the formation and rotation of plastic hinges in beams, must be obtained without a critical loss in strength.

Previous research has shown that factors such as beam geometry, strength and load history affect energy dissipation capacity and cyclic behavior (Popov et. al 1972, Wight & Sozen 1973, 1975, Bertero et. al 1974, Ma et. al 1976, Scribner & Wight 1978, 1980, Hwang 1982, Ehsani & Wight 1982, 1985, Hwang & Scribner 1984, Nmai & Darwin 1984, 1986, Darwin & Nmai 1986). However, it has been inherently difficult to determine the dominant parameters controlling cyclic performance due to the fact that research concerning hinge degradation covers such a wide range of member properties and testing variables.

One recent development, that provides a method to evaluate cyclic performance and takes into consideration the influence of

variations in member properties and test variables, is the "energy dissipation index", D_i (Nmai & Darwin 1984, 1986, Darwin & Nmai 1986). D_i represents a measure of cyclic performance and is dependent upon the energy dissipated or work done by the member normalized with respect to the beam's elastic energy at yield.

Based on a statistical analysis of the test results from six major experimental studies (Wight & Sozen 1973, Bertero et al. 1974, Ma et al. 1976, Scribner & Wight 1978, Hwang & Scribner 1984, Nmai & Darwin 1984), Nmai & Darwin concluded that the parameters most significantly affecting D_i were the maximum applied shear stress, v_m, nominal stirrup strength expressed in terms of stress, v_s, and concrete strength, f'_c. The combination of parameters providing a good correlation with D_i was $(v_s f'_c)^{0.5}(v_m)^{-1.5}$. Although the dominance of v_m is evident by its exponential magnitude, this expression also indicates that factors which maintain the integrity or confinement of the concrete, such as a reduced stirrup spacing to increase v_s and an increase in beam width to reduce v_m, improve D_i.

Despite the fact that the positive correlation between D_i and $(v_s f'_c)^{0.5}(v_m)^{-1.5}$ provides a means to evaluate the effect of variations in beam properties and load history, this relationship has limitations. One limitation arises from the fact that the statistical analysis performed by Nmai & Darwin is based upon members fabricated with concrete strengths ranging from 3750 to

5900 psi. Although this narrow range represents a significant percentage of concrete strengths currently specified for beam elements, there is no explicit guarantee that the term $(v_s f'_c)^{0.5}(v_m)^{-1.5}$ will provide a consistent measure of cyclic performance when concrete in excess of 6000 psi is used. A second limitation of using v_s, f'_c and v_m as the only controlling parameters is that the influence of beam geometry is only partially represented by the term $(v_s f'_c)^{0.5}(v_m)^{-1.5}$. The addition of a parameter representing member shape (or any other member property) may reduce or increase the exponential magnitude of the remaining parameters and thus provide more insight when evaluating the impact of each parameter on D_i.

The main purpose of this study is to test and evaluate the influence of high strength concrete on the cyclic behavior of reinforced concrete beams. A statistical analysis of the test results from this study and those of previous research are used to develop a relationship which more accurately describes the influence of concrete strength on cyclic performance. The test results from the high strength concrete specimens (11310 psi $\leq f'_c \leq$ 12860 psi) investigated in this study and the results from four previous researchers (Wight & Sozen 1973, Scribner & Wight 1978, Hwang & Scribner 1984, Nmai & Darwin 1984) representing members fabricated with ordinary strength concrete, are correlated with the cyclic behavior of beams through the use of the energy dissipation index, D_i. A linear regression analysis is used to

evaluate the effect of concrete strength, beam geometry and reinforcement on cyclic performance.

3.2 ENERGY DISSIPATION

The energy dissipated by a beam is dependent upon concrete strength, flexural and shear reinforcement, shear span (Fig. 3.1), and displacement ductility. The "dissipated energy" also depends on the definition of specimen failure. To reduce ambiguities in defining failure, several researchers (Gosain et al. 1977, Scribner & Wight 1978 and 1980, Hwang 1982, Hwang & Scribner 1984, Nmai & Darwin 1984, 1986, Darwin & Nmai 1986) have defined the energy dissipated, E, as the summation of the work done for cycles with a maximum load, P_n, greater than or equal to 75% of the beam's initial yield load, P_y.

The influence of concrete strength on energy dissipation capacity is illustrated by six specimens of similar geometry, strength, and load history. These specimens include two beams tested by Nmai & Darwin (1984, 1986), F-2 and F-3 and four beams tested in the current study, G-1 thru G-4. A comparison of Beams G-1 (ρ = 0.68%, f'_c = 11,610 psi, E = 225 kip-in) and G-3 (ρ = 0.68%, f'_c = 12,860 psi, E = 231 kip-in.) with Beam F-3 (ρ = 0.68%, f'_c = 4260 psi, E = 201 kip-in.) shows that a higher concrete strength increases energy dissipation capacity. Similarly, the increase in energy dissipated by Beams G-2 (ρ = 1.02%, f'_c = 11,310 psi, E = 229 kip-in.) and G-4 (ρ = 1.02%, f'_c = 12,700 psi,

E = 227 kip-in.) compared with Beam F-2 (ρ = 1.02%, f'_c = 4220 psi, E = 169 kip-in.), results from the increase in concrete strength.

The increase in energy dissipation, associated with increased concrete strength, appears to be due principally to the fact that high strength concrete is subjected to a lower percentage of its compressive strength for a given steel percentage and applied loading. Therefore it degrades less rapidly under each cycle. However, an increase in concrete strength does not appear to be the most economical method to increase cyclic performance since a 200% increase in concrete strength improved energy dissipation capacities by 13 and 35%, respectively, for the two reinforcement ratios considered. High strength concrete does appear to be more effective as the reinforcement ratio increases.

3.3 ENERGY DISSIPATION INDEX, D_i

The energy dissipation index, D_i (Nmai & Darwin 1984, 1986, Darwin & Nmai 1986) is a measure of the inelastic cyclic performance of a reinforced concrete beam. D_i is expressed as the ratio of the energy dissipated under cyclic loading to the elastic energy of an equivalent full span beam at initial yielding. The energy dissipation index is expressed as

$$D_i = \frac{E}{0.5P_y\Delta_y\left[\,1 + \left(\frac{A'_s}{A_s}\right)^2\,\right]} \qquad (3.1)$$

in which E = summation of the energy dissipated for all cycles in which $P_n \geq 0.75P_y$, P_y and Δ_y = the initial yield load and yield deflection in negative bending, A'_s = area of bottom steel, and A_s = area of top steel. The normalizing term $0.5P_y\Delta_y[1 + (A'_s/A_s)^2]$ is an approximation of the total elastic energy at yield (Fig. 3.2) for both negative and positive bending at the near and far ends, respectively, of a full span beam in a frame subjected to lateral displacement.

3.4 D_i versus $[(v_s f'_c)^{0.5}(v_m)^{-1.5}]$

The original correlation of v_s, f'_c and v_m with D_i (Nmai & Darwin 1984, 1986, Darwin & Nmai 1986) involved a linear regression analysis of individual and combined test results from six investigations (Wight & Sozen 1973, Bertero et al. 1974, Ma et al. 1976, Scribner & Wight 1978, Hwang & Scribner 1984, Nmai & Darwin 1984). Excluded from the analysis were specimens in which the flexural reinforcement in the hinging zone suffered severe anchorage deterioration, the beam incorporated special reinforcing schemes, or the testing program used a maximum displacement ductility factor, μ (defined as the ratio of maximum displacement to the initial yield displacement), less than 3.9. The restriction imposed upon μ resulted from the fact that specimens subjected to low ductilities exhibited much higher values of D_i than members subjected to $\mu \geq 3.9$. Specimens tested with $3.9 \leq \mu \leq 6.0$ were thought to be more indicative of members subjected to

severe cyclic loading. When the cumulative test results from the six studies (representing 26 specimens fabricated with concrete strengths ranging from 3750 to 5900 psi) were subjected to linear regression analysis, Nmai and Darwin reported that the best fit equation using the least squares method was

$$D_i = 188[(v_s f'_c)^{0.5}(v_m)^{-1.5}] - 9 \qquad (3.2)$$

with a correlation coefficient r = 0.910 (Fig. 3.3). The coefficient, 188, was substantially lower than the coefficients obtained for separate analyses of the individual test series. Nmai & Darwin felt that this was due to a bias in the data. The seven specimens that they tested, which tended to be below the statistical mean, predominated at high values of $(v_s f'_c)^{0.5}(v_m)^{-1.5}$. Most of the other tests were above the statistical mean, but had low values of $(v_s f_c)^{0.5}(v_m)^{-1.5}$. To correct this bias and insure that the deterministic effects of the individual test results were introduced into the regression analysis of the combined data, Nmai & Darwin used the concept of "dummy" variables. An improved best fit equation was obtained, reflecting a more realistic representation of the overall trend line. The expression representing the improved correlation of test results was

$$D_i = 222[(v_s f'_c)^{0.5}(v_m)^{-1.5}] - 17 \qquad (3.3)$$

When Eq. 3.3 was plotted with respect to the 26 discrete data points (Fig. 3.4), Nmai & Darwin observed that beams with larger effective depths, d, and smaller width-to-depth ratios, b/d, lie below the regression line, and thus appeared to produce lower values of D_i than the "average" beam. On the other hand, beams with smaller effective depths and larger b/d ratios lie above the best fit line, producing higher values of D_i and better cyclic performance than deeper, more slender members. These observations imply that both the size and the shape of a beam may affect cyclic performance. Nmai & Darwin further suggested that concrete confinement may not only depend on stirrup spacing, s, expressed as a multiple of effective depth (e.g. $s \leq d/4$), but may also depend upon beam width and possibly some critical material dimension, such as the size of coarse aggregate, d_a.

3.5 INFLUENCE of CONCRETE STRENGTH on D_i

Eq. 3.3 suggests that changes in D_i are dependent upon the square root of f'_c. Experimentally, the influence of concrete strength on member response may be determined by comparing the value of D_i for beams with similar geometry, shear reinforcement, and load history. Specimens meeting these requirements are Beams F-1 thru F-3 ($f'_c \approx$ 4000 psi) (Nmai & Darwin 1984, 1986) and Beams G-1 thru G-4 ($f'_c \approx$ 12,000 psi). The shear reinforcement for these seven beams varied from 161 psi to 176 psi. In addition, variations in the flexural reinforcement ratio ($0.68\% \leq \rho \leq 1.03\%$)

produced different values of applied shear stress (145 psi $\leq v_m \leq$ 215 psi). When the values of D_i for these specimens are subjected to a linear regression analysis using $(v_s f'_c)^{0.5}(v_m)^{-1.5}$ as the predictor variable, the best fit equation is

$$D_i = 82[(v_s f'_c)^{0.5}(v_m)^{-1.5}] + 9.6 \qquad (3.4)$$

with r = 0.972. Eq. 3.4 is compared to Eq. 3.3 in Fig. 3.5. Fig. 3.5 indicates that an increase in concrete strength results in an increase in D_i, and that Eq. 3.4 predicts lower values of D_i than Eq. 3.3. Thus, it appears that the assumption of a one-half power influence of f'_c on D_i is incorrect or additional parameters must be included in the predictor variable to improve the correlation with D_i, or both. As a first step, a better estimate of the influence of concrete strength on D_i must be obtained.

This can be done if the exponential magnitude of each parameter in Eq. 3.4 is characterized individually. Application of optimizing principles (Appendix C) to solve for each exponent provides a method to perform the characterization. Since the nominal stirrup strength, v_s, is nearly constant for the seven specimens, a regression analysis using f'_c and v_m as the controlling parameters provides an approximate, yet acceptable, correlation of data. Thus, the optimum correlation of f'_c and v_m with D_i becomes

$$D_i = 1789[(f'_c)^{0.38}(v_m)^{-1.35}] - 0.3 \qquad (3.5)$$

with correlation coefficient r = 0.980 (Fig. 3.6).

To facilitate evaluation of the correlation between D_i and the predictor variable, the square of r, or coefficient of determination is introduced (r^2 = 0.961 for Eq. 3.5). As discussed in Appendix C, the optimum correlation of data is one in which r or r^2 is maximized. Both r and r^2 express the strength of a linear relationship and have a value of one when the correlation is exact and zero when there is no correlation. However, r^2 specifically represents the percentage of the variation in the response variable that is explained by the predictor variable (Morrison 1983). In addition, r^2, as compared to r, is a more sensitive measure of linearity.

For the seven beams used in this analysis, Eq. 3.5 indicates that the applied shear stress, v_m, has considerably greater influence on D_i than does concrete strength. The ranking or order of significance between v_m and f'_c in Eq. 3.5 is qualitatively similar to Eqs. 3.3 and 3.4. Also, the optimized exponential values of 0.38 and -1.35 in Eq. 3.5 are of comparable magnitudes to v_m and f'_c in the previous equations. Thus, the difference in the value of D_i calculated in Eq. 3.5, as opposed to Eq. 3.4, is likely due to member properties that are not accounted for by v_s, f'_c, and v_m.

Before additional properties are considered, the optimized exponents of v_s, f'_c, and v_m for all 30 test results will be obtained (26 normal and 4 high strength concrete specimens). As

seen in Table 3.1, 121 psi $\leq v_s \leq$ 832 psi. This wide range necessitates the inclusion of stirrup strength in the predictor variable. For all 30 tests, the optimized best fit line is

$$D_i = 15909[(v_s)^{0.95}(f'_c)^{-0.01}(v_m)^{-2.02}] + 1.2 \qquad (3.6)$$

with $r^2 = 0.873$ (Fig. 3.7).

The fit of the data in Eq. 3.6 is not as good as that obtained in either Eq. 3.3 or Eq. 3.5. The negative exponent for f'_c in Eq. 3.6 contradicts the earlier observations that increases in concrete strength result in increases in both dissipated energy and D_i. Therefore, Eq. 3.6 does not correctly reflect the true influence of concrete strength on cyclic performance.

The negative exponent of f'_c in Eq. 3.6 may be attributed to two factors. First, the distribution of data is biased. Specifically, concrete strength is dominated by values between 4000 and 5000 psi, as compared to the uniform distribution of v_s and v_m (Fig. 3.8). The 26 specimens fabricated with normal strength concrete represent the full range of v_s and v_m while the 4 high strength concrete beams represent the lower end of the respective ranges. A non-biased analysis must include high strength concrete specimens with higher values of v_s and v_m.

Second, the negative exponent of f'_c may be the result of an insufficient number of parameters in the predictor variable to adequately describe the influence of v_s, f'_c, and v_m on D_i (as previously suggested to explain the differences in Eqs. 3.3 and 3.4). While the presence or absence of any parameter can affect

the exponential magnitude of the remaining parameters in the predictor variable (i.e. "latent" parameters) (Draper & Smith 1981), the absence of a controlling parameter can substantially distort the true influence of the parameters used in the analysis.

3.6 ADDITIONAL PARAMETERS INFLUENCING D_i

Further insight into the choice of which parameters dominate cyclic performance can be obtained by including the influence of beam shape and size (as proposed by Nmai & Darwin 1984, 1986 and Darwin & Nmai 1986) in the regression analysis. In addition, the development of a parameter which more accurately describes the improvement in ductility obtained with an increase in beam width and decrease in stirrup spacing, will be shown to improve the correlation of available data. This parameter will represent the combined influence of beam width and stirrup spacing not currently represented by the stirrup strength term, v_s.

Beam shape is introduced into the regression analysis through the addition of the width-to-depth ratio, b/d (i.e. aspect ratio). The influence of beam size expressed as a function of coarse aggregate diameter, d_a, is introduced through the parameter d_a/d. d_a is normalized with respect to d, as opposed to b, so as to maintain the influence of the b/d ratio.

An additional factor, which influences cyclic performance, pertains to the confinement of the concrete core. The nominal

stirrup strength term, v_s, does not always reflect improved ductility with reduced stirrup spacing. This occurs in beams of equal nominal stirrup strength obtained by proportionate changes in the area of transverse reinforcement and stirrup spacing. As shown by Nmai & Darwin (1984 and 1986) and Darwin & Nmai (1986), a reduced stirrup spacing increases the energy dissipation capacity of beams subjected to severe cyclic loading by providing greater concrete confinement and delaying buckling of the compression reinforcement. For the case of monotonic compression loading in reinforced concrete tied columns, strength and ductility have been shown to be influenced more by tie spacing and configuration than by tie size (Sheikh & Uzumeri 1980). The development of a parameter reflecting concrete confinement, including factors such as stirrup spacing, s, core width, b_c, and core depth, d_c, should improve the correlation between D_i and the parameters controlling cyclic performance.

A parameter relating hinge or core integrity to D_i may be defined as the ratio of a confined concrete volume to the volume of the core. For the region between adjacent stirrups, the volume of the core is the product of the stirrup spacing, the core width, and the core depth (for this study, the core dimensions are based on the outside stirrup dimensions). The confined concrete volume is delineated by planes containing the four stirrup legs and oriented at an angle of 45° with respect to the surface of the beam. When the stirrup spacing is less than the

core width, the volume of confined concrete takes the form of two truncated pyramids (Fig. 3.9.(a)). As seen in Fig. 3.9.(b), a reduction in stirrup spacing increases the volume of confined concrete relative to the core volume and should provide an improvement in D_i.

The volume of confined concrete between two adjacent stirrups is

$$\text{Volume} = \frac{s}{6}\left[6b_c d_c - 3s(b_c + d_c) + 2s^2\right] \tag{3.7}$$

The ratio of the confined concrete volume to the core volume or "Confinement Ratio", C_r, is

$$C_r = \frac{\frac{s}{6}\left[6b_c d_c - 3s(b_c + d_c) + 2s^2\right]}{sb_c d_c} \tag{3.8}$$

$$= 1 - \frac{s}{2b_c} - \frac{s}{2d_c} + \frac{1}{3}\left(\frac{s}{b_c}\right)\left(\frac{s}{d_c}\right) \tag{3.9}$$

The influence of s, b_c and d_c on the confinement ratio may be determined by evaluating a plot of C_r isobars on the s/d_c-s/b_c plane (Fig. 3.10). A reduction in stirrup spacing decreases s/b_c and s/d_c and thus improves confinement (i.e. provides a larger value of C_r). The influence of b_c and d_c on the confinement ratio may be illustrated by evaluating Fig. 3.10 at a constant s/d_c ratio. An increase in beam width reduces s/b_c and thus

results in a larger value of C_r at the constant value of s/d_c. The increase in energy dissipation arising from an increase in beam width, which improves the state of triaxial confinement for concrete in compression, can now be correlated with D_i through the term C_r. Evaluation of Eq. 3.9 and Fig. 3.10 also indicates that square-shaped beams will provide better cyclic performance than slender rectangular-shaped beams.

The inclusion of b/d, d_a/d, and C_r in the regression analysis should facilitate the determination of which parameters dominate the behavior of beams subjected to severe cyclic loading. However, as shown in Fig. 3.11, the distribution of these parameters is also somewhat biased, but not to the extent of f'_c (Fig. 3.8).

3.7 EVALUATION of PARAMETERS INFLUENCING D_i

The determination of which parameters dominate cyclic performance is dependent upon the choice of parameters to be included in the regression analysis. As more parameters are added to the predictor variable, the ability to both "predict" and "describe" each parameter's influence on D_i will be improved. A relative comparison of the exponential magnitudes provides a means to qualitatively evaluate the dominance of the respective parameters.

When b/d, d_a/d and C_r are included in an analysis which already considers v_s, f'_c and v_m, the overall strength of the relationship between D_i and the controlling parameters can be determined by evaluating the new value of r^2. As more parameters

are added to the predictor variable, the effect is an increase in r^2. Based on the relationship between r^2 and the number of parameters, the best correlation of data would be one in which all six of the proposed controlling parameters are considered. The practical choice of which combination of parameters provide a reasonably "good" correlation with D_i is one in which a value of r^2 is close to the maximum and obtained with a minimum number of parameters.

The bias in the distribution of parameters (Fig. 3.8 and 3.11) necessitates further discussion relative to evaluating the influence of a given parameter on D_i. As compared to the other parameters, the obvious bias in the distribution of f'_c limits the interpretation of its exponential magnitude. In addition, the intercorrelation of terms such as b/d and C_r (which are both dependent upon b and d) may reduce the descriptive ability of the predictor variable. The choice of which parameters are to be included in the regression analysis and the subsequent evaluation of their relative exponential magnitudes is subjective.

3.7.1 D_i versus $(v_s)^{c_1}(f'_c)^{c_2}(\frac{b}{d})^{c_3}(\frac{d_a}{d})^{c_4}(C_r)^{c_5}(v_m)^{c_6}$

When beam size and shape and the confinement ratio are included in a statistical analysis of the data, the optimization of exponential values results in a least squares best fit line of

$$D_i = 9281\left[(v_s)^{0.48}(f'_c)^{0.11}(\frac{b}{d})^{0.48}(\frac{d_a}{d})^{-0.09}(C_r)^{0.96}(v_m)^{-1.56}\right] - 0.4 \qquad (3.10)$$

with r^2 = 0.951 (Fig. 3.12). As compared to Eq. 3.6 in which r^2 = 0.873, the 8% increase in r^2 can be directly attributed to the inclusion of the parameters b/d, d_a/d, and C_r.

As previously discussed, the significance of applied shear stress, v_m, on cyclic performance is well established. Beams subjected to large shear stresses have lower values of D_i resulting from the loss in concrete confinement and reduction in shear stiffness. The dominance of v_m on D_i is seen in Eq. 3.10. The parameter v_m has the largest exponential magnitude and has the greatest influence on D_i of the six parameters evaluated.

The parameter in Eq. 3.10 having the least impact on D_i is the ratio of coarse aggregate diameter to effective depth, d_a/d. The negative sign and low exponential magnitude indicate that beam size, as represented by d_a/d, has little effect on D_i. The negative sign of the exponent also suggests that d_a primarily affects concrete strength (concrete strength generally increases as aggregate size decreases), and its removal from the regression analysis should increase the exponential magnitude of f'_c. A positive correlation (i.e. positive exponent for d_a/d in Eq. 3.10), as stated by Darwin & Nmai (1986), would have suggested improved confinement with increased aggregate size.

When the parameter d_a/d is removed from the predictor variable, the resulting optimized linear expression is

$$D_i = 9828[(v_s)^{0.50}(f'_c)^{0.14}(\frac{b}{d})^{0.47}(C_r)^{0.95} (v_m)^{-1.58}] - 0.4 \quad (3.11)$$

with $r^2 = 0.950$ (Fig. 3.13). The increase in the exponential magnitude of f'_c in Eq. 3.11, as compared to Eq. 3.10, and the negligible change in the exponents of the remaining parameters, indicates that the analysis of available data adequately represents the dependency of f'_c on d_a.

The bias in the distribution of parameters and the apparent intercorrelation of terms limit the evaluation of the relative influence of b/d and C_r on D_i. However, some insight into the importance of these parameters is possible by removing b/d or C_r from the regression analysis and comparing the new value of r^2 to that obtained with Eq. 3.11. It should be noted that as parameters are removed from the analysis, the descriptive abilities of the predictor variable are diminished.

3.7.2 D_i versus $(v_s)^{c_1}(f'_c)^{c_2}(C_r)^{c_3}(v_m)^{c_4}$

Eliminating the b/d ratio from the regression analysis, (note, it has less influence in Eq. 3.11 than C_r), results in the optimized relationship

$$D_i = 7518[(v_s)^{0.80}(f'_c)^{0.07}(C_r)^{1.12}(v_m)^{-1.77}] + 0.7 \quad (3.12)$$

with $r^2 = 0.921$. As compared to Eq. 3.6, the 5% increase in r^2 is due singularly to the inclusion of the confinement ratio C_r. The ranking, or order of significance of the controlling parameters in Eq. 3.12 is consistent with Eq. 3.11. This suggests that factors such as stirrup spacing and beam width (which affect v_s and C_r) influence D_i more than f'_c. The parameter dominating D_i remains the applied shear stress, v_m.

When C_r is replaced with the aspect ratio, b/d, the optimized expression becomes

$$D_i = 17136[(v_s)^{0.53}(f'_c)^{0.10}(\frac{b}{d})^{0.61}(v_m)^{-1.71}] - 0.7 \qquad (3.13)$$

with $r^2 = 0.920$. The evaluation of r^2 for Eq. 3.12 and Eq. 3.13 indicates that both expressions provide an exceptionally good prediction of D_i for the range of parameters investigated.

3.8 PRACTICAL IMPLICATIONS

In addition to the bias in the distribution of parameters, another factor to be considered when evaluating a limited quantity of data is prediction bias (i.e. developing a correlation between variables that fits the range of data and not necessarily the true trend). The effect of prediction bias can be readily seen by performing a regression analysis on the 26 normal concrete strength specimens and then comparing each parameter's exponential magnitude to the values in Eq. 3.10. When the

predictor variable representing the six controlling parameters is optimized for the 26 specimens, the best fit line is

$$D_i = 28[(v_s)^{0.44}(f'_c)^{0.79}(\frac{b}{d})^{0.40}(\frac{d_a}{d})^{-0.17} (C_r)^{0.94}(v_m)^{-1.55}] - 0.8 \qquad (3.14)$$

with $r^2 = 0.960$.

A comparison of the exponents with those in Eq. 3.10, shows that only the exponents of f'_c and d_a/d (which is related to concrete strength) have changed significantly. These large changes clearly indicate prediction bias. This bias affects Eqs. 3.10 through 3.14 and therefore restricts interpretation of the true influence of f'_c on D_i.

To remove the bias and obtain a better representation of the true impact of concrete strength on cyclic performance, a controlled series of tests are required for the full range of beam parameters.

An evaluation Eqs. 3.10 through 3.13, based on r^2, indicates that the linear regression analyses using all 30 applicable test results provide a good correlation of parameters with D_i. v_m is the dominant parameter influencing D_i.

Considering the dominance of v_m on cyclic performance, the use of high strength concrete to reduce member width does not appear to be a good design philosophy. In fact, reductions in

beam width should cause a degradation in cyclic performance under severe earthquake loading.

Improvements in cyclic performance can be obtained with a reduction in stirrup spacing and an increase in beam width. Reduced stirrup spacing, however, does not facilitate the placement of the reinforcement or concrete. Therefore, the more economical means to improve cyclic performance is to increase beam width. This is readily seen by expressing the applied shear stress term as

$$v_m = \frac{V_m}{bd} \approx \frac{(A_s f_y)d}{a(bd)} \approx \frac{A_s f_y}{ab} \qquad (3.15)$$

in which the product $(A_s f_y)d$ approximates the moment capacity of the section and a = shear span. For a given d, $A_s f_y$ controls the flexural strength and thus the applied shear force, V_m. v_m is not effected by d. Therefore, a reduction in v_m can only be obtained by increasing b. Larger beam widths reduce conjestion of the reinforcement and facilitate concrete placement.

CHAPTER 4

SUMMARY AND CONCLUSIONS

4.1 SUMMARY

The main objective of this study was to test and evaluate the cyclic behavior of high strength, lightly reinforced concrete beams. Four specimens representing beam-to-column subassemblies in a moment resistant frame were fabricated with concrete strengths ranging from 11,310 to 12,860 psi and flexural reinforcement ratios of 0.68 and 1.02%. Nominal stirrup strength and stirrup spacing were approximately 170 psi and d/4, respectively. All specimens were subjected to beam tip deflections corresponding to a displacement ductility factor of five. Maximum applied shear stress varied from 145 to 210 psi.

Standard numerical optimizing principles and linear regression analysis techniques were used to qualitatively evaluate the influence of concrete strength, specimen geometry, and reinforcement on cyclic behavior. Recommendations are made concerning the choice of which member properties affect and improve the cyclic performance of beams designed to resist severe seismic loading.

4.2 CONCLUSIONS

For beams with similar geometry, reinforcement and load history, an increase in concrete strength increases the energy dissipated by the member.

Considering the available measures correlating seismic loading to hinge performance for specimens without axial loading, the energy dissipation index, D_i, provides a consistent measure of cyclic performance.

Based on the range of available data analyzed in this report, improvements in D_i can primarily be obtained with a decrease in the maximum applied shear stress. To a lesser extent, an increase in D_i is possible with increased concrete strength, nominal stirrup strength, and confinement ratio.

As seen by the development of the confinement ratio and its influence on the correlation of data, factors which contribute to confining the concrete core and facilitate transfer of shear within the hinging zone improve energy dissipation capacity. The use of square-shaped beams, as opposed to slender rectangular members, appears to provide improved cyclic performance.

An increase in D_i can be obtained by reducing stirrup spacing and increasing beam width. However, reduced stirrup spacing leads to conjestion of the reinforcement and restricts concrete placement. Increases in beam width also improve the state of triaxial confinement for concrete in compression and provide the most effective means to increase the energy dissipation capacity

by reducing the maximum applied shear stress without increasing the energy demand on the beam.

Beam size, relative to the coarse aggregate size, does not appear to be a factor influencing cyclic performance.

4.3 RECOMMENDATIONS for FUTURE WORK

Although applicable research concerning hinge degradation represents a wide range of beam geometry, strength, and load history, the analysis presented in this study indicates that applied shear stress dominates cyclic performance. Investigations specifically designed to reduce the bias in the distribution of concrete strength should provide additional information required to evaluate the influence of concrete strength on cyclic performance. In addition, research programs designed to study the influence of beam width on cyclic performance may also modify existing minimum code requirements concerning the b/d ratio. Testing programs designed to supplement existing data could ultimately provide a means to quantitatively evaluate the appropriateness of constructing reinforced concrete flat beams to resist earthquake induced forces.

REFERENCES

Abdel-Fattah, B. A., and Wight, J. K. (1985). "Experimental Study of Moving Beam Plastic Hinging Zones for Earthquake Resistant Deign of R/C Buildings," Report No. UMCE 85-11, Department of Civil Engineering, University of Michigan, Ann Arbor, MI, December, 291 pp.

Abdel-Fattah, B., and Wight, J. K. (1987). "Study of Moving Beam Plastic Hinging Zones for Earthquake-Resistant Design of R/C Buildings," ACI Structural Journal, Vol. 84, No. 1, January-February, pp. 31-39.

ACI Committee 318 (1983). "Building Code Requirements for Reinforced Concrete (ACI 318-83)," American Concrete Institute, Detroit, Michigan, 111 pp.

ACI Committee 318 (1983). "Commentary on Building Code Requirements for Reinforced Concrete (ACI 318-83) (ACI 318R-83)," American Concrete Institute, Detroit, Michigan, 155 pp.

Bertero, V. V., Popov, E. P., and Wang, T. Y. (1974). "Hysteretic Behavior of Reinforced Concrete Flexural Members with Special Web Reinforcement," Earthquake Engineering Research Center, University of California, Berkeley, Report No. EERC 74-9, August, 126 pp.

Burr, I. W. (1974). Applied Statistical Methods, Academic Press, Inc., New York, pp. 372-400.

Darwin, D. and Nmai, C. K. (1986). "Energy Dissipation in RC Beams Under Cyclic Load," Journal of Structural Engineering, ASCE, Vol. 112, No. 8, August, pp. 1829-1846.

Draper, N. R., and Smith, H. (1981). Applied Regression Analysis, John Wiley & Sons, Inc., New York, pp. 294-305.

Ehsani, M. R., and Wight, J. K. (1982). "Behavior of External Reinforced Concrete Beam to Column Connections Subjected to Earthquake Type Loading," Report No. UMEE 82R5, Department of Civil Engineering, University of Michigan, Ann Arbor, MI, July, 243 pp.

Ehsani, M. R., and Wight, J. K. (1985). "Exterior Reinforced Concrete Beam-to-Column Connections Subjected to Earthquake-Type Loading," Journal of the American Concrete Institute, Vol. 82, No. 4, July-August, pp. 492-499.

Ehsani, M. R., Moussa, A. E., and Vallenilla, C. R. (1987). "Comparison of Inelastic Behavior of Reinforced Ordinary- and High-Strength Concrete Frames," ACI Structural Journal, Vol. 84, No. 2, March-April, pp. 161-169.

Gosain, N. K., Brown, R. H., and Jirsa, J. O. (1977). "Shear Requriements for Load Reversals on RC Members," Journal of the Structural Division, ASCE, Vol. 103, No. ST7, July, pp. 1461-1476.

Hwang, T. H. (1982). "Effects of Variation in Load History on Cyclic Response of Concrete Flexural Members," Thesis submitted to the University of Illinois at Urbana-Champaign in partial fulfillment of the requirements for the degree of Doctor of Philosophy, July, 232 pp.

Hwang, T. H., and Scribner, C. F. (1984). "R/C Member Cyclic Response During Various Loadings," Journal of Structural Engineering, ASCE, Vol. 110, No. 3, March, pp. 477-489.

IMSL Library (1985). Edition 9.2, IMSL, Inc., Houston, Texas.

Ma, S. M., Bertero, V. V., and Popov, E. P. (1976). "Experimental and Analytical Studies on the Hysteretic Behavior of Reinforced Concrete Rectangular and T-Beams," Earthquake Engineering Research Center, University of California, Berkeley, Report No. EERC 76-2, May, 254 pp.

Morrison, D. F., (1983). Applied Linear Statistical Models, Prentice-Hall, Inc., New Jersey, pp. 57-68.

Neter, J., and Wasserman, W. (1974). Applied Linear Statistical Models, Richard D. Irwin, Inc., Illinois, pp. 53-93.

Nmai, C. K., and Darwin, D. (1984). "Cyclic Behavior of Lightly Reinforced Concrete Beams," SM Report No. 12, University of Kansas Center for Research, Inc., Lawrence, KS., June, 139 pp.

Nmai, C. K., and Darwin, D. (1986). "Lightly Reinforced Concrete Beams under Cyclic Load," Journal of the American Concrete Institute, Vol. 83, No. 5, September-October, pp. 777-783.

Popov, E. P., Bertero, V. V., and Krawinkler, H. (1972). "Cyclic Behavior of Three R. C. Flexural Members with High Shear," Earthquake Engineering Research Center, University of California, Berkeley, Report No. EERC 72-5, October, 82 pp.

Scribner, C. F., and Wight, J. K. (1978). "Delaying Shear Strength Decay in Reinforced Concrete Flexural Members Under Large Load Reversals," Report No. UMEE 78R2, Department of Civil Engineering, University of Michigan, Ann Arbor, MI, May, 221 pp.

Scribner, C. F., and Wight, J. K. (1980). "Strength Decay in R/C Beams Under Load Reversals," Journal of the Structural Division, ASCE, Vol. 106, No. ST4, April, pp. 861-876.

Sheikh, S. A., and Uzumeri, S. M. (1980). "Strength and Ductility of Tied Concrete Columns," Journal of the Structural Division, ASCE, Vol. 106, No. ST5, May, pp. 1079-1102.

Uniform Building Code, (1985), International Conference of Building Officals, Whittier, CA, 817 pp.

Wight, J. K., and Sozen, M. A. (1973). "Shear Strength Decay in Reinforced Concrete Columns Subjected to Large Deflection Reversals," Civil Engineering Studies, SRS No. 403, University of Illinois at Urbana-Champaign, August, 290 pp.

Wight, J. K., and Sozen, M. A. (1975). "Strength Decay of RC Columns Under Shear Reversals," Journal of the Structural Division, ASCE, Vol. 101, No. ST5, May, pp. 1053-1065.

Zsutty, T. C. (1968). "Beam Shear Strength Prediction by Analysis of Existing Data," Journal of the American Concrete Institute, Vol. 65, No. 11, November, pp. 943-951.

TABLE 2.1 BEAM AND REINFORCEMENT PROPERTIES

	BEAM			
	G-1	G-2	G-3	G-4
PROPERTY:				
Length, l (in.)	68	68	68	68
Height, h (in.)	18	18	18	18
Width, b (in.)	7.5	7.5	7.5	7.5
Effective depth, d (in.)	15.69	15.75	15.62	15.62
Effective depth, d_1 (in.)	16.56	16.62	16.59	16.59
Core Width, b_c (in.)	5.5	5.6	5.6	5.5
Core Depth, d_c (in.)	15.94	16.06	15.9	15.9
Shear Span, a (in.)	60	60	60	60
a/d	3.8	3.7	3.8	3.8
Reinforcement Ratio, ρ (%)	0.68	1.02	0.68	1.02
Top Reinforcement, A_s	4#4	6#4	4#4	6#4
Bottom Reinforcement, A'_s	2#4	3#4	2#4	3#4
A'_s/A_s	0.5	0.5	0.5	0.5
f_y (ksi)	69.4	69.4	69.4	69.4
Stirrup diameter (in.)	0.222	0.222	0.222	0.222
Stirrup spacing, s (in.)	3.6	3.6	3.6	3.6
f_{vy} (ksi)	58.9	58.6	61.5	58.6
v_s (psi)	169	168	176	168

TABLE 2.2 AGGREGATE AND CONCRETE PROPERTIES

Fine Aggregate: (FA)
Bulk Specific Gravity (SSD) = 2.61
Absorption (SSD) = 0.4%
Unit Weight = 109 pcf
Fineness Modulus = 2.57

Sieve Analysis (% Passing):	3/8"	#4	#8	#16	#30	#50	#100
	100	99.4	94.0	79.5	53.3	15.2	1.5

Coarse Aggregate: (CA)
Bulk Specific Gravity (SSD) = 2.59
Absorption (SSD) = 2.6%
Unit Weight = 96 pcf
Fineness Modulus = 6.40

Sieve Analysis (% Passing):	3/4"	1/2"	3/8"	#4	#8	#16
	100	83.7	51.4	6.7	1.5	0.8

	Actual Mix Proportions for 1.0 Cubic Yard[1]									
Beam	Water	Cement	Fly Ash	FA (SSD)	CA (SSD)	Silica Fume Slurry	Superplasticizer (fl. oz.)	Slump (in.)	Age at Testing (days)	f'_c[3] (psi)
G-1	66[2]	694	-	1182	1755	314	-	8.75	76	11,610
G-2	297	824	169	977	1631	-	118	2.5	108	11,310
G-3	49[2]	920	-	1049	1558	416	-	8.5	185	12,860
G-4	51[2]	706	-	1205	1758	316	-	9.75	73	12,700

(1) Measured in pounds unless noted otherwise
(2) Free surface moisture on aggregate
(3) Compressive strength from 6 x 12 in. cylinders

TABLE 2.3 COMPUTED AND MEASURED SHEARS

	BEAM			
	G-1	G-2	G-3	G-4
Nominal Stirrup Capacity:				
$V_s = A_v f_{vy} d/s$ (kips)	19.8	19.8	20.6	19.7
$v_s = A_v f_{vy}/(bs)$ (psi)	169	168	176	168
Calculated Shears:				
V_y (1) (kips)	14.2	21.1	14.1	21.0
V_c (2) (kips)	25.4	25.1	26.6	26.4
V_m (3) (kips)	17.6	26.1	17.6	26.0
Test Shears:				
V_y (kips)	13.7	20.8	14.1	20.8 (4)
V_m (kips)	17.1	24.7	17.7	24.7 (4)
Maximum Shear Stress:				
v_m (psi)	145	208	151	210
$v_m/\sqrt{f'_c}$	1.35	1.97	1.33	1.87

(1) V_y = Shear force at yielding of longitudinal beam reinforcement

(2) $V_c = 2\sqrt{f'_c} b_w d$

(3) V_m = Maximum shear force = $V_c + V_s$

(4) Value based on the test results of Beam G-2

TABLE 2.4 PRINCIPAL EXPERIMENTAL RESULTS

	BEAM			
	G-1	G-2	G-3	G-4
Yield Load (kips)	13.7	20.8	14.1	20.8
Maximum Load (kips)	17.1	24.7	17.7	24.7
Yield Deflection (in.)	0.328	0.368	0.372	0.368
Maximum Deflection (in.)	1.64	1.84	1.86	1.84
μ(1)	5.0	5.0	5.0	5.0
Maximum Growth (in.)	0.444	0.382	0.418	0.382
Number of Cycles:				
$P_n \geq 0.75P_y$	8.5	5.0	7.0	5.0
Total	8.5	7.25	8.5	7.5

(1) μ = Displacement ductility factor

TABLE 3.1 TEST RESULTS OF APPLICABLE RESEARCH

Reference	Beam	b (in.)	d (in.)	b_c (in.)	d_c (in.)	s (in.)	A_v (sq in.)	f_{vy} (lbs/sq in.)
Hanks & Darwin (Current Study)	* G-1	7.5	15.69	5.5	15.94	3.6	0.077	58,900
	* G-2	7.5	15.75	5.6	16.06	3.6	0.077	58,600
	* G-3	7.5	15.62	5.6	15.9	3.6	0.077	61,500
	* G-4	7.5	15.62	5.5	15.9	3.6	0.077	58,600
Nmai & Darwin (1984)	* F-1	7.5	15.25	4.5	15.0	3.8	0.141	32,500
	* F-2	7.5	15.38	5.5	16.0	3.8	0.141	32,500
	* F-3	7.5	15.38	5.5	16.0	3.8	0.141	32,500
	* F-4	7.5	15.25	5.25	15.75	1.6	0.05	37,700
	* F-5	7.5	15.25	5.25	15.75	2.1	0.05	37,900
	* F-6	7.5	15.38	5.5	16.0	3.8	0.141	32,300
	* F-7	7.5	15.38	5.5	15.75	3.8	0.101	37,600
Scribner & Wight (1978)	* 1	8.0	8.6	5.0	8.5	2.0	0.098	43,700
	2(1)	8.0	8.6	5.0	8.5	2.0	0.098	43,700
	3(2)	8.0	10.1	5.0	9.5	2.5	0.098	43,400
	4(1)	8.0	10.1	5.0	9.5	2.5	0.098	43,400
	* 5	8.0	8.6	5.0	8.5	2.0	0.098	43,700
	6(1)	8.0	8.6	5.0	8.5	2.0	0.098	43,700
	7(3)	8.0	10.1	5.0	9.7	2.5	0.221	45,700
	8(1)	8.0	10.1	5.0	9.5	2.5	0.098	43,400
	* 9	10.0	12.1	7.0	12.0	3.0	0.221	53,500
	10(1)	10.0	12.1	7.0	12.0	3.0	0.221	53,500
	* 11	10.0	12.1	7.0	12.0	3.0	0.221	53,500
	12(1)	10.0	12.1	7.0	12.0	3.0	0.221	53,500
Wight & Sozen (1973)	* 00.033W	6.0	10.05	4.35	9.25	5.0	0.098	50,600
	* 00.048W	6.1	10.0	4.35	9.15	3.5	0.098	50,700
	* 00.067W	6.1	10.05	4.25	9.25	2.5	0.098	50,400
	* 00.105E	6.1	10.0	4.45	9.5	3.5	0.221	45,800
	* 00.105W	6.0	9.95	4.5	9.3	3.5	0.221	46,000
	* 00.147E	6.0	10.0	4.45	9.4	2.5	0.221	45,800
	* 00.147W	5.9	9.95	4.55	9.3	2.5	0.221	46,000
Hwang & Scribner (1984)	1-1(4)	8.0	9.9	5.0	8.6	2.5	0.098	55,600
	* 1-2	8.0	10.1	5.0	8.8	2.5	0.098	53,400
	* 1-4	8.0	9.9	5.0	8.6	2.5	0.098	59,000
	2-1(4)	8.0	9.6	5.0	8.4	2.5	0.098	54,400
	* 2-2	8.0	9.6	5.0	8.4	2.5	0.098	54,600
	* 2-3	8.0	9.7	5.0	8.5	2.5	0.098	58,700
	* 2-4	8.0	9.6	5.0	8.4	2.5	0.098	54,000
	3-1(4)	8.0	9.7	5.0	8.8	2.5	0.221	75,300
	* 3-2	8.0	9.8	5.0	8.9	2.5	0.221	75,100
	* 3-3	8.0	9.6	5.0	8.7	2.5	0.221	75,300
	* 3-4	8.0	9.7	5.0	8.8	2.5	0.221	75,100
Ma, Bertero & Popov (1976)	R-2(3)	9.0	14.0	7.5	13.88	3.5	0.098	63,200
	R-4(3)	9.0	14.0	7.5	13.88	3.5	0.196	63,200
	R-5(3)	9.0	14.0	7.5	13.88	3.5	0.196	63,200
	R-6(3)	9.0	14.0	7.5	13.88	3.5	0.196	63,200
	T-1(3)	9.0	14.0	7.5	13.88	3.5	0.196	63,200
	T-2(3)	9.0	14.0	7.5	13.88	3.5	0.196	63,200
	T-3(3)	9.0	14.0	7.5	13.88	3.5	0.196	63,200
Bertero, Popov & Wang (1974)	33(5)	15.0	25.5	12.0	25.88	3.0	0.442	71,700
	35I(5)	15.0	25.5	12.0	25.88	5.0	0.442	71,700

TABLE 3.1 TEST RESULTS OF APPLICABLE RESEARCH (con't)

Reference	Beam	ρ, as a percentage	A'_s/A_s	d_a (in.)	P_y (kips)	Δ_y (in.)	Energy Dissipated(6) (kip-in.)
Hanks & Darwin (Current Study)	* G-1	0.68	0.5	0.5	13.7	0.33	225
	* G-2	1.02	0.5	0.5	20.8	0.37	229
	* G-3	0.68	0.5	0.5	14.1	0.37	231
	* G-4	1.02	0.5	0.5	20.8	0.37	227
Nmai & Darwin (1984)	* F-1	1.03	0.5	0.75	18.2	0.66	287
	* F-2	1.02	0.5	0.75	19.7	0.53	169
	* F-3	0.69	0.5	0.75	13.5	0.47	201
	* F-4	0.69	0.5	0.75	13.0	0.40	297
	* F-5	0.69	0.5	0.75	13.0	0.45	262
	* F-6	0.69	0.75	0.75	13.3	0.38	328
	* F-7	0.69	0.5	0.75	13.3	0.40	201
Scribner & Wight (1978)	* 1	1.27	0.69	0.37	8.9	0.39	366
	2(1)	1.27	0.69	0.37	8.9	0.47	394
	3(2)	1.63	0.69	0.37	14.4	0.54	274
	4(1)	1.63	0.69	0.37	16.4	0.66	407
	* 5	1.27	0.69	0.37	11.6	0.43	275
	6(1)	1.27	0.69	0.37	12.0	0.37	327
	7(3)	1.63	0.69	0.37	15.0	0.70	365
	8(1)	1.63	0.69	0.37	17.0	0.80	418
	* 9	2.62	0.77	0.37	34.2	1.10	1,267
	10(1)	2.62	0.77	0.37	35.8	1.07	1,358
	* 11	2.62	0.77	0.37	41.0	0.72	723
	12(1)	2.62	0.77	0.37	46.0	0.90	792
Wight & Sozen (1973)	* 00.033W	1.47	1.0	0.37	17.3	0.44	131
	* 00.048W	1.47	1.0	0.37	16.3	0.50	182
	* 00.067W	1.47	1.0	0.37	15.2	0.44	240
	* 00.105E	1.47	1.0	0.37	18.4	0.50	189
	* 00.105W	1.47	1.0	0.37	18.4	0.53	220
	* 00.147E	1.47	1.0	0.37	17.0	0.44	293
	* 00.147W	1.47	1.0	0.37	18.1	0.47	327
Hwang & Scribner (1984)	1-1(4)	1.65	0.69	0.75	18.9	0.41	590
	* 1-2	1.65	0.69	0.75	18.6	0.41	343
	* 1-4	1.65	0.69	0.75	17.2	0.40	248
	2-1(4)	2.34	0.73	0.75	25.9	0.38	360
	* 2-2	2.34	0.73	0.75	24.6	0.37	160
	* 2-3	2.34	0.73	0.75	25.9	0.44	171
	* 2-4	2.34	0.73	0.75	25.9	0.37	151
	3-1(4)	2.34	0.73	0.75	35.8	0.25	320
	* 3-2	2.34	0.73	0.75	34.4	0.25	155
	* 3-3	2.34	0.73	0.75	35.5	0.25	196
	* 3-4	2.34	0.73	0.75	36.1	0.25	178
Ma, Bertero & Popov (1976)	R-2(3)	1.4	0.53	0.5	22.5	0.56	267
	R-4(3)	1.4	0.53	0.5	22.8	0.60	336
	R-5(3)	1.4	1.0	0.5	39.3	0.36	349
	R-6(3)	1.4	1.0	0.5	24.0	0.62	738
	T-1(3)	1.4	0.53	0.5	32.9	0.72	519
	T-2(3)	1.4	0.53	0.5	32.0	0.75	234
	T-3(3)	1.4	1.0	0.5	31.2	0.75	803
Bertero, Popov & Wang (1974)	33(5)	1.58	1.0	-	130.0	0.80	6,470
	35I(5)	1.58	1.0	-	132.0	0.80	9,510

TABLE 3.1 TEST RESULTS OF APPLICABLE RESEARCH (con't)

Reference	Beam	v_s (lbs/sq in.)	f'_c (lbs/sq in.)	b/d	d_a/d	C_r	v_m (lbs/sq in.)
Hanks & Darwin (Current Study)	* G-1	169	11,610	0.48	0.032	0.61	145
	* G-2	168	11,310	0.48	0.032	0.62	208
	* G-3	176	12,860	0.48	0.032	0.61	151
	* G-4	168	12,700	0.48	0.032	0.61	210
Nmai & Darwin (1984)	* F-1	161	4,260	0.49	0.049	0.52	197
	* F-2	161	4,220	0.49	0.049	0.59	215
	* F-3	161	4,260	0.49	0.049	0.59	145
	* F-4	158	4,330	0.49	0.049	0.81	141
	* F-5	121	4,370	0.49	0.049	0.75	143
	* F-6	160	4,320	0.49	0.049	0.59	145
	* F-7	133	4,220	0.49	0.049	0.59	144
Scribner & Wight (1978)	* 1	268	4,970	0.93	0.044	0.71	144
	2(1)	268	4,970	0.93	0.044	0.71	158
	3(2)	213	4,970	0.79	0.037	0.66	213
	4(1)	213	4,970	0.79	0.037	0.66	241
	* 5	268	3,980	0.93	0.044	0.71	212
	6(1)	268	3,980	0.93	0.044	0.71	221
	7(3)	830	3,980	0.79	0.037	0.66	221
	8(1)	213	3,980	0.79	0.037	0.66	238
	* 9	394	4,940	0.83	0.031	0.70	342
	10(1)	394	4,940	0.83	0.031	0.70	353
	* 11	394	4,940	0.83	0.031	0.70	426
	12(1)	394	4,940	0.83	0.031	0.70	432
Wight & Sozen (1973)	* 00.033W	167	4,640	0.59	0.037	0.41	294
	* 00.048W	235	3,750	0.61	0.038	0.51	319
	* 00.067W	327	4,610	0.60	0.037	0.62	336
	* 00.105E	478	4,850	0.61	0.038	0.52	390
	* 00.105W	484	4,850	0.60	0.038	0.64	385
	* 00.147E	675	4,900	0.60	0.038	0.64	382
	* 00.147W	690	4,900	0.59	0.038	0.64	388
Hwang & Scribner (1984)	1-1(4)	273	5,900	0.81	0.076	0.65	255
	* 1-2	262	5,880	0.79	0.074	0.66	270
	* 1-4	290	4,980	0.81	0.076	0.65	242
	2-1(4)	267	5,100	0.83	0.078	0.65	366
	* 2-2	268	5,390	0.83	0.078	0.65	383
	* 2-3	288	4,710	0.82	0.077	0.65	406
	* 2-4	265	4,780	0.83	0.078	0.65	390
	3-1(4)	832	4,910	0.82	0.077	0.66	495
	* 3-2	830	4,970	0.82	0.077	0.66	506
	* 3-3	832	4,980	0.83	0.078	0.65	495
	* 3-4	829	5,060	0.82	0.077	0.66	528
Ma, Bertero & Popov (1976)	R-2(3)	197	4,190	0.64	0.036	0.68	190
	R-4(3)	394	4,380	0.64	0.036	0.68	224
	R-5(3)	394	4,580	0.64	0.036	0.68	349
	R-6(3)	394	4,340	0.64	0.036	0.68	234
	T-1(3)	394	4,790	0.64	0.036	0.68	266
	T-2(3)	394	4,610	0.64	0.036	0.68	298
	T-3(3)	394	4,470	0.64	0.036	0.68	279
Bertero, Popov & Wang (1974)	33(5)	699	5,400	0.59	-	0.83	426
	35I(5)	884	5,500	0.59	-	0.72	463

TABLE 3.1 TEST RESULTS OF APPLICABLE RESEARCH (con't)

Reference	Beam	v_s/v_m	$v_m/\sqrt{f'_c}$	μ_{max}	Number of Cycles (6) $\mu \geq 2$	Number of Cycles (6) $\mu \geq 4$	D_i
Hanks & Darwin (Current Study)	* G-1	1.16	1.35	5.0	8	8	80
	* G-2	0.81	1.97	5.0	7	7	48
	* G-3	1.17	1.33	5.0	8	8	70
	* G-4	0.80	1.87	5.0	7	7	47
Nmai & Darwin (1984)	* F-1	0.80	3.01	3.9	5	5	38
	* F-2	0.78	3.31	5.1	2	2	26
	* F-3	1.15	2.22	4.4	6	6	51
	* F-4	1.16	2.14	5.1	9	9	91
	* F-5	0.87	2.16	4.6	8	8	72
	* F-6	1.15	2.20	5.3	9	9	82
	* F-7	0.95	2.22	5.1	6	6	60
Scribner & Wight (1978)	* 1	1.85	2.06	6.0	12	12	142
	2(1)	1.68	2.24	6.0	12	12	127
	3(2)	1.01	3.06	6.0	7	7	47
	4(1)	0.89	3.45	6.0	8	8	51
	* 5	1.29	3.35	6.0	10	10	74
	6(1)	1.23	3.44	6.0	12	12	99
	7(3)	3.72	3.60	6.0	10	10	47
	8(1)	0.89	3.84	6.0	10	10	41
	* 9	1.14	4.92	6.0	7	7	42
	10(1)	1.12	5.09	6.0	7	7	45
	* 11	0.92	6.16	6.0	4	4	31
	12(1)	0.91	6.23	6.0	5	5	24
Wight & Sozen (1973)	* 00.033W	0.57	4.34	4.0	7	1	17
	* 00.048W	0.74	5.20	4.0	7	1	22
	* 00.067W	0.98	4.85	4.0	9	3	36
	* 00.105E	1.22	5.50	4.0	3	3	21
	* 00.105W	1.26	5.33	4.0	3	3	22
	* 00.147E	1.77	5.45	4.0	6	6	39
	* 00.147W	1.77	5.45	4.0	6	6	38
Hwang & Scribner (1984)	1-1(4)	1.07	3.3	2.0	110	-	103
	* 1-2	0.97	3.6	4.0	13	13	61
	* 1-4	1.20	3.5	4.0	13	7	49
	2-1(4)	0.73	5.1	2.0	60	-	48
	* 2-2	0.70	5.2	4.0	4	4	23
	* 2-3	0.71	6.0	4.0	7	3	20
	* 2-4	0.68	5.6	4.0	5	3	21
	3-1(4)	1.68	7.1	2.0	50	-	47
	* 3-2	1.64	7.3	4.0	4	4	23
	* 3-3	1.68	7.0	4.0	8	4	29
	* 3-4	1.57	7.4	4.0	6	4	26
Ma, Bertero & Popov (1976)	R-2(3)	1.03	2.94	4.9	7	1	32
	R-4(3)	1.76	3.38	7.2	1	1	38
	R-5(3)	1.13	5.16	4.4	10	3	21
	R-6(3)	1.68	3.55	4.4	13	5	47
	T-1(3)	1.48	3.84	4.1	7	1	33
	T-2(3)	1.32	4.38	5.5	-	-	15
	T-3(3)	1.41	4.18	4.2	10	4	33
Bertero, Popov & Wang (1974)	33(5)	1.64	5.80	5.25	13	6	62
	35I(5)	1.91	6.20	6.4	14	7	90

* Designates specimen used in D_i analysis
(1) Intermediate reinforcement
(2) Performed poorly
(3) Severe anchorage deterioration
(4) Displacement ductility
(5) Special web reinforcement
(6) Cycles where $P_n \geq 0.75P_y$

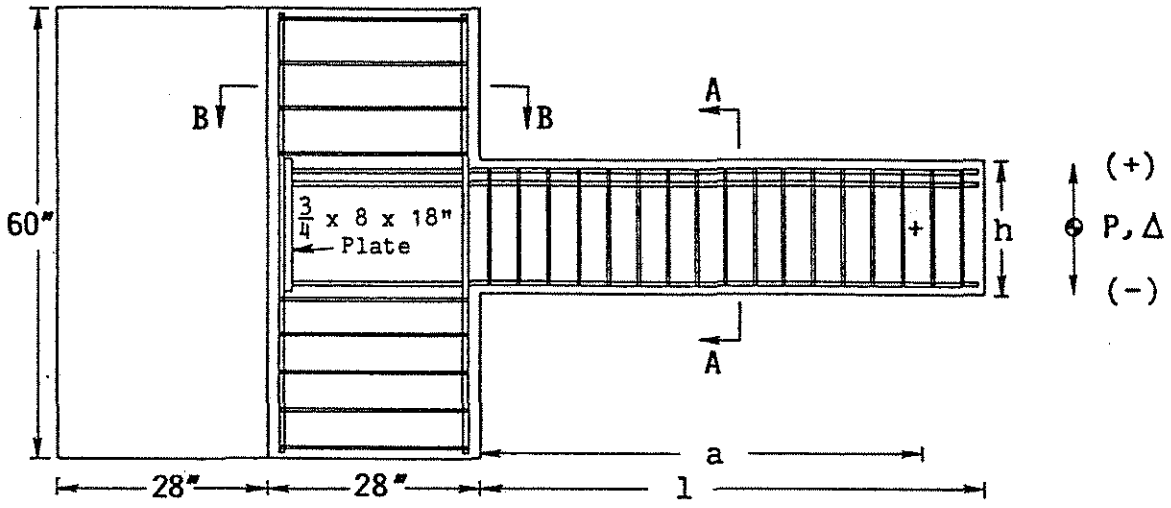

Elevation

(G-1 & G-3) (G-2 & G-4)

Section A-A

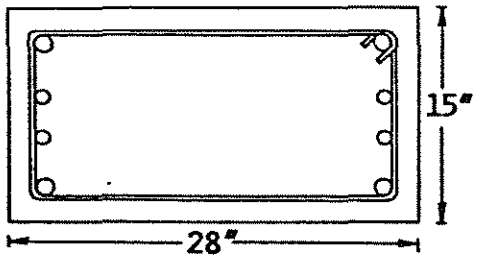

Section B-B

Fig. 2.1 Test Specimen and Reinforcing Details (Nmai & Darwin 1984, 1986)

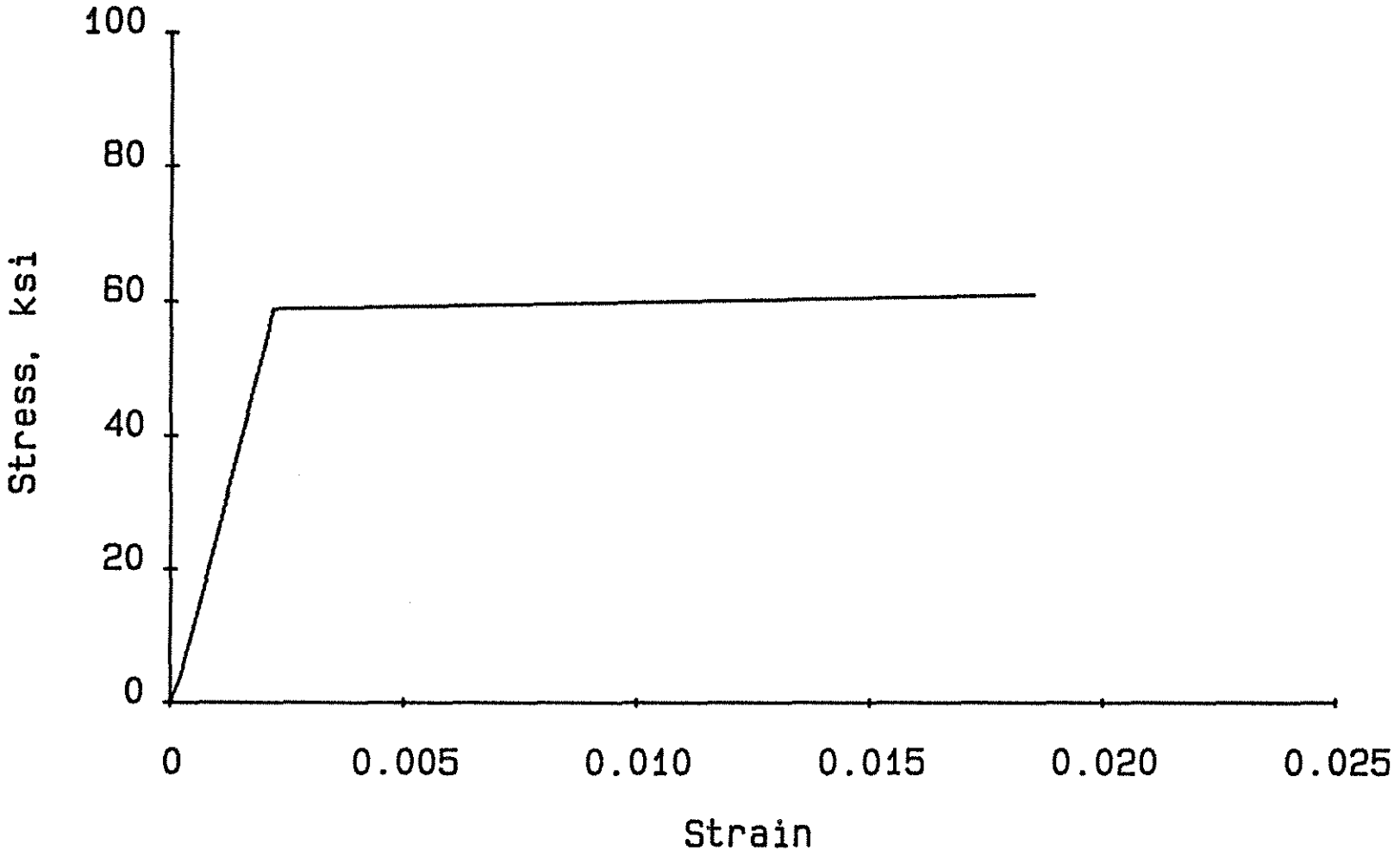

Fig. 2.2 Stress-Strain Relationship for the Transverse Reinforcement

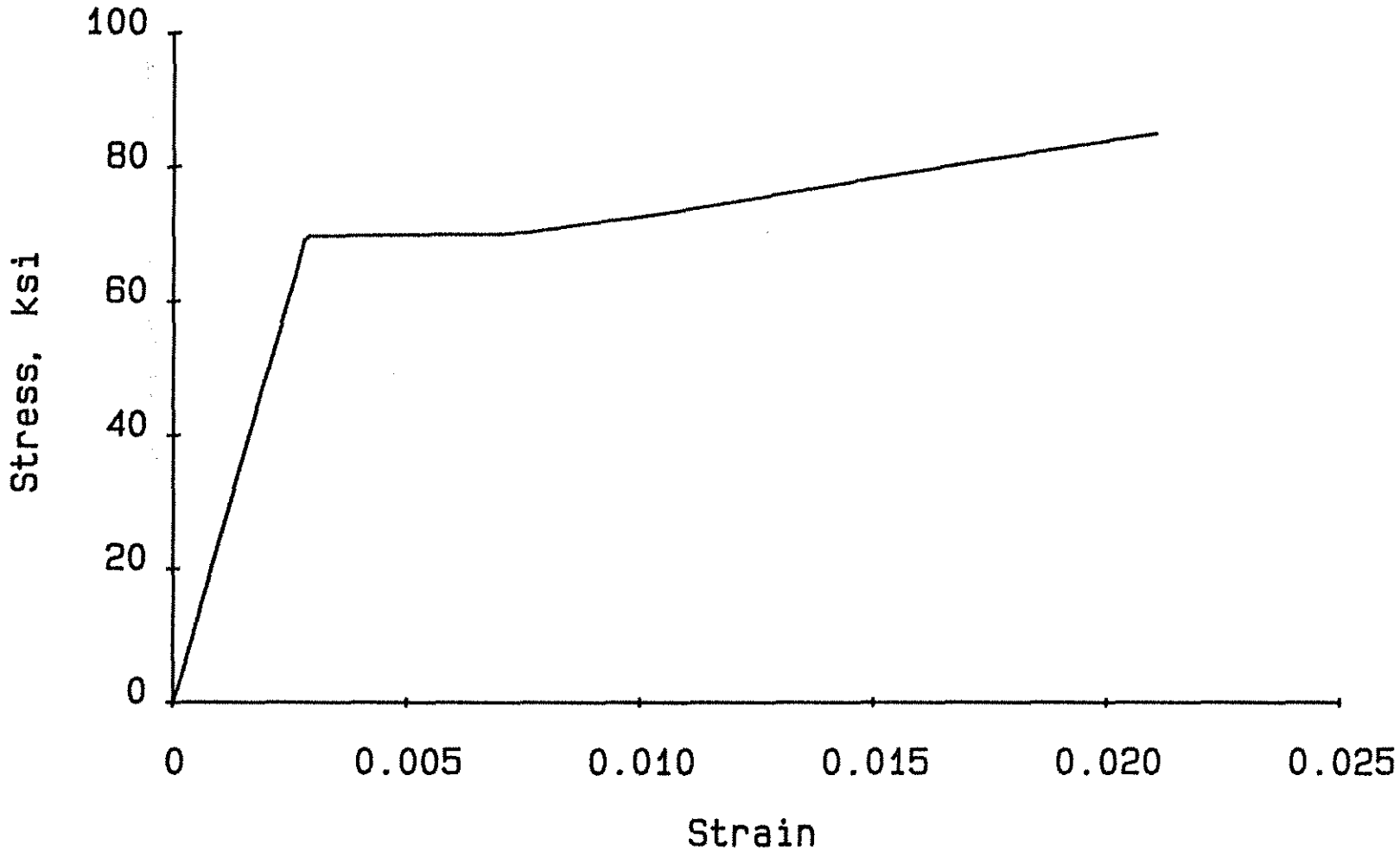

Fig. 2.3 Stress-Strain Relationship for the Longitudinal Reinforcement

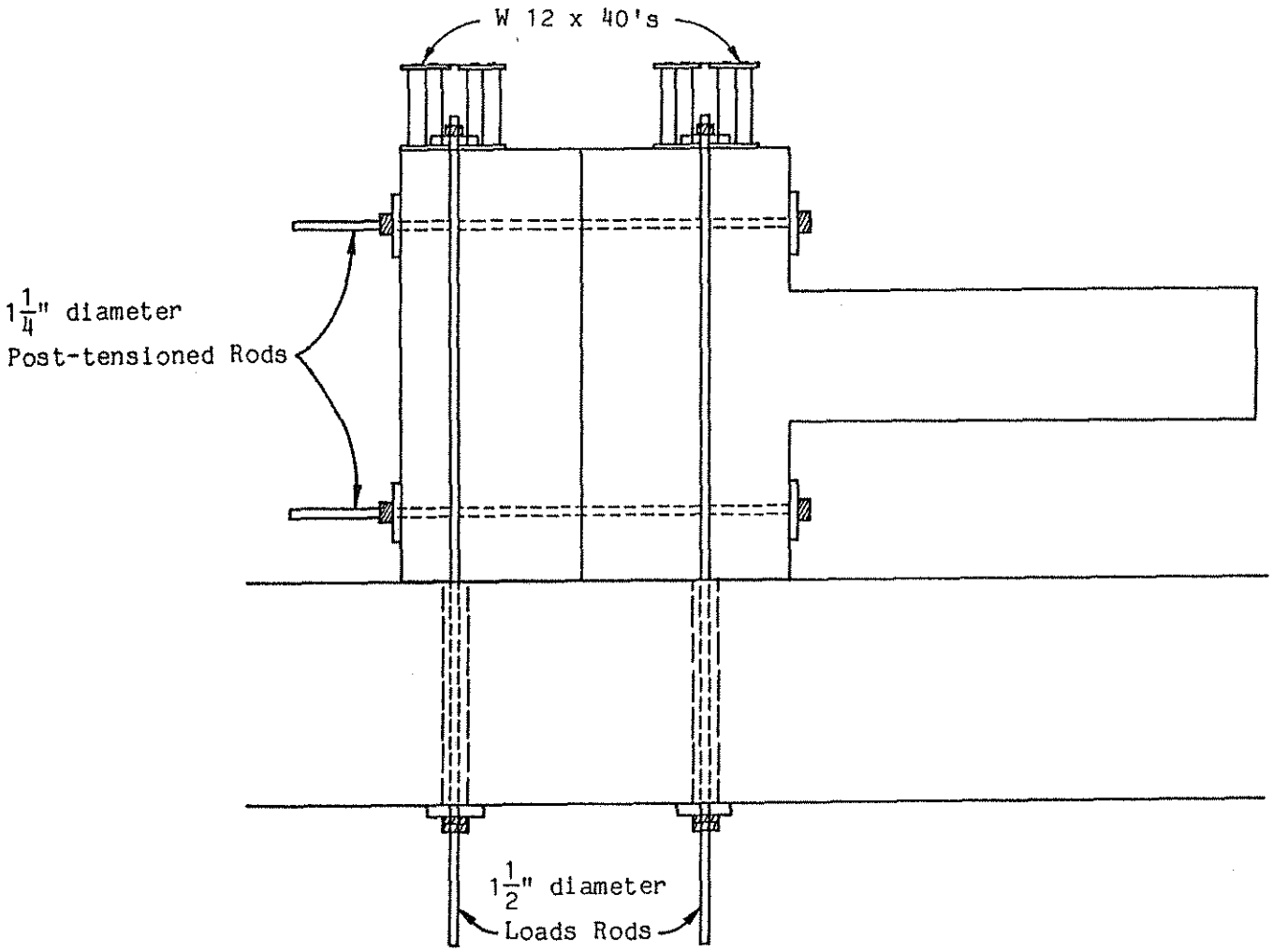

Fig. 2.4 Beam-Column Subassembly (Nmai & Darwin 1984)

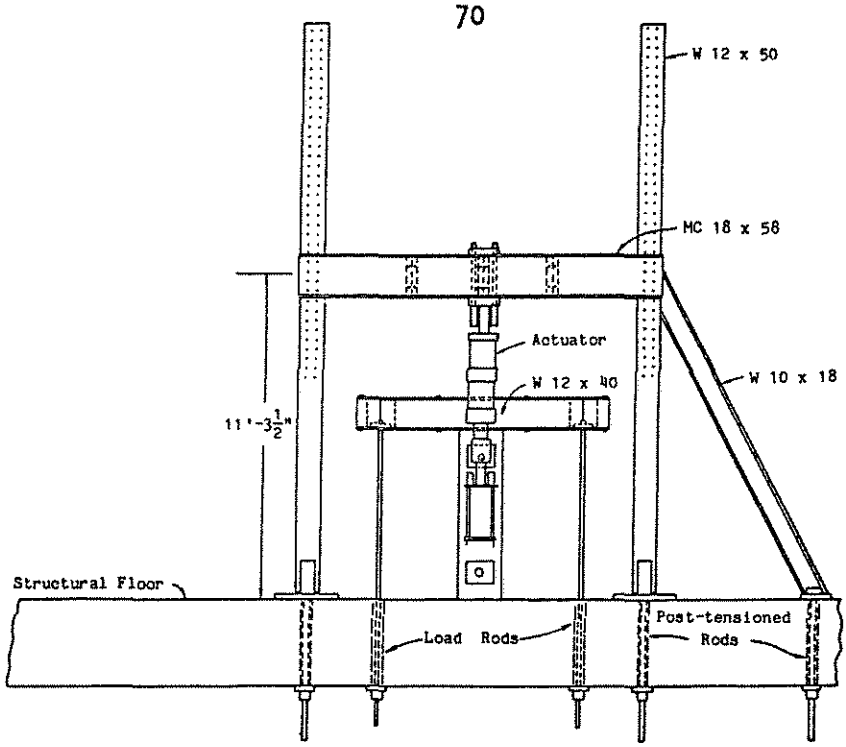

Fig. 2.5(a) Specimen in Test Position, End View (Nmai & Darwin 1984)

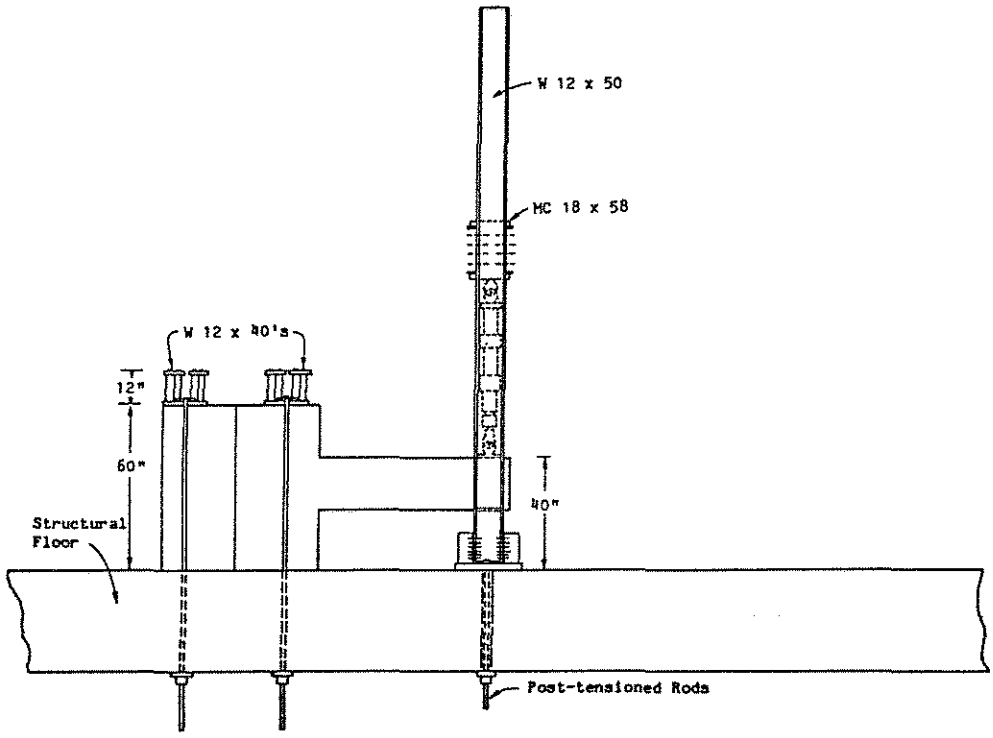

Fig. 2.5(b) Specimen in Test Position, Side View (Nmai & Darwin 1984)

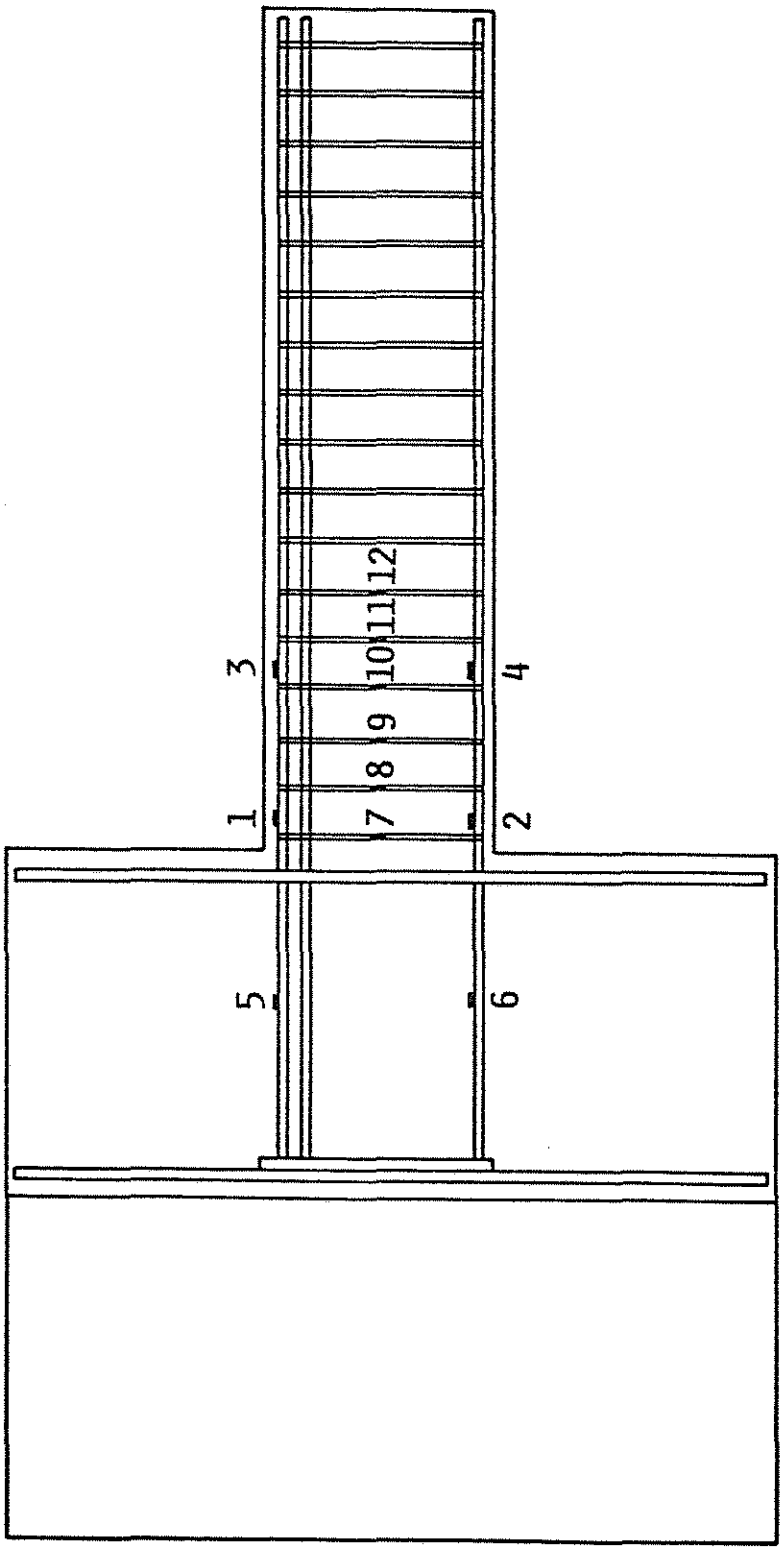

Fig. 2.6 Location of Strain Gages (Nmai & Darwin 1984)

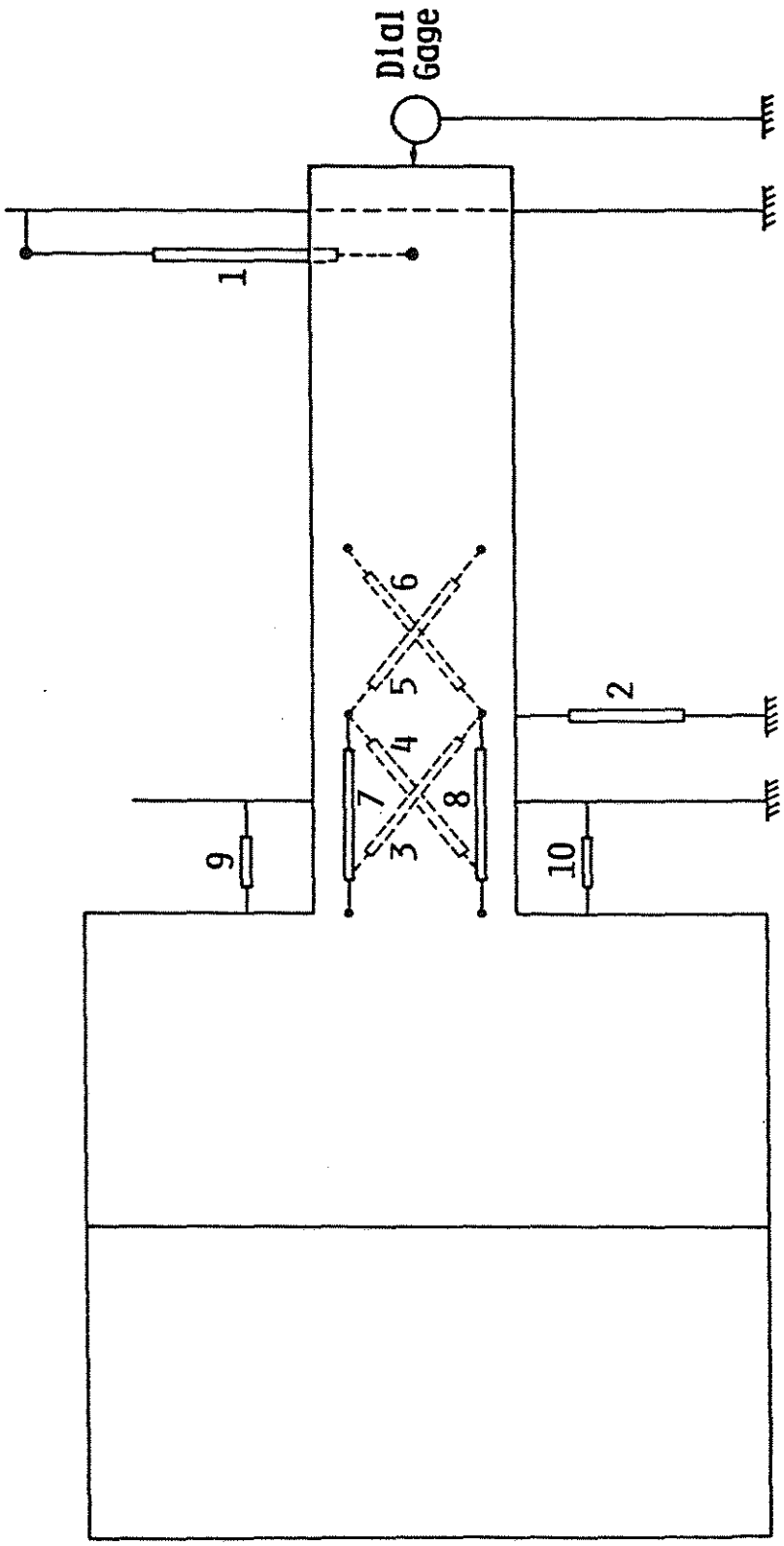

Fig. 2.7 Location of LVDT'S and Dial Gage (Nmai & Darwin 1984)

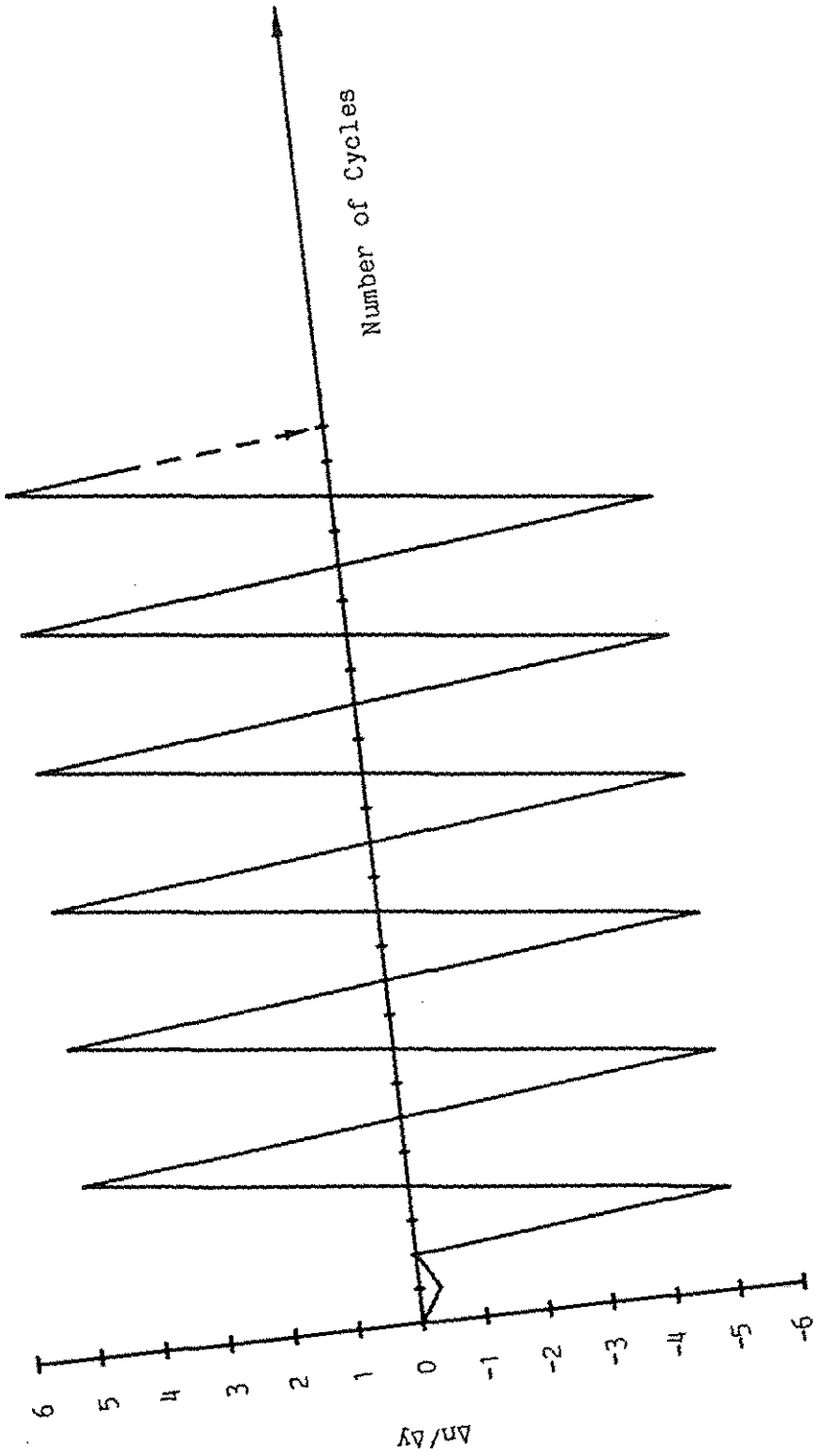

Fig. 2.8 Loading Schedule

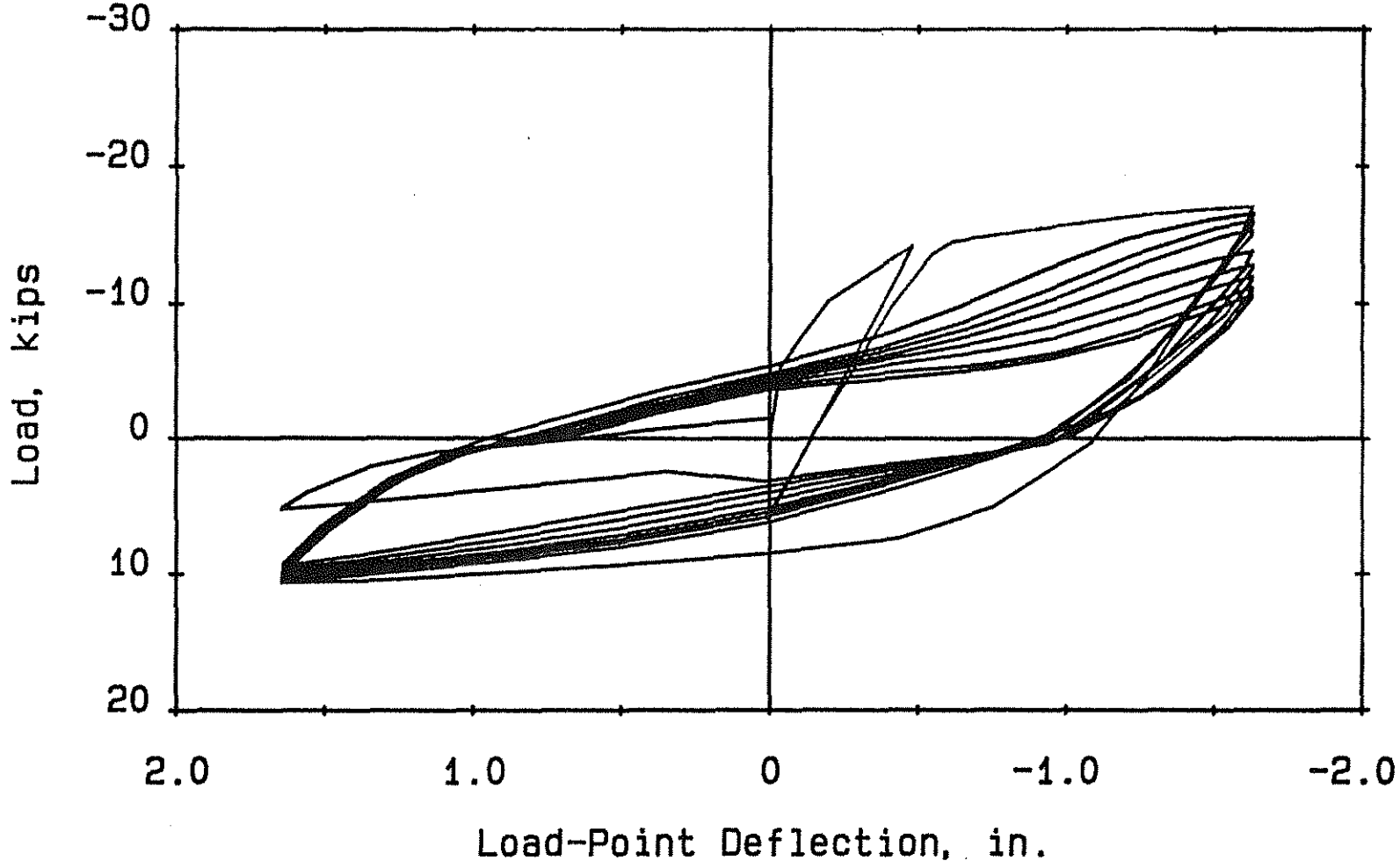

Fig. 2.9(a) Load-Deflection Curve, Beam G-1

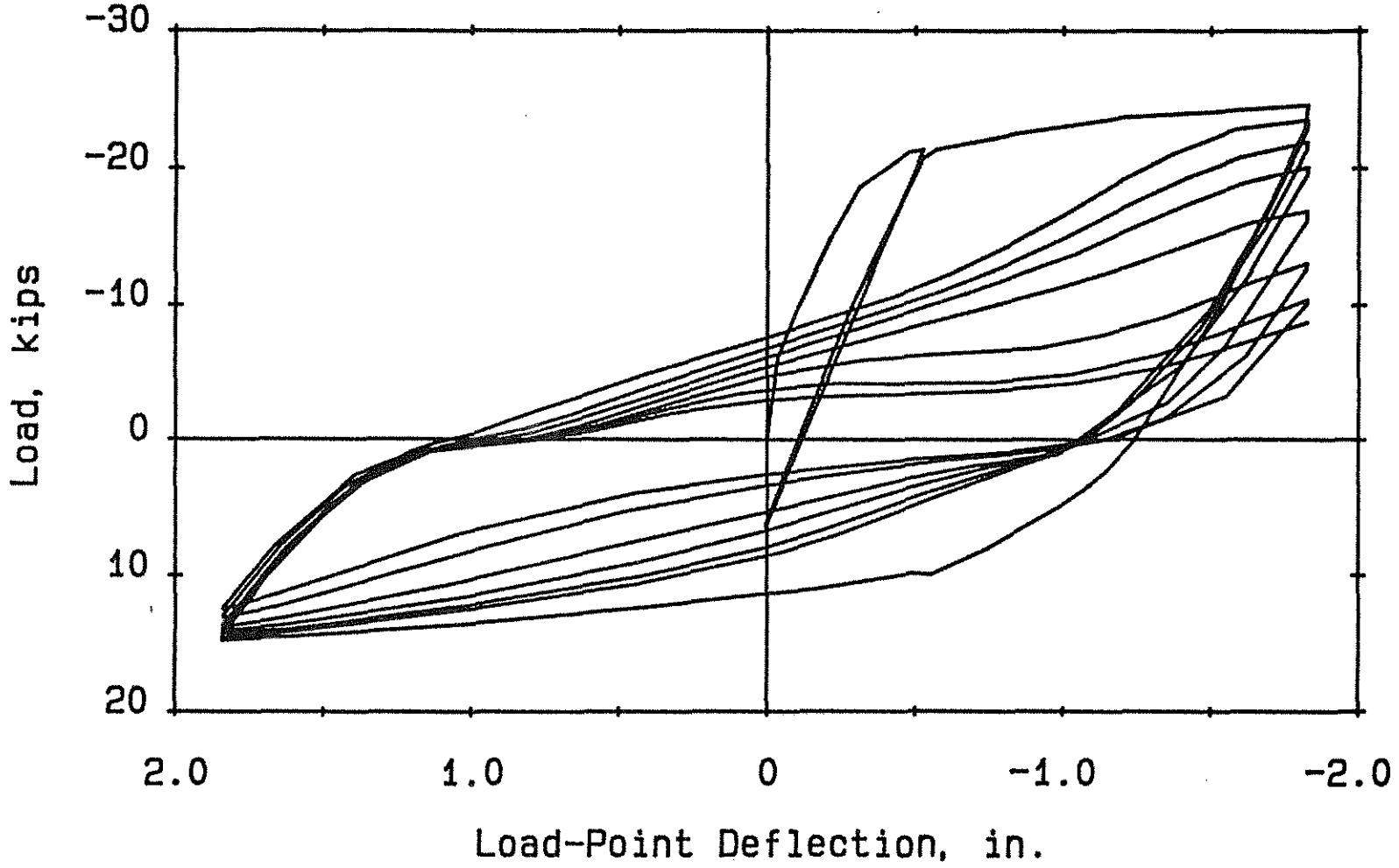

Fig. 2.9(b) Load-Deflection Curve, Beam G-2

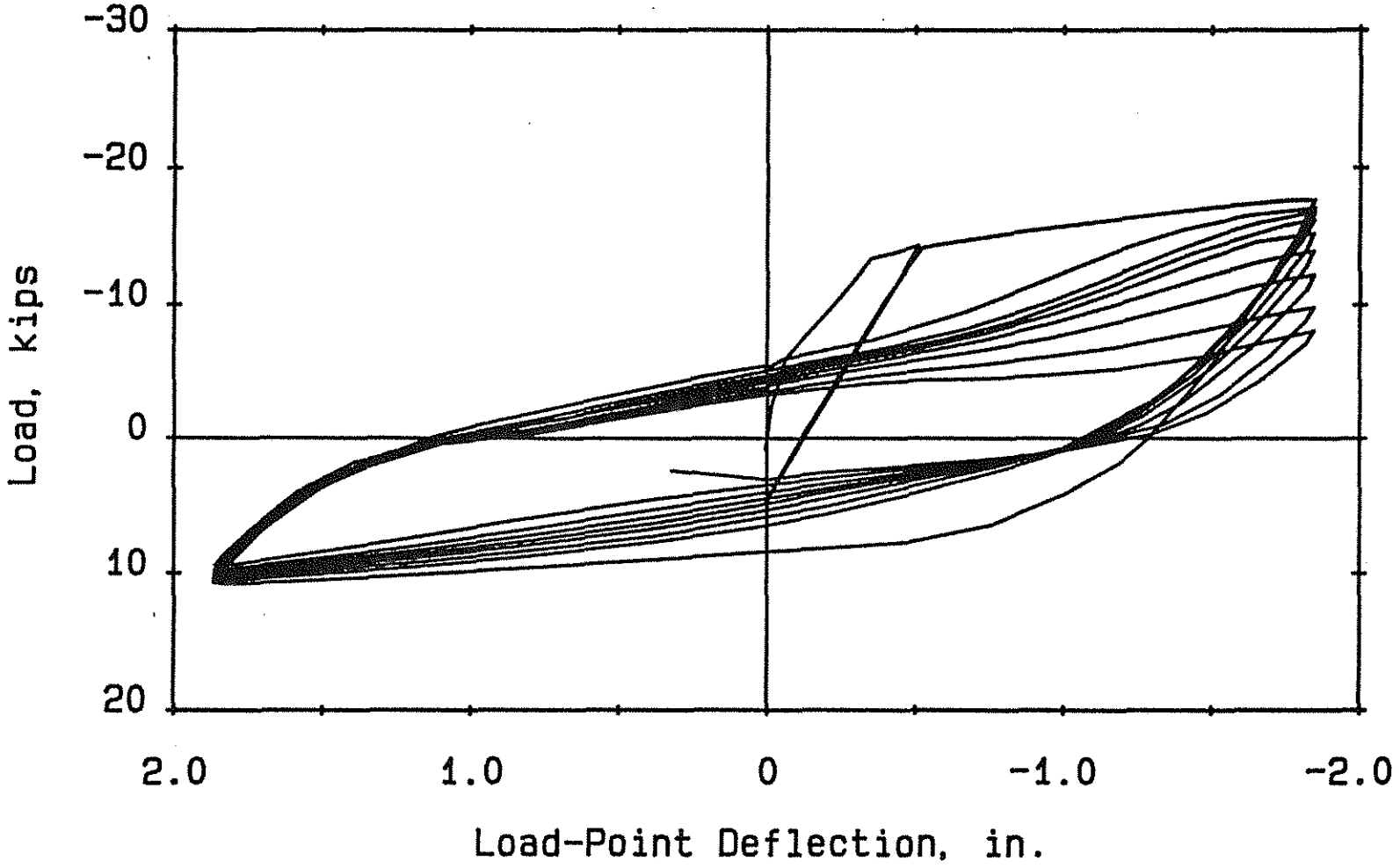

Fig. 2.9(c) Load-Deflection Curve, Beam G-3

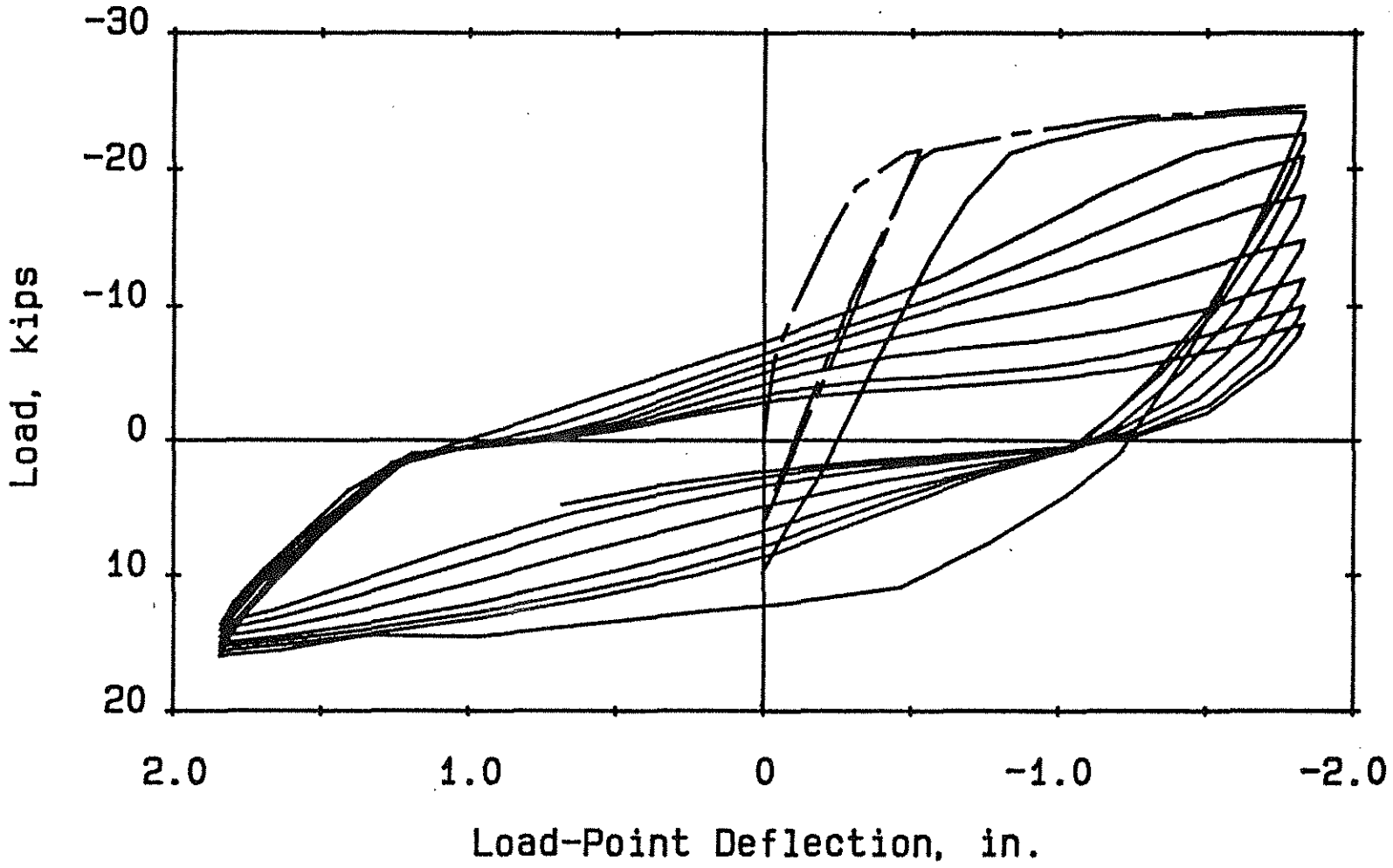

Fig. 2.9(d) Load-Deflection Curve, Beam G-4

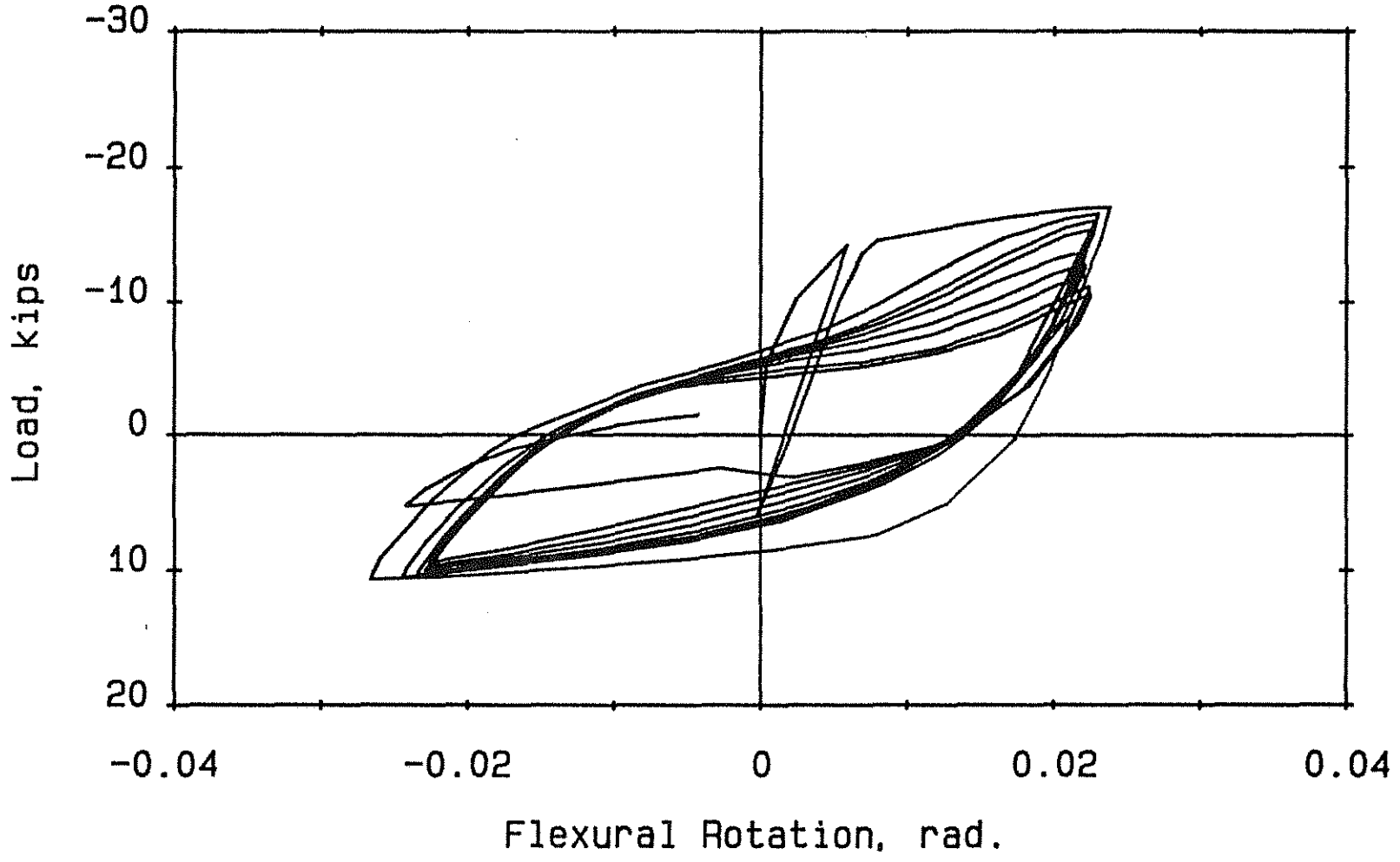

Fig. 2.10(a) Load versus Hinging Zone Flexural Rotation, Beam G-1

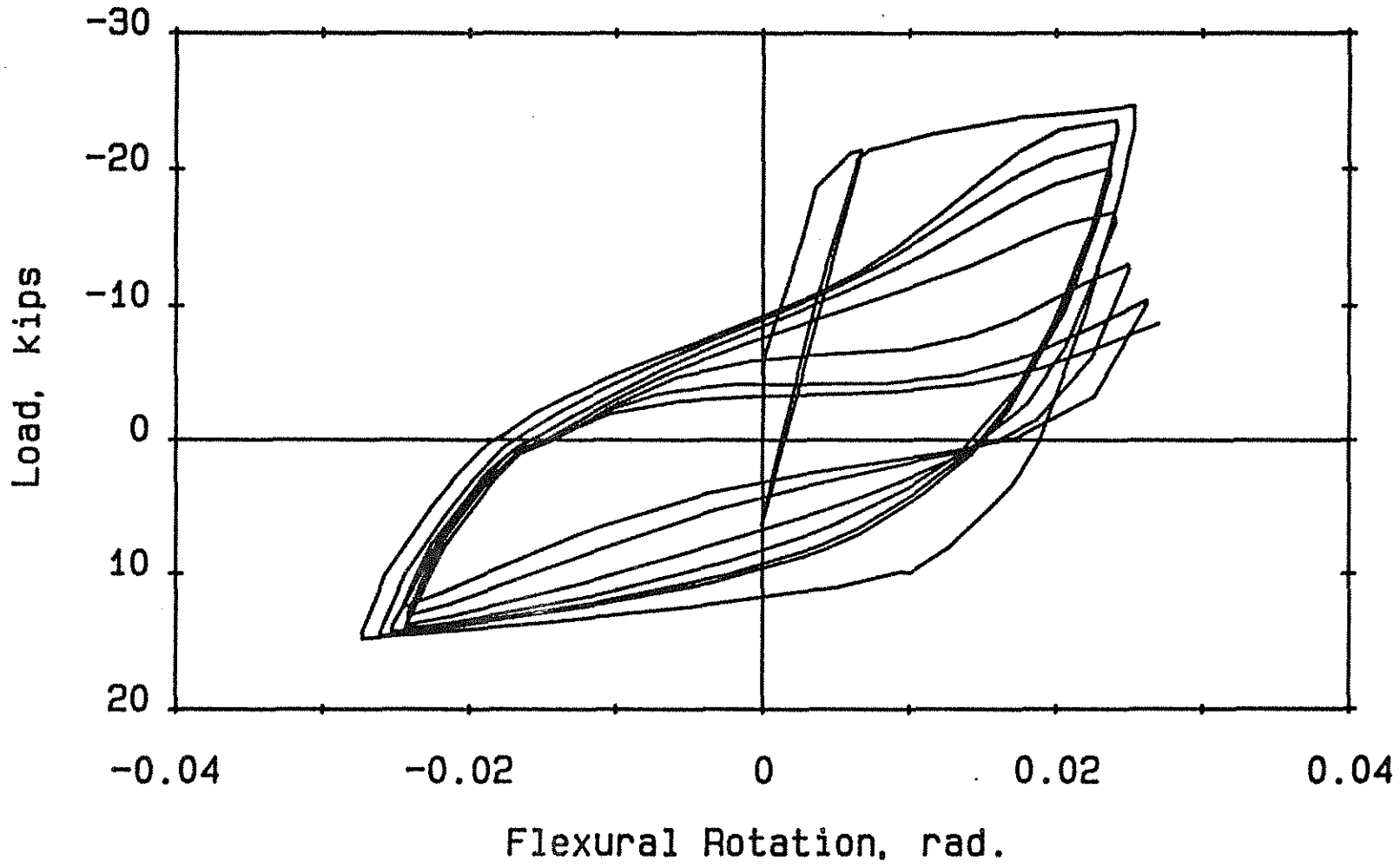

Fig. 2.10(b) Load versus Hinging Zone Flexural Rotation, Beam G-2

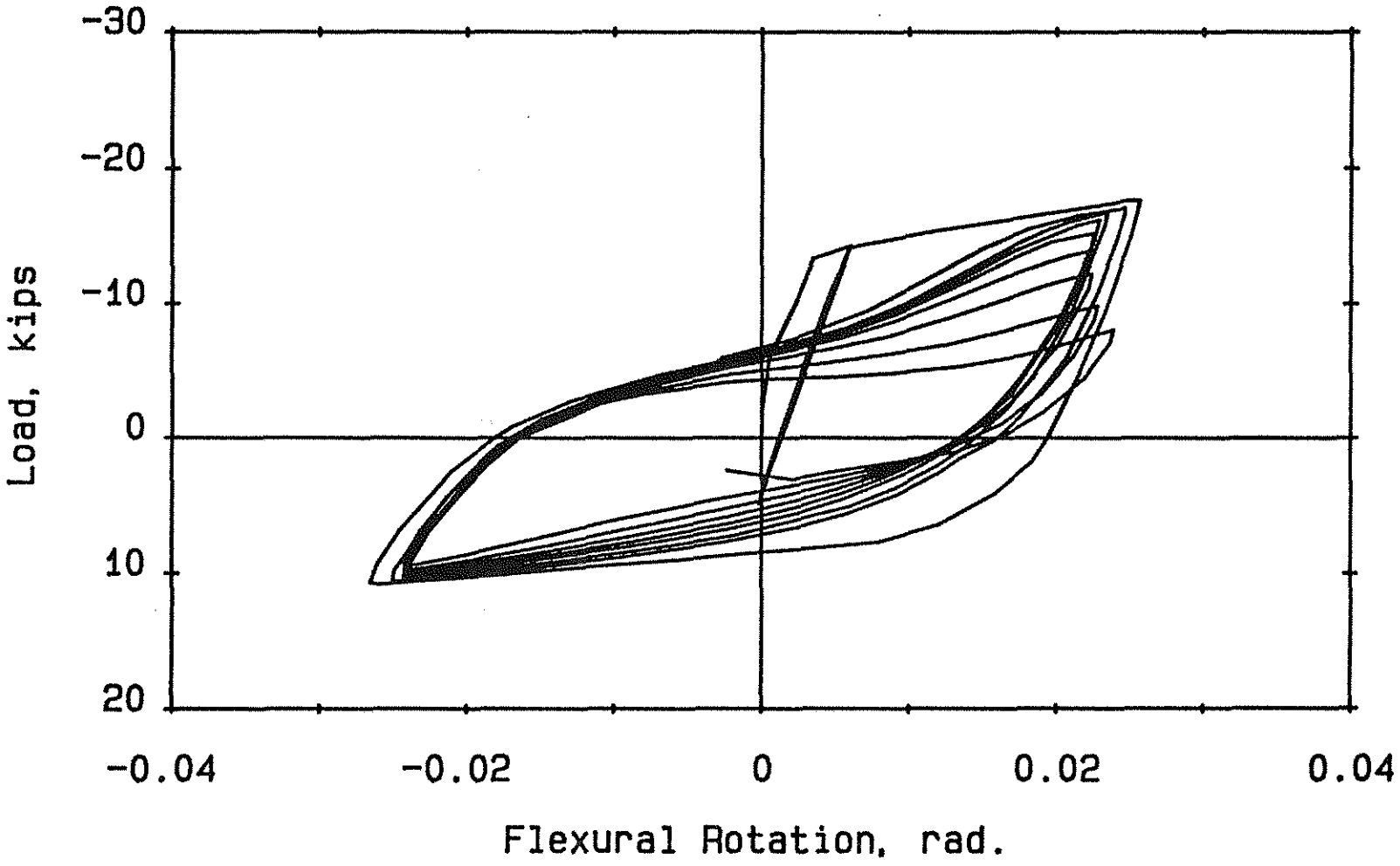

Fig. 2.10(c) Load versus Hinging Zone Flexural Rotation, Beam G-3

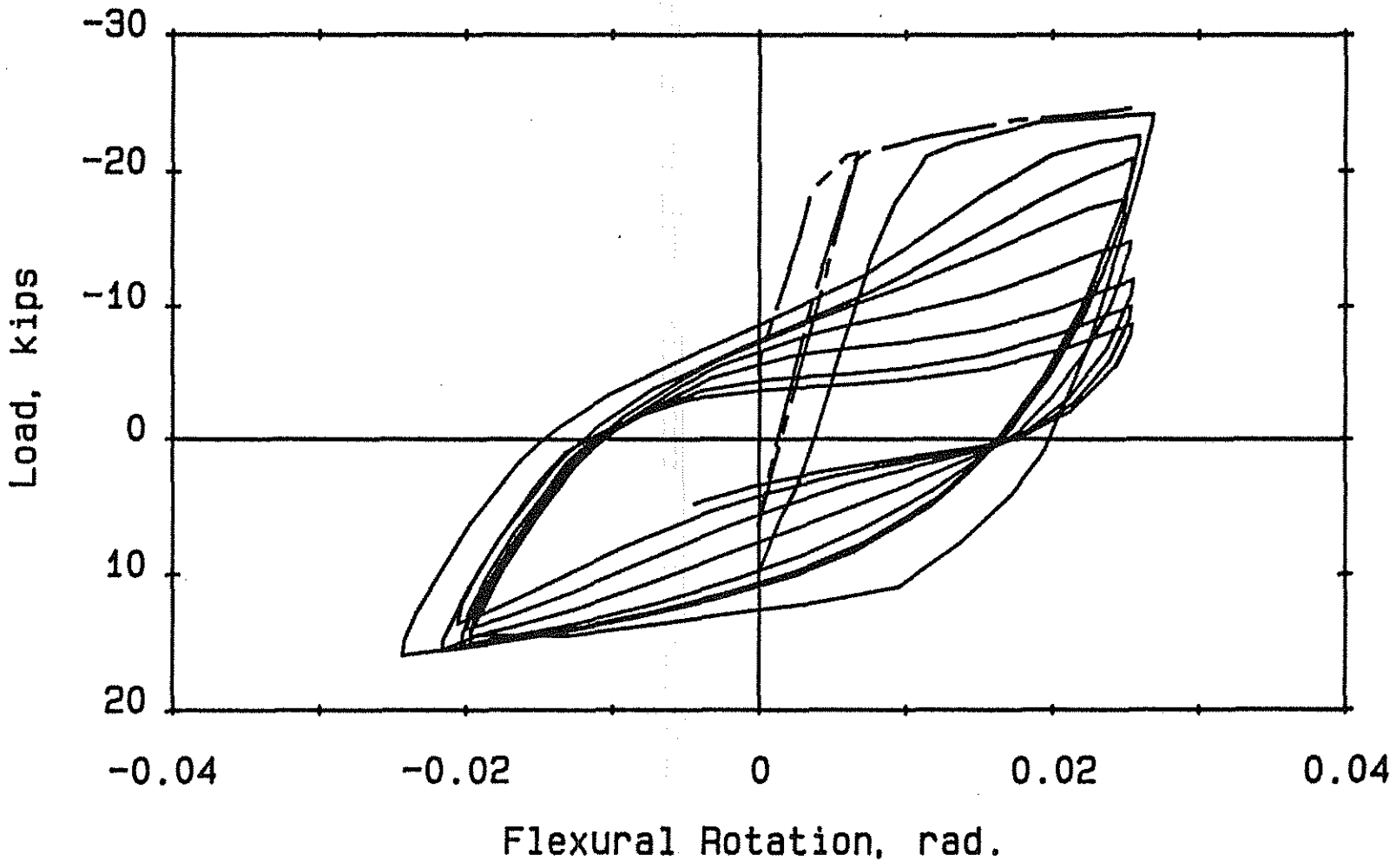

Fig. 2.10(d) Load versus Hinging Zone Flexural Rotation, Beam G-4

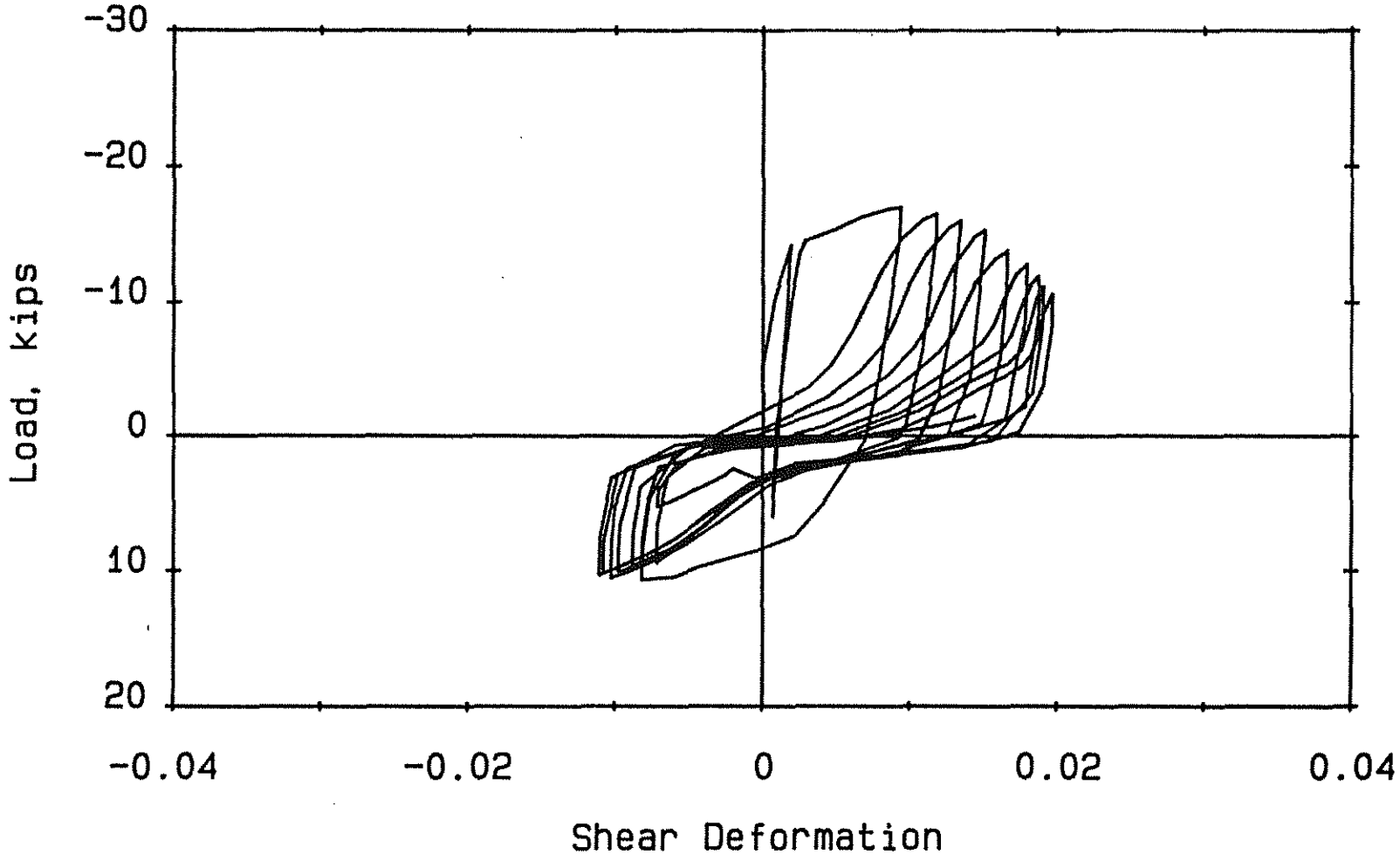

Fig. 2.11(a) Load versus Hinging Zone Shear Deformation, Beam G-1

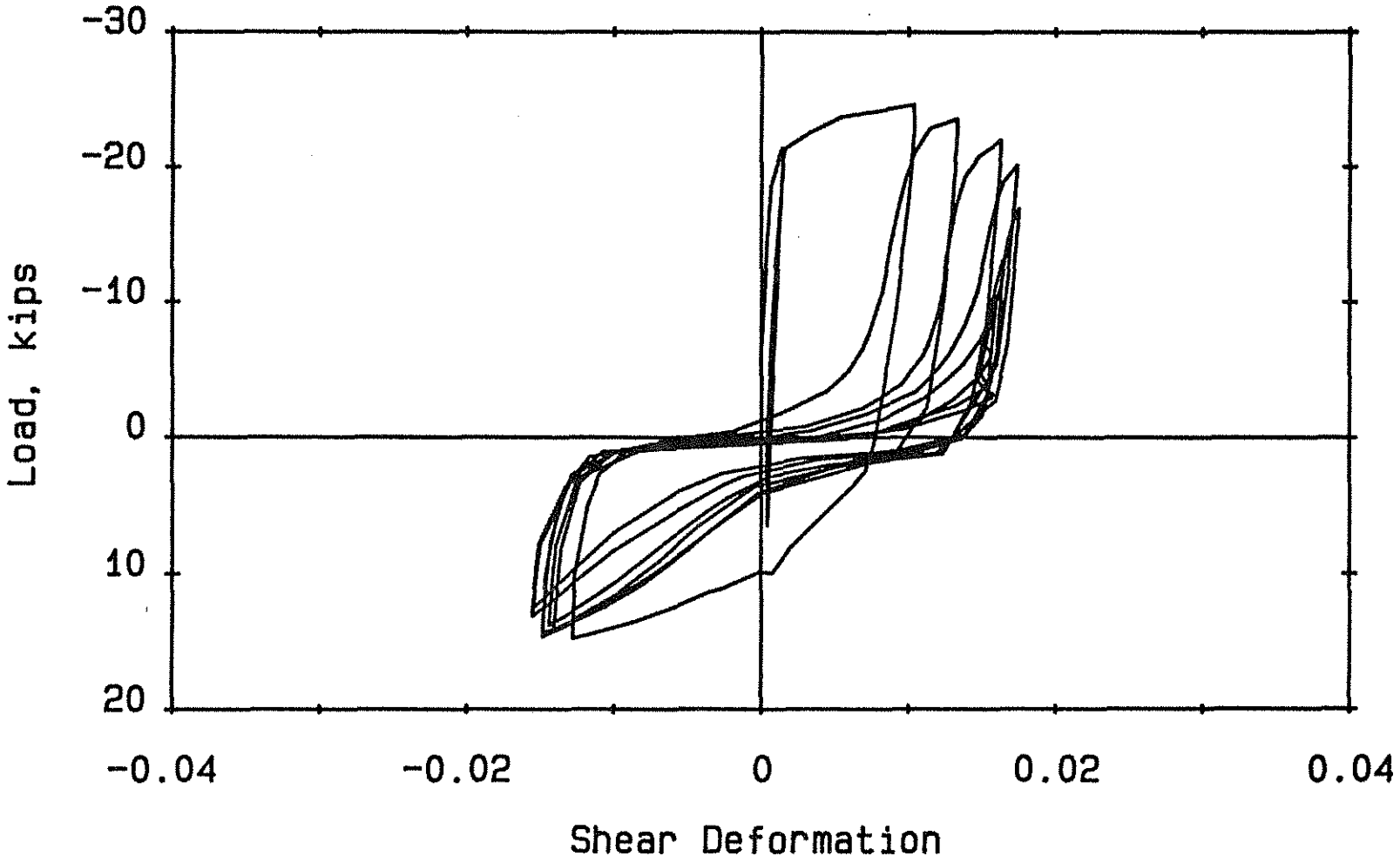

Fig. 2.11(b) Load versus Hinging Zone Shear Deformation, Beam G-2

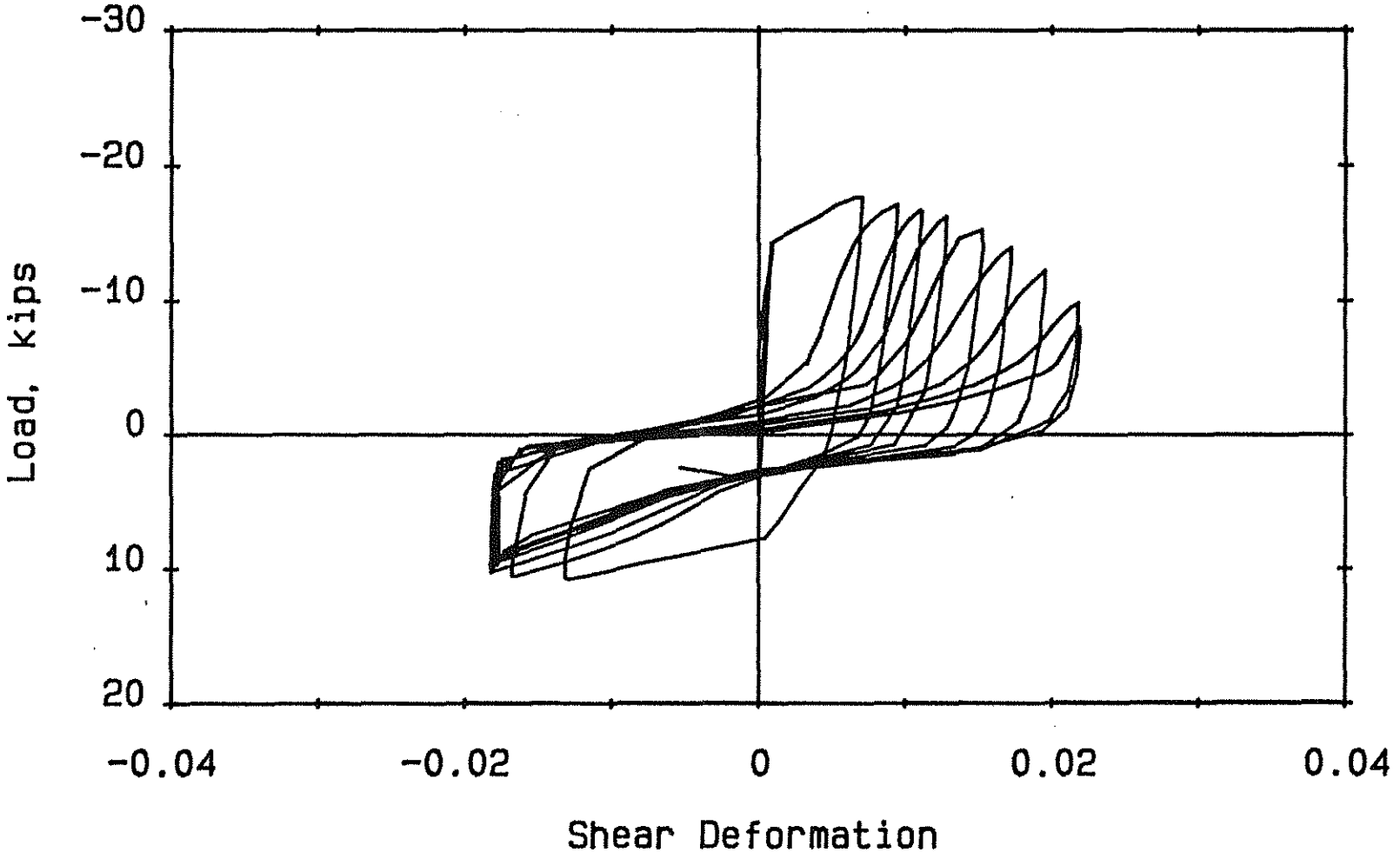

Fig. 2.11(c) Load versus Hinging Zone Shear Deformation, Beam G-3

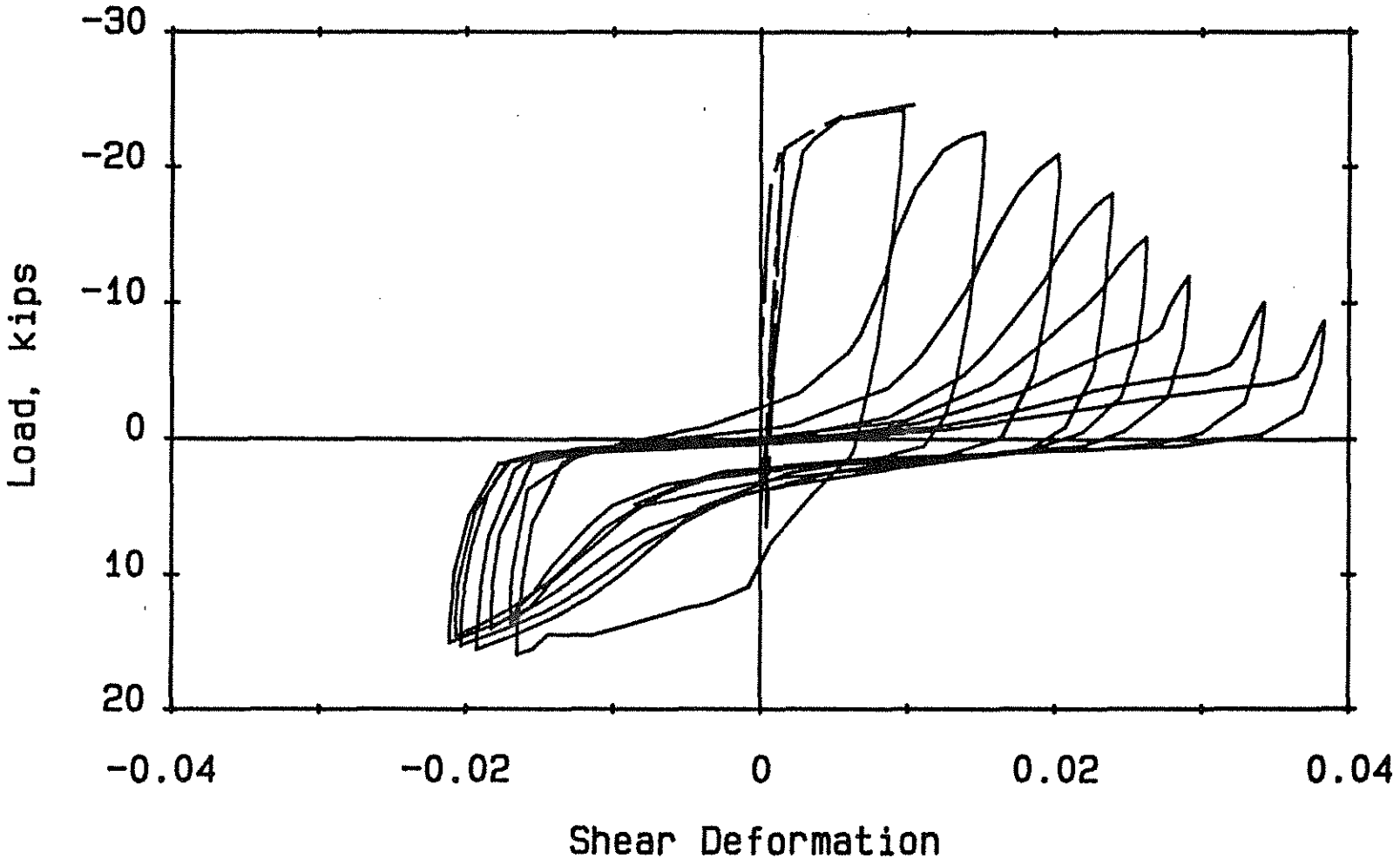

Fig. 2.11(d) Load versus Hinging Zone Shear Deformation, Beam G-4

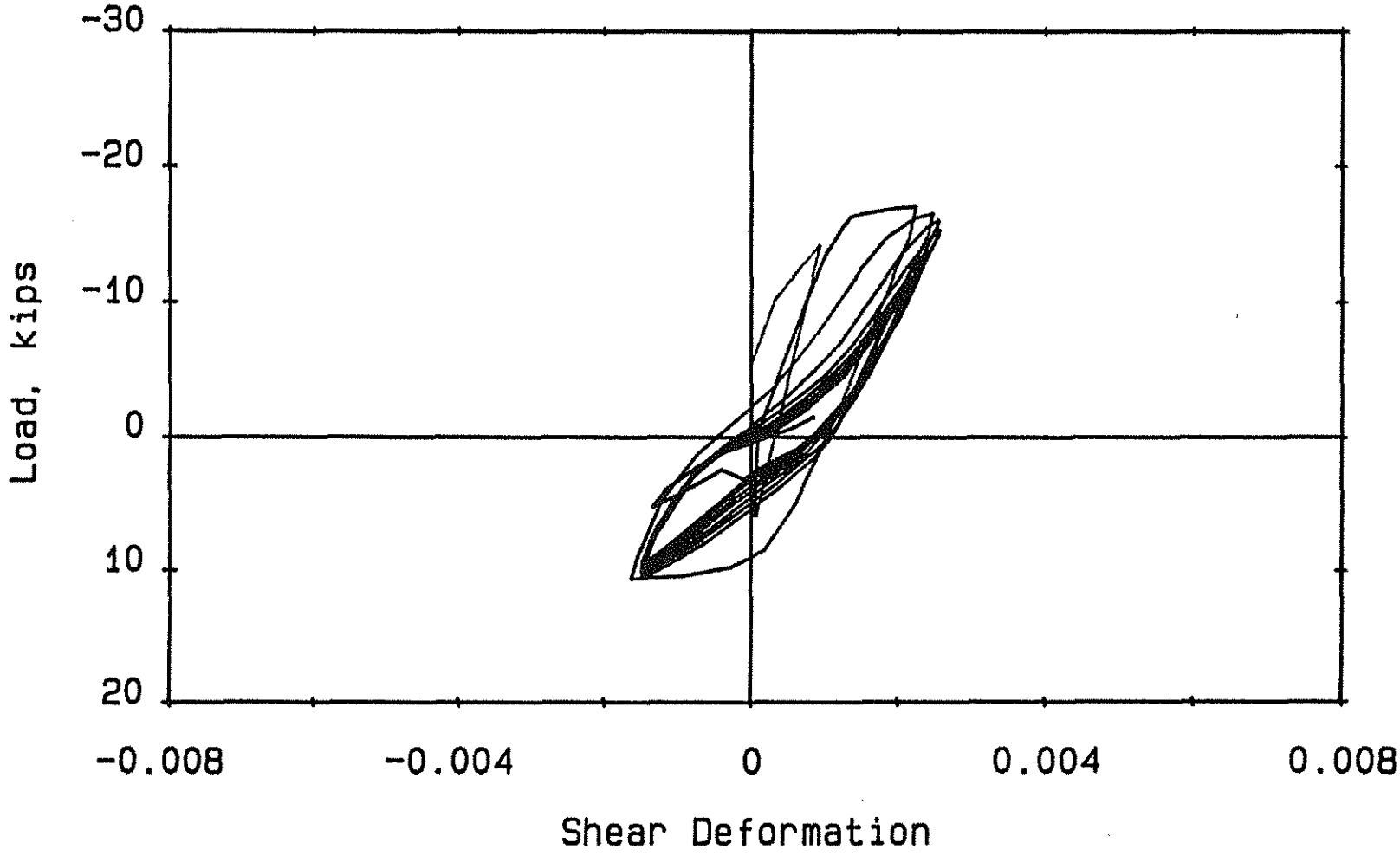

Fig. 2.12(a) Load versus Shear Deformation over Region Extending d to 2d from Column Face, Beam G-1

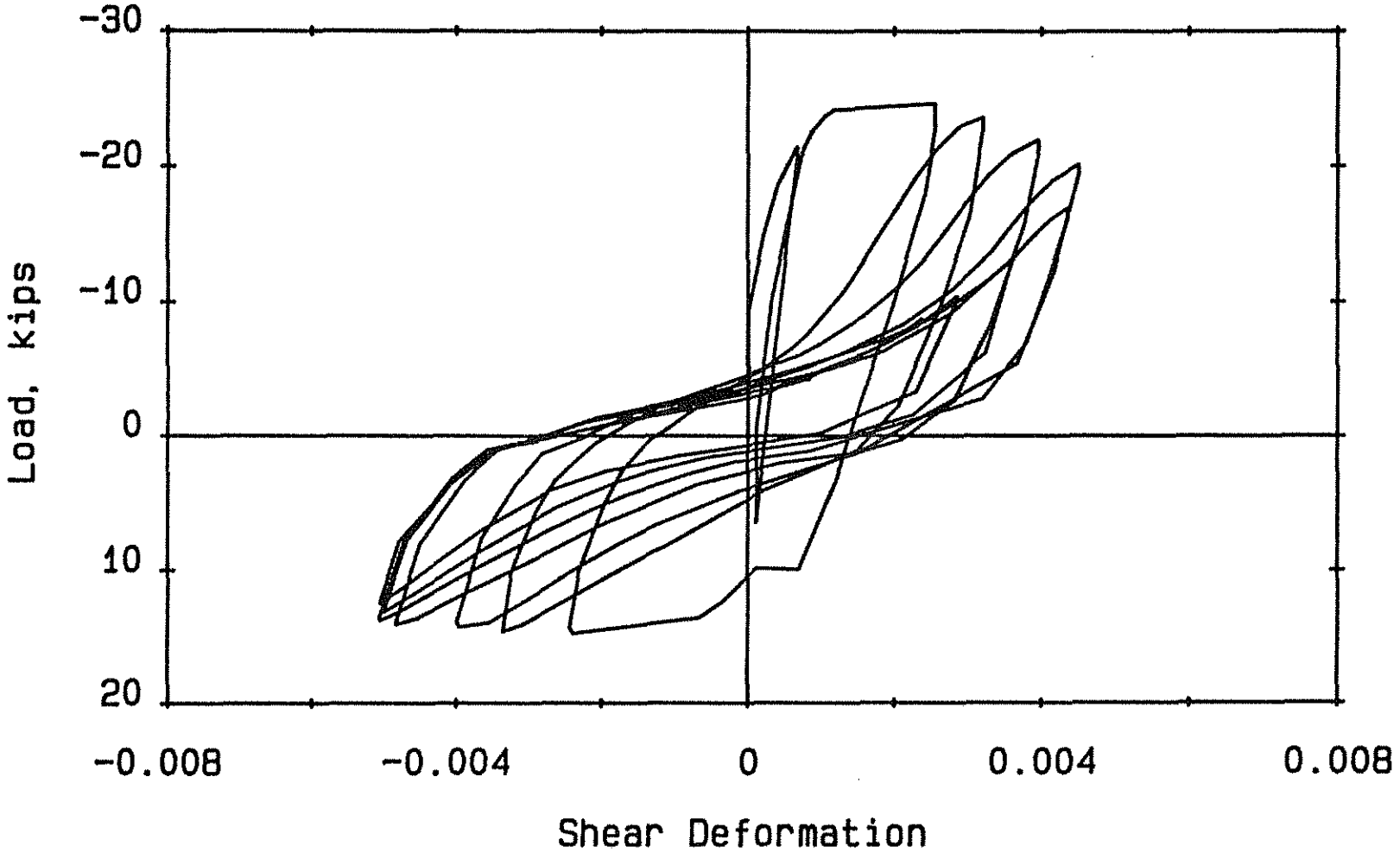

Fig. 2.12(b) Load versus Shear Deformation over Region Extending d to 2d from Column Face, Beam G-2

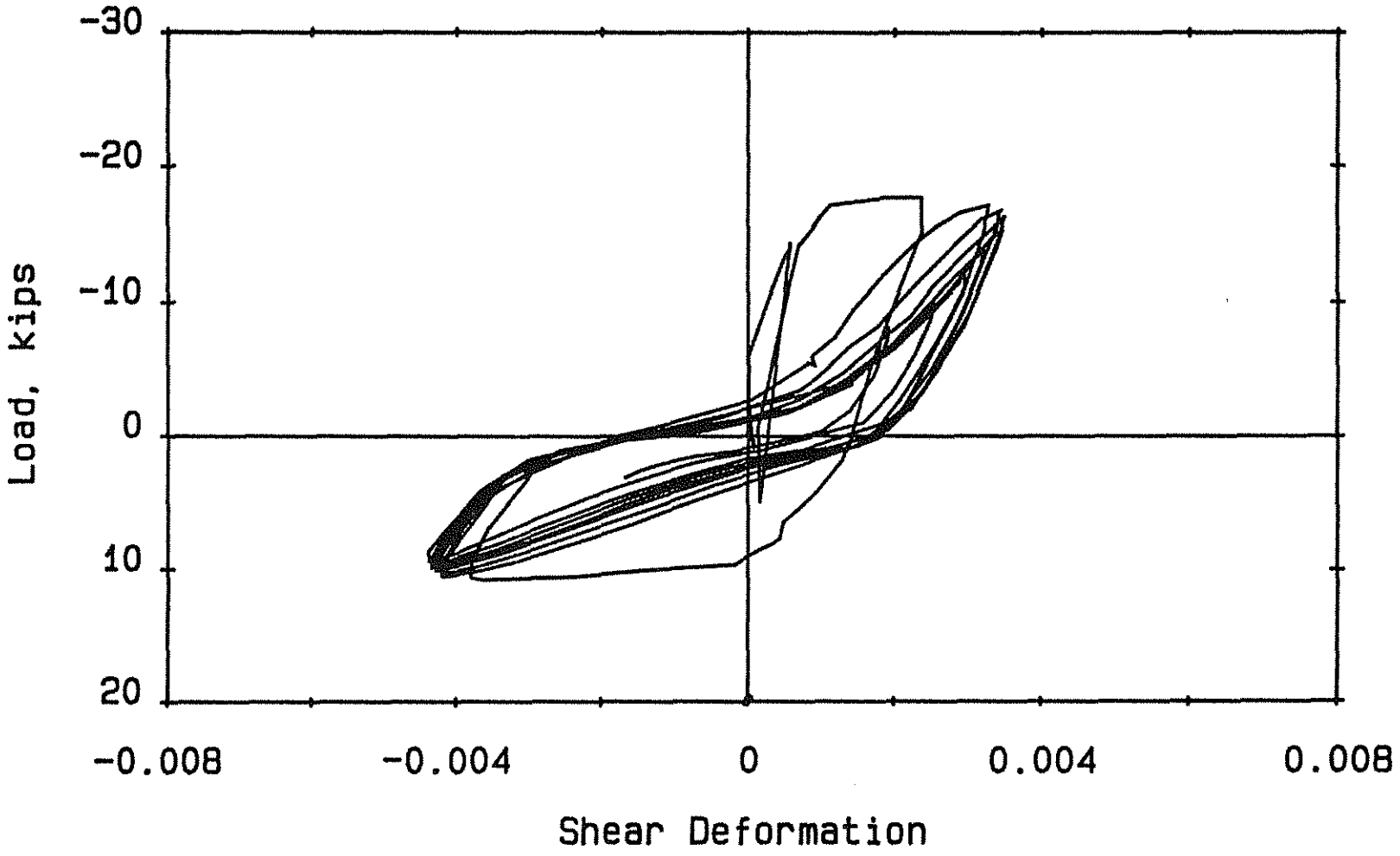

Fig. 2.12(c) Load versus Shear Deformation over Region Extending d to 2d from Column Face, Beam G-3

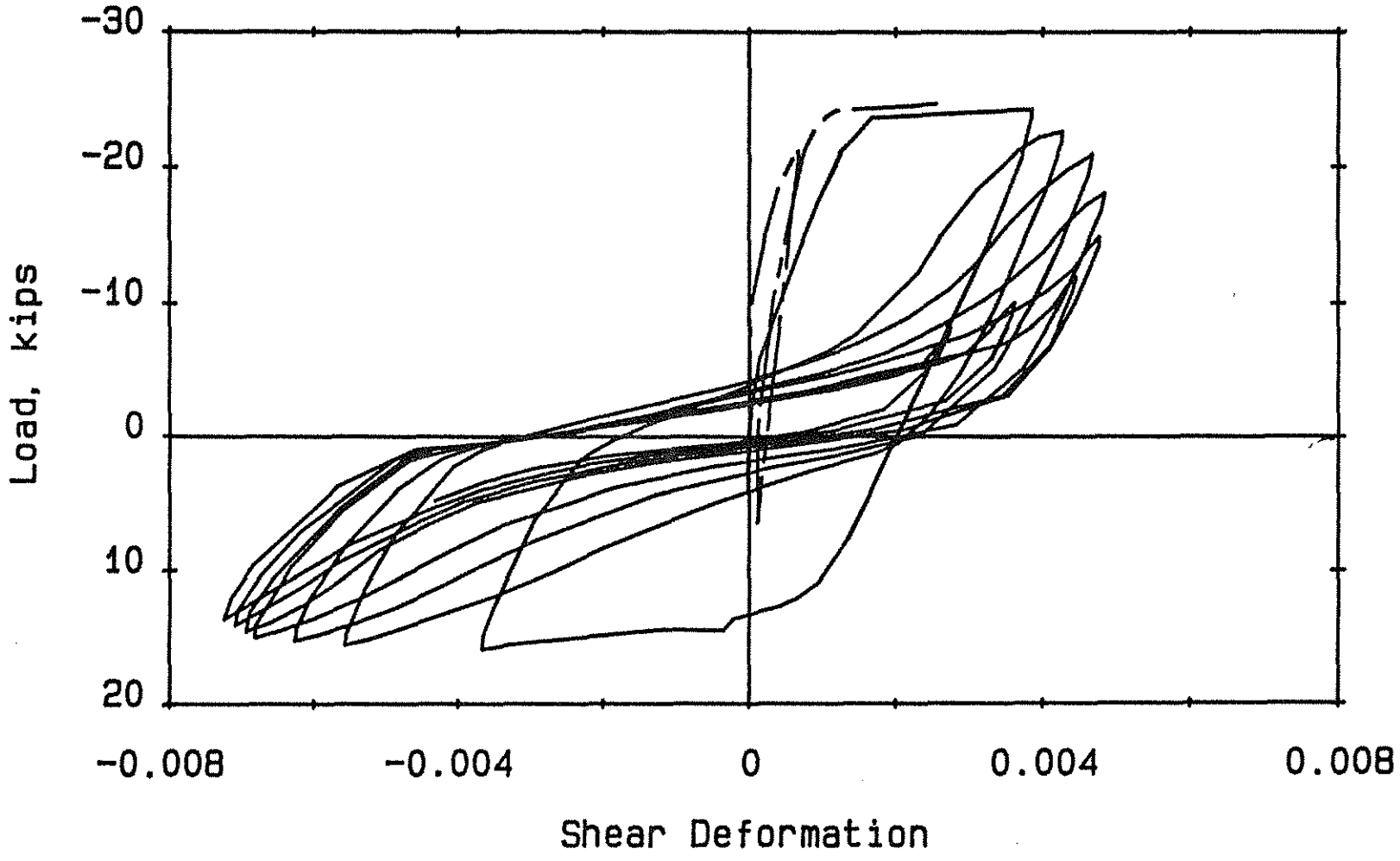

Fig. 2.12(d) Load versus Shear Deformation over Region Extending d to 2d from Column Face, Beam G-4

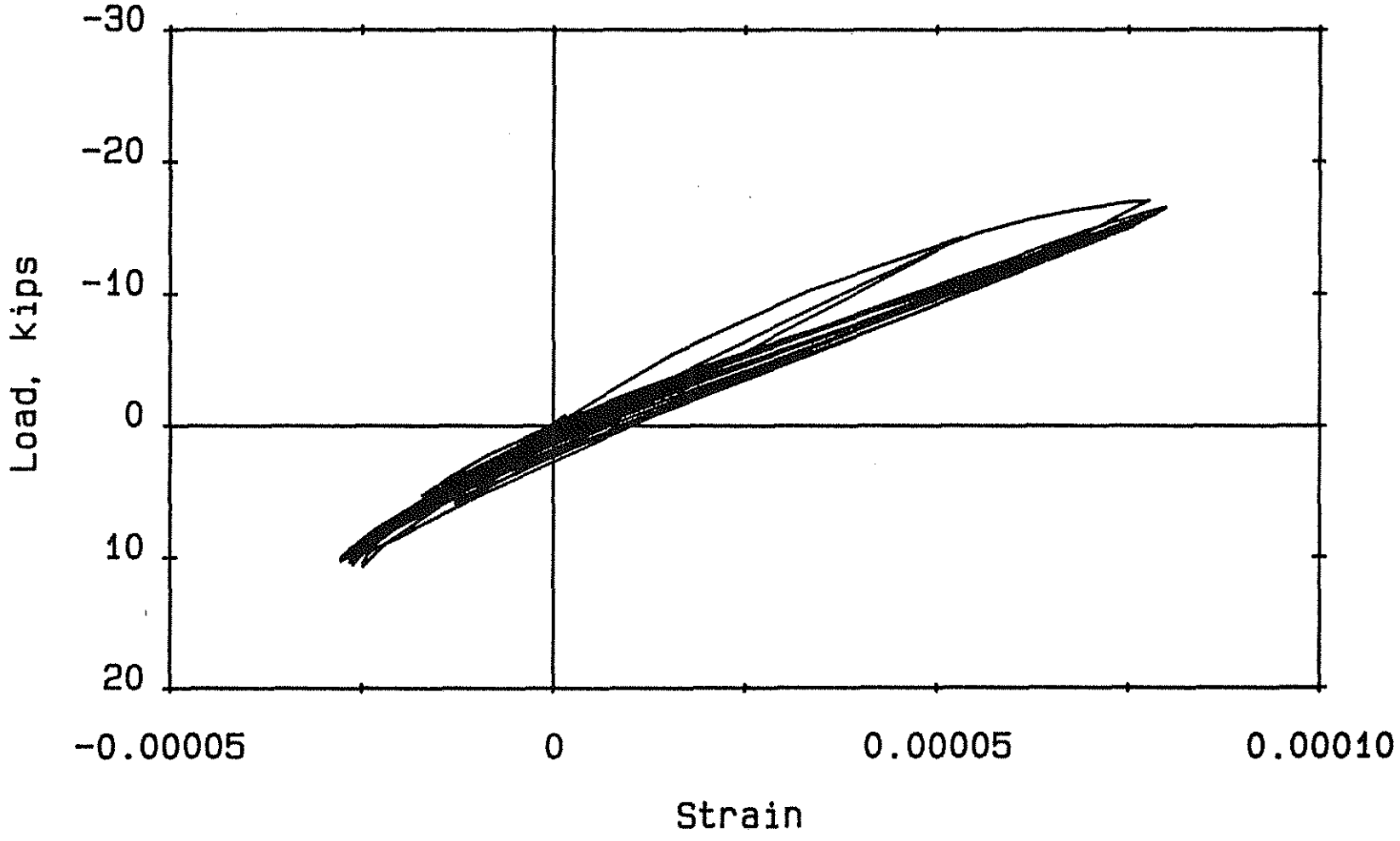

Fig. 2.13(a) Load versus Strain, Beam G-1 Gage #5

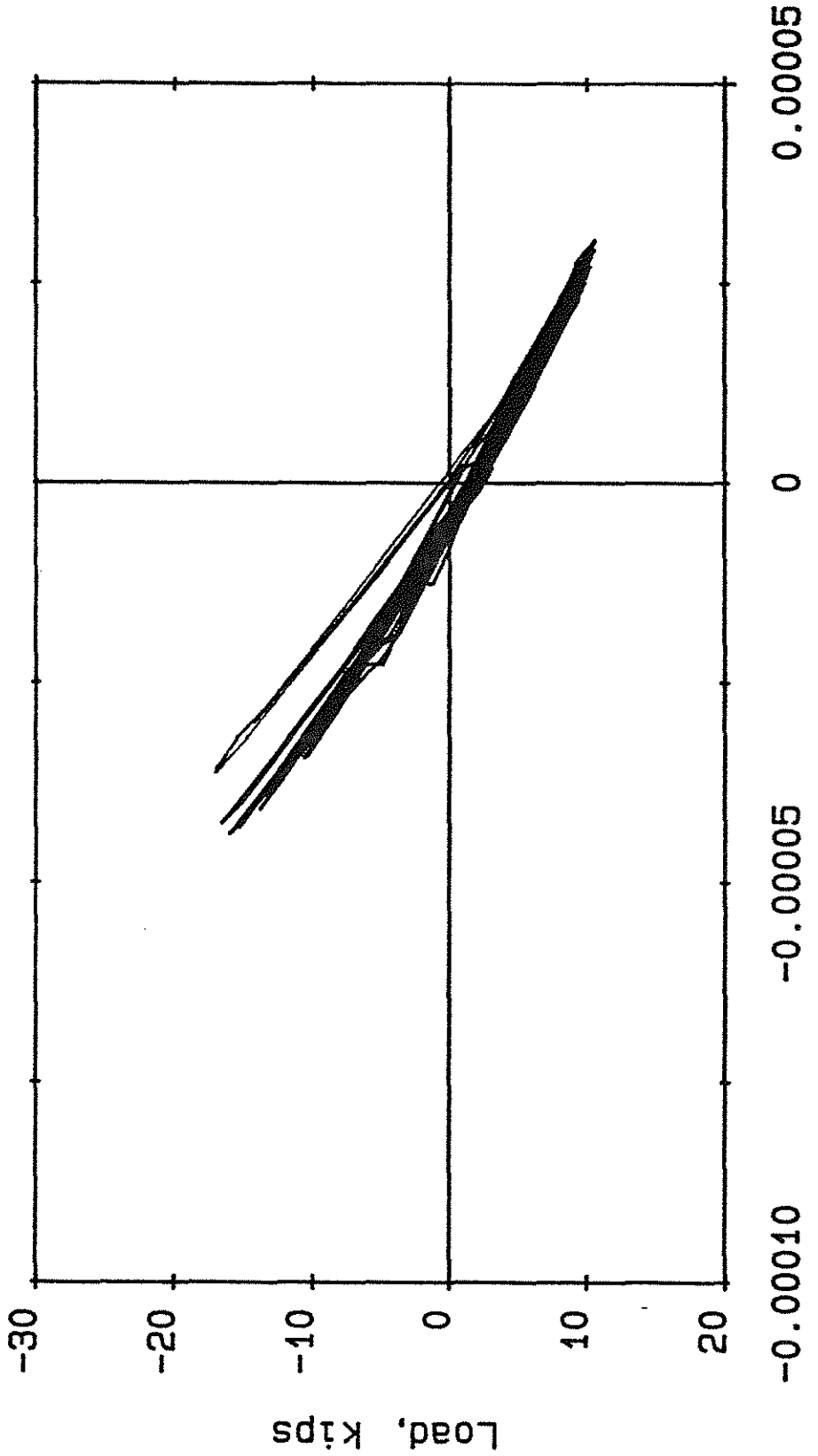

Fig. 2.13(b) Load versus Strain, Beam G-1 Gage #6

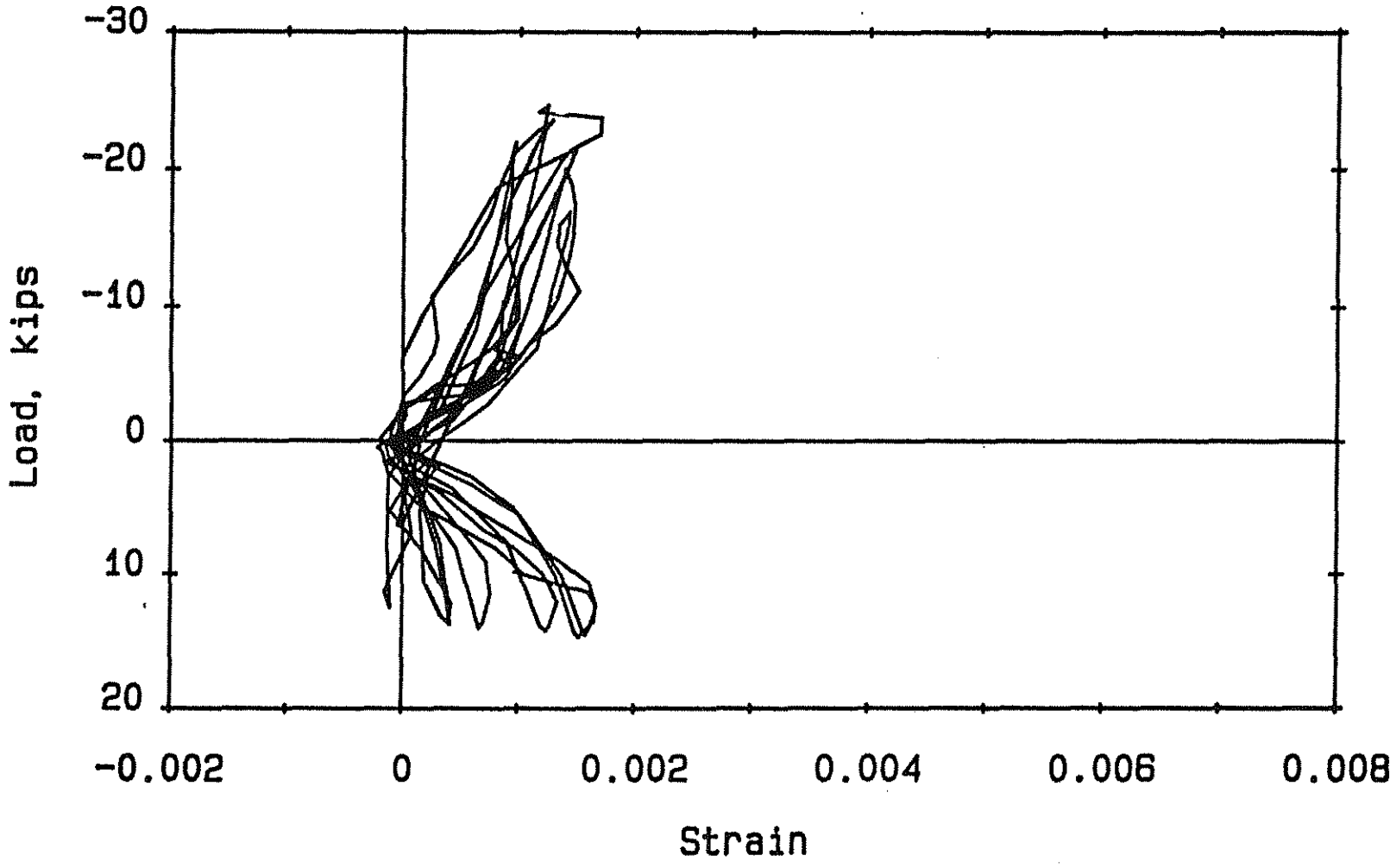

Fig. 2.14(a) Load versus Strain, Beam G-2 Gage #8

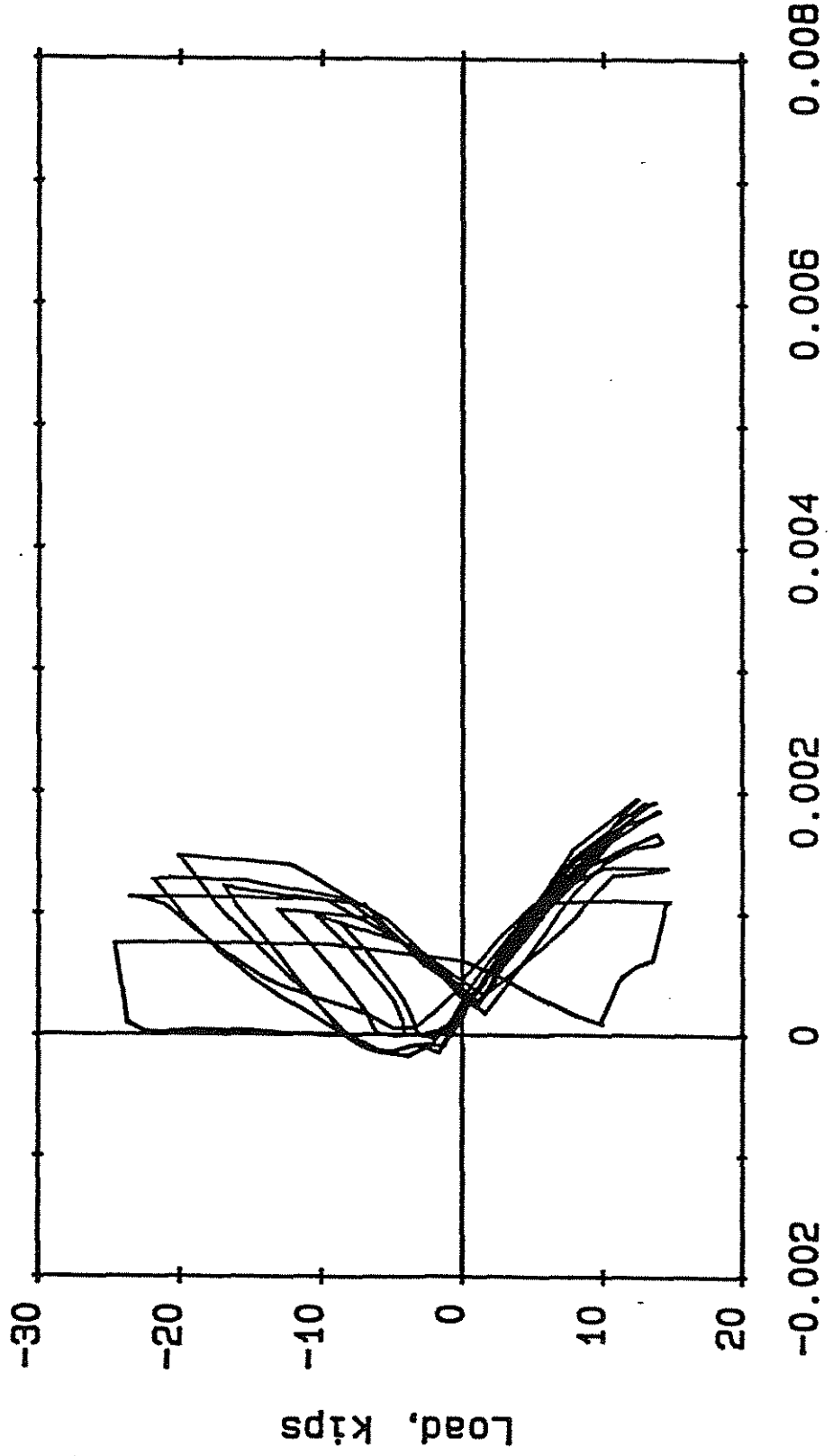

Fig. 2.14(b) Load versus Strain, Beam G-2 Gage #12

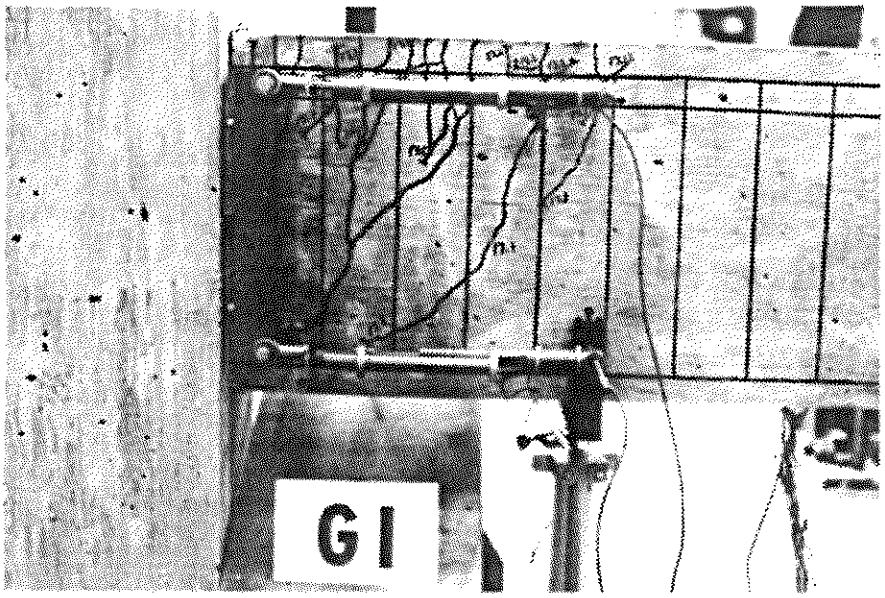

Fig. 2.15(a) Initial Crack Pattern, Beam G-1

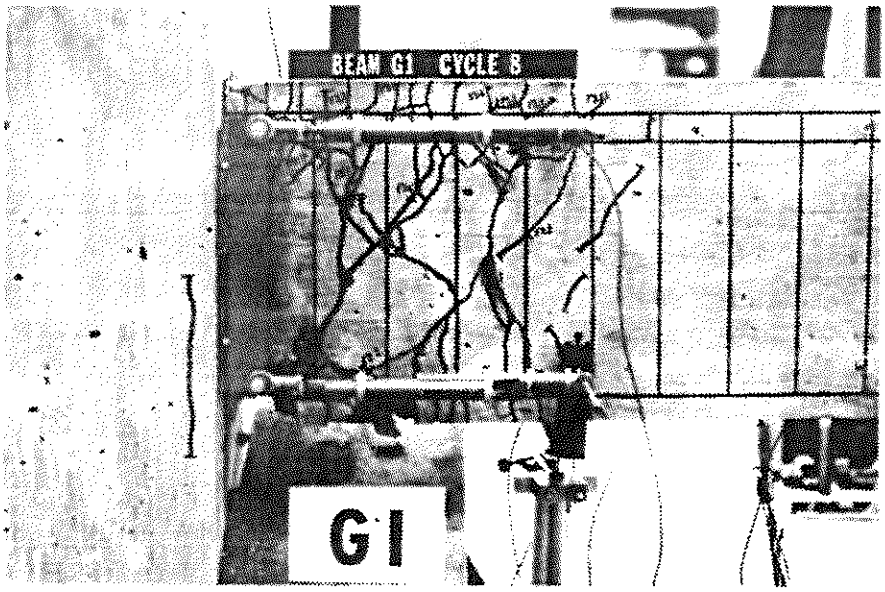

Fig. 2.15(b) Final Crack Pattern, Beam G-1

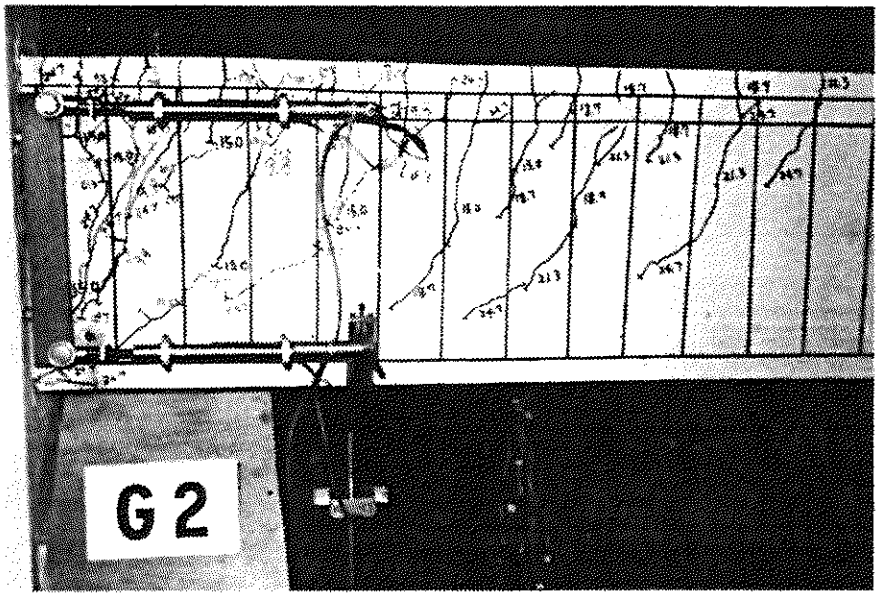

Fig. 2.16(a) Initial Crack Pattern, Beam G-2

Fig. 2.16(b) Buckled Flexural Reinforcement, Beam G-2

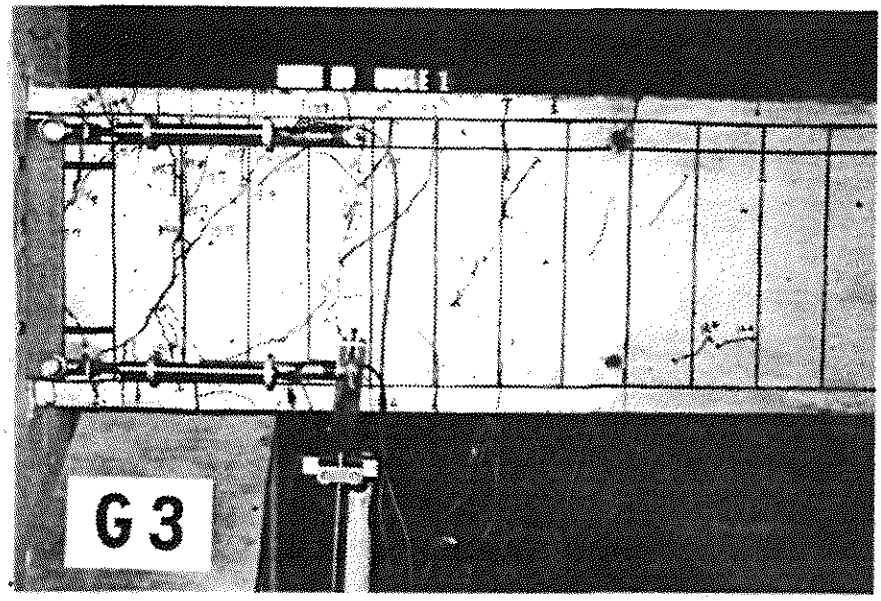

Fig. 2.17(a) Crack Pattern at the End of Cycle 1, Beam G-3

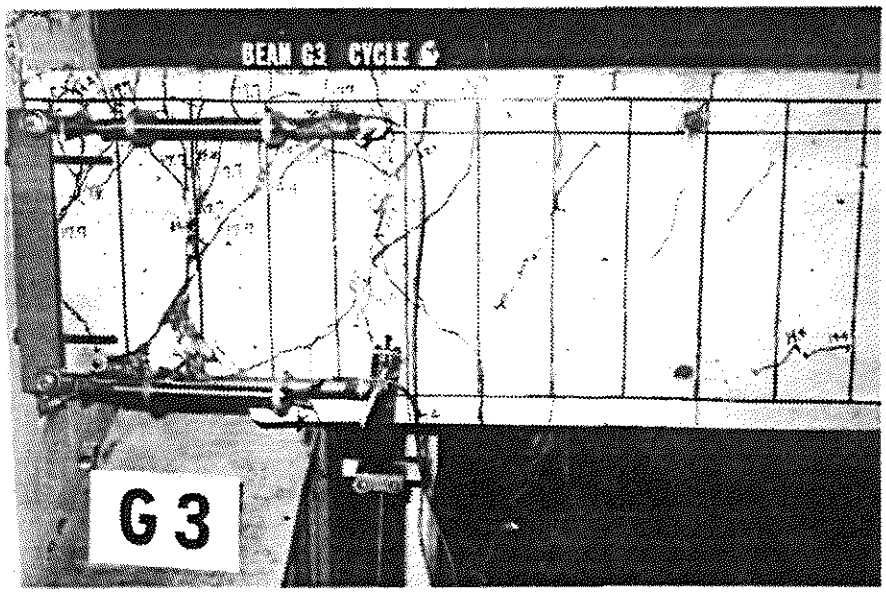

Fig. 2.17(b) Concrete Spalling at the End of Cycle 6, Beam G-3

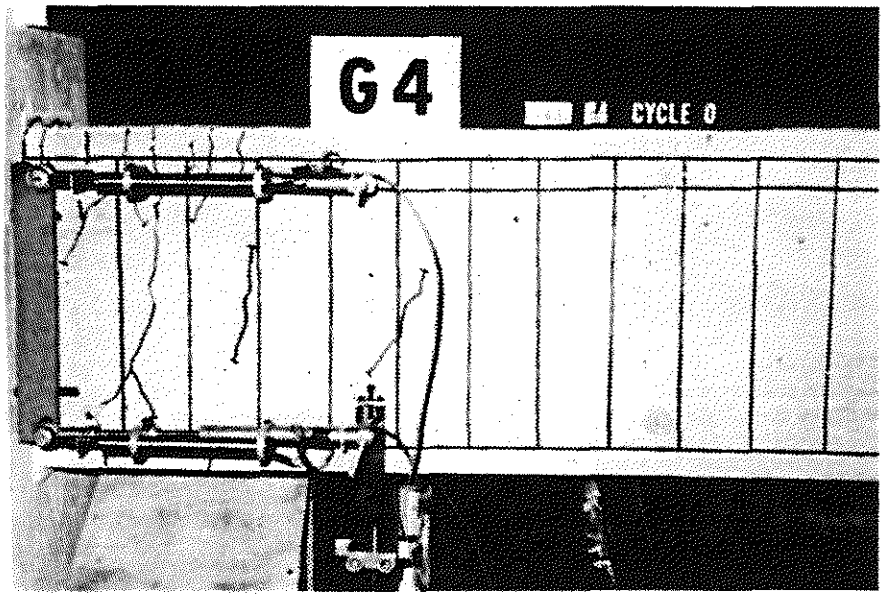

Fig. 2.18(a) Pretest Crack Pattern, Beam G-4

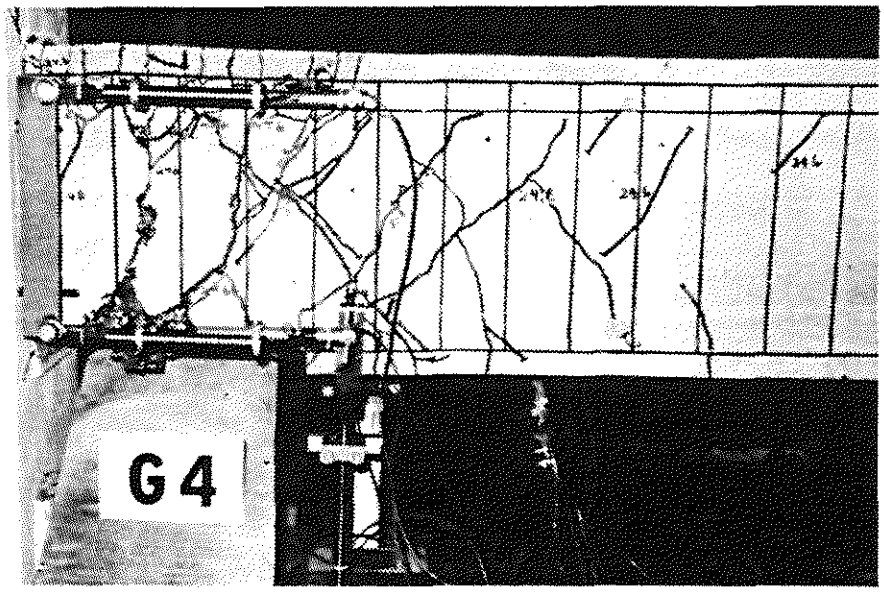

Fig. 2.18(b) Crack Pattern at the End of Cycle 7, Beam G-4

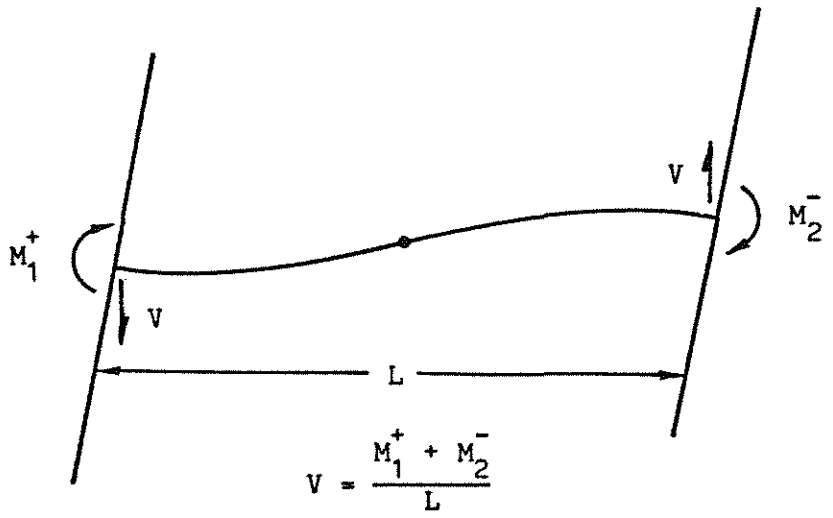

Fig. 3.1 Beam Shear Force Due to Lateral Deformation (Darwin & Nmai 1986)

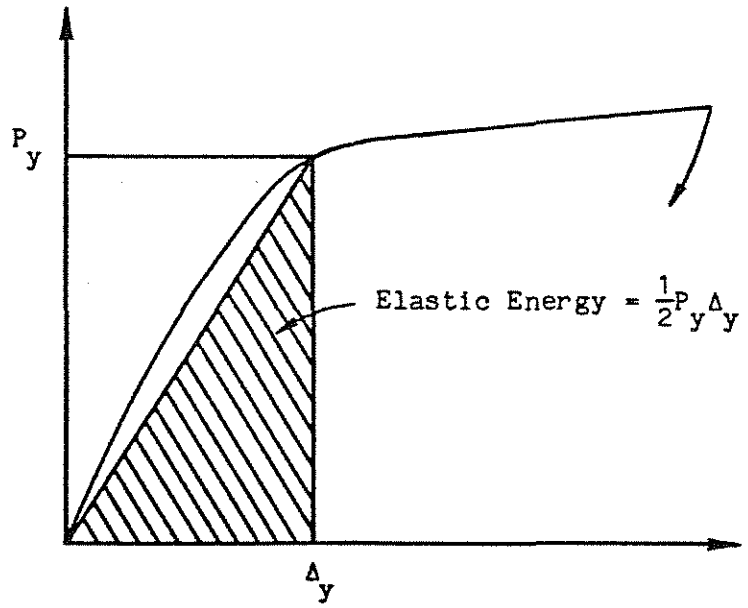

Fig. 3.2 Elastic Energy in Negative Bending (Nmai & Darwin 1984)

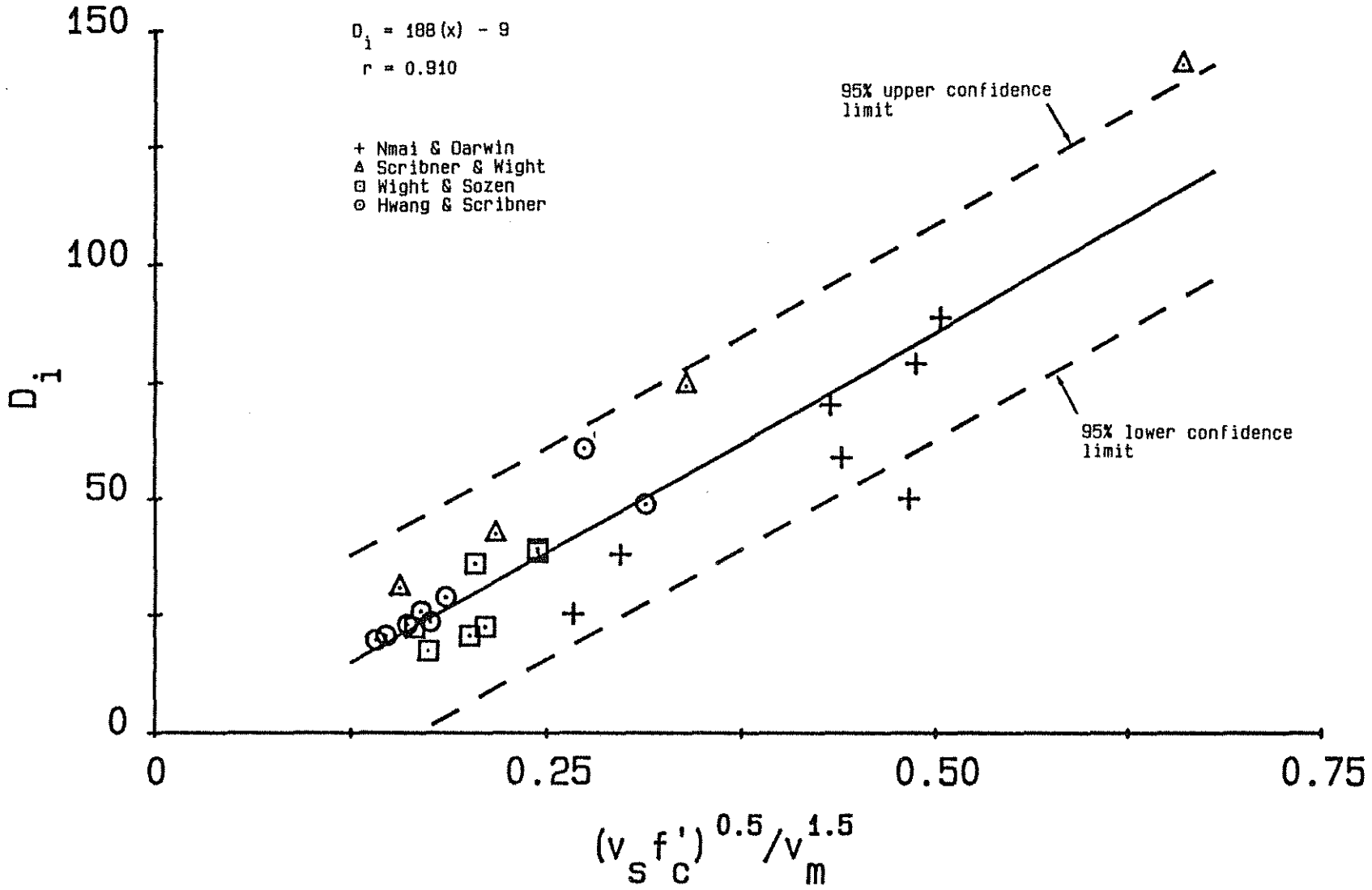

Fig. 3.3 D_i versus $(v_s f'_c)^{0.5}(v_m)^{-1.5}$, Nmai & Darwin (1984)

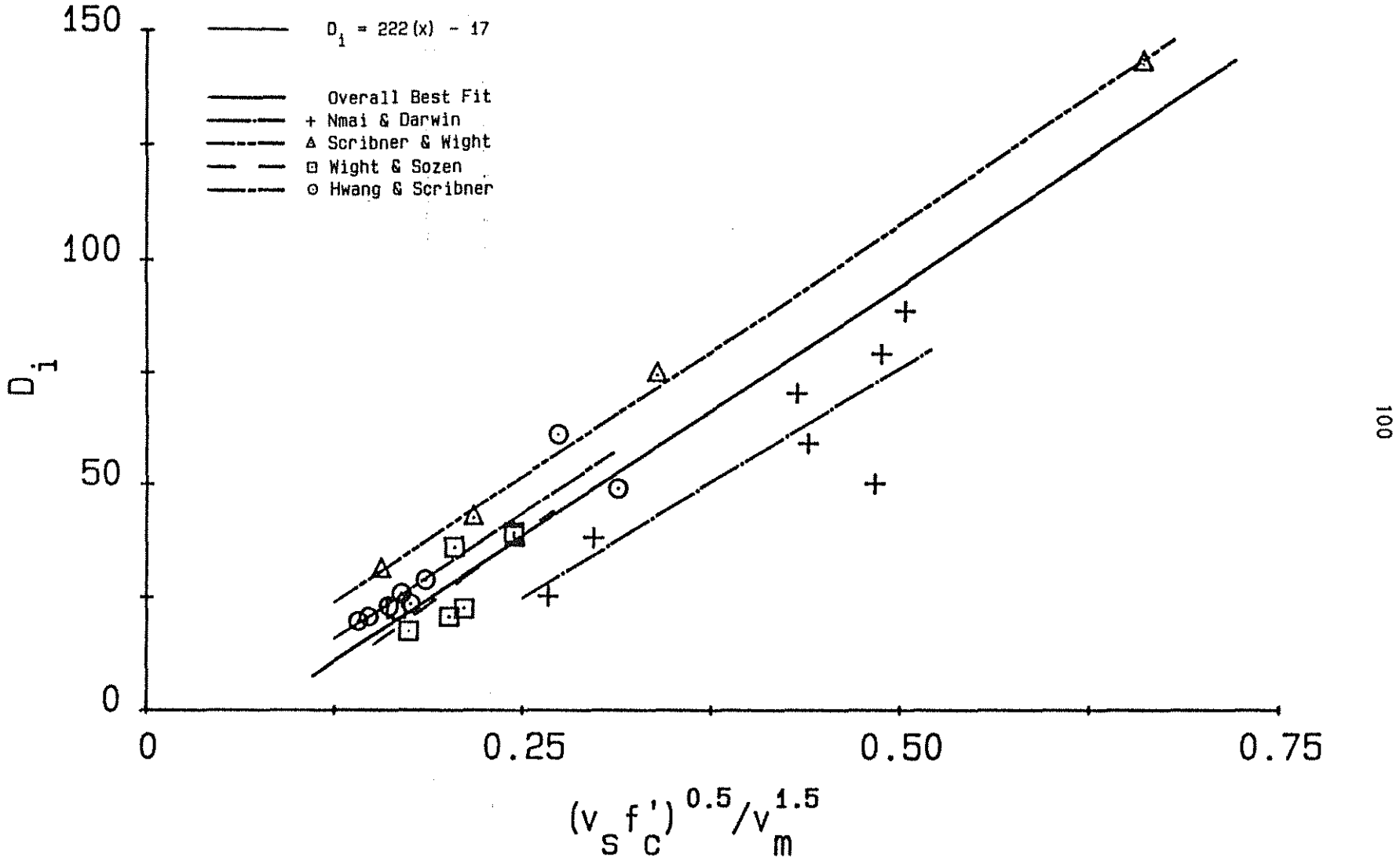

Fig. 3.4 D_i versus $(v_s f'_c)^{0.5}(v_m)^{-1.5}$, Nmai & Darwin (1984)

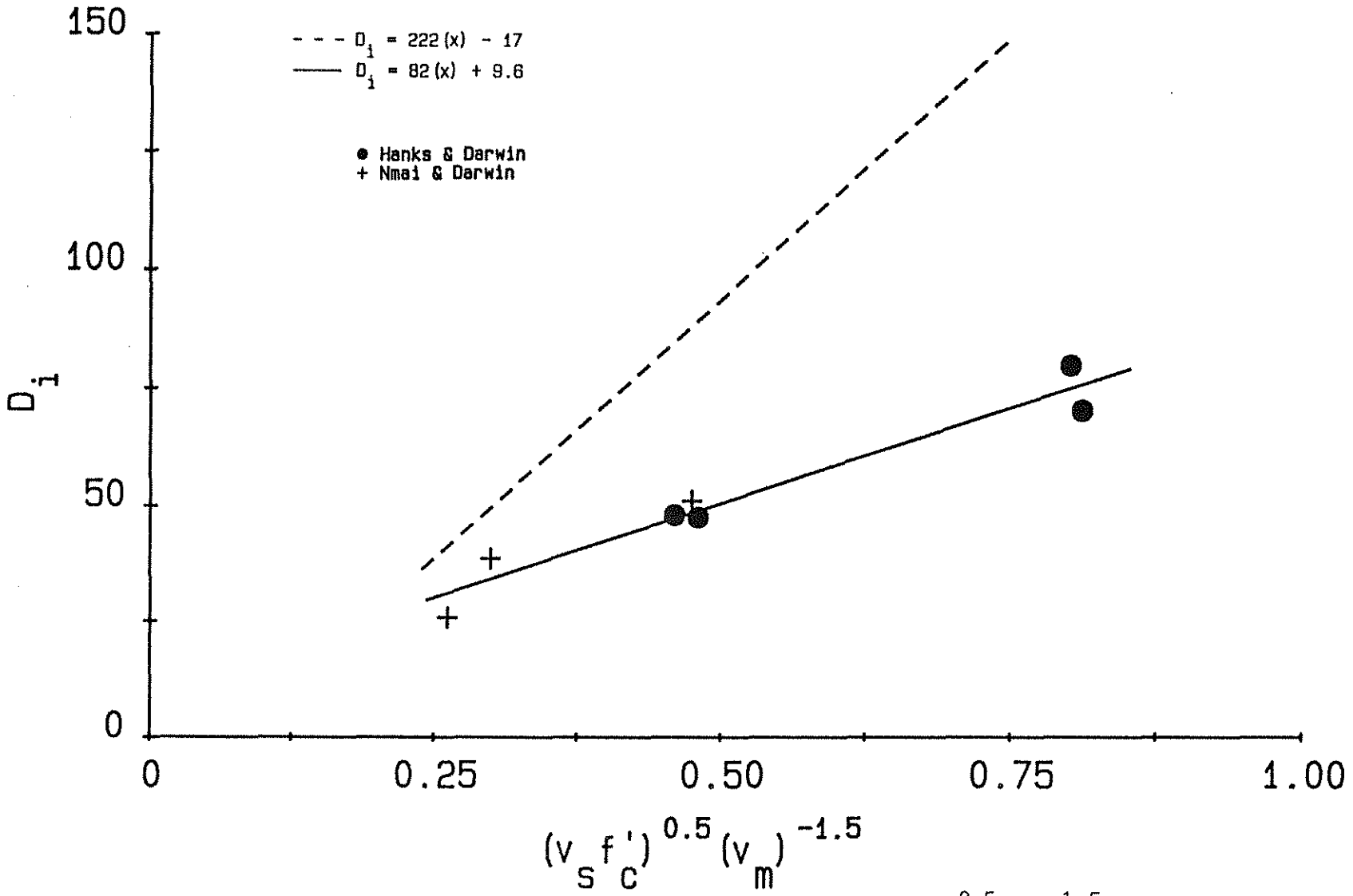

Fig. 3.5 Influence of Concrete Strength, D_i versus $(v_s f'_c)^{0.5}(v_m)^{-1.5}$, Nmai & Darwin (1984) and Current Study

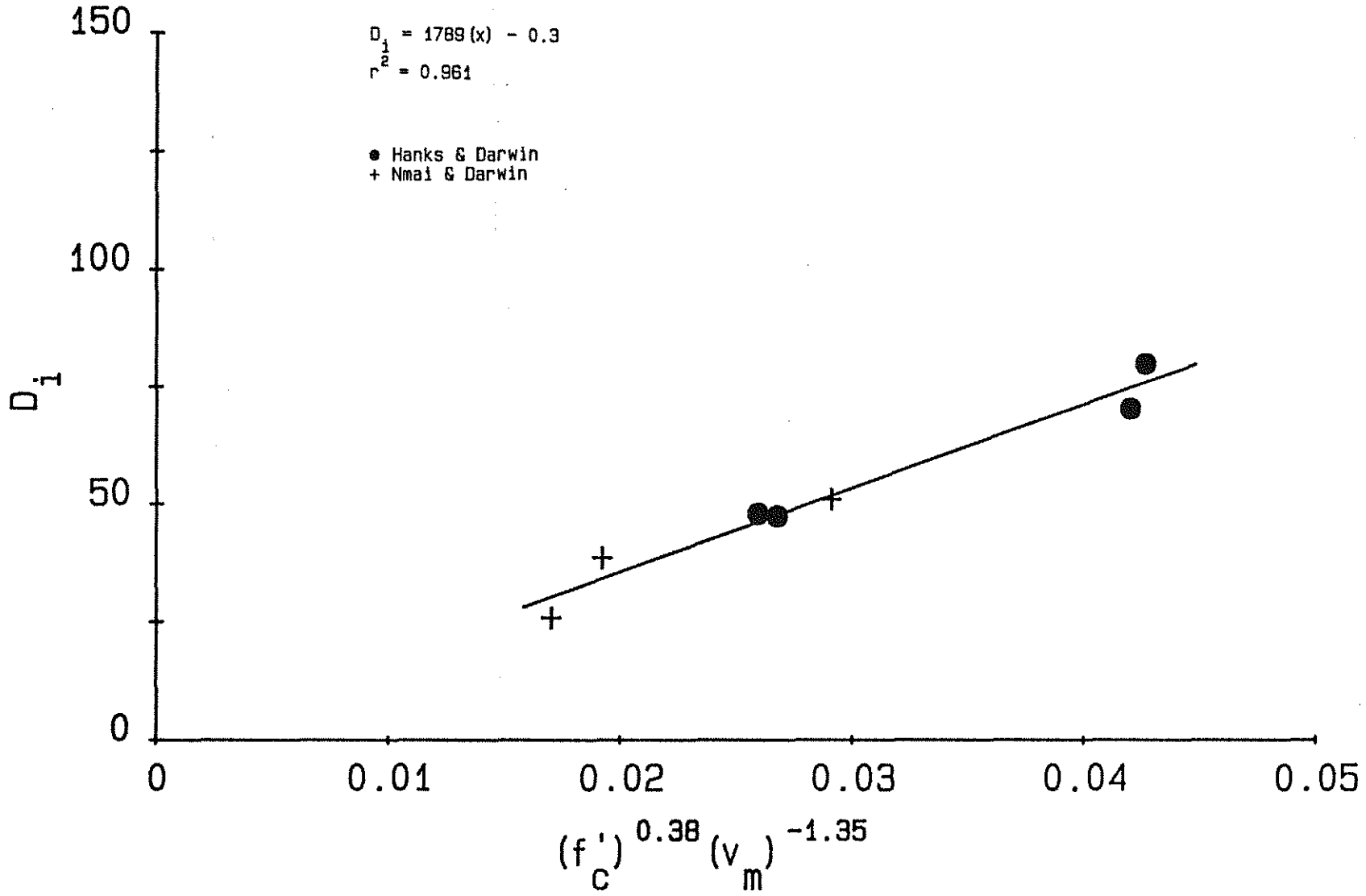

Fig. 3.6 D_i versus $(f'_c)^{0.38}(v_m)^{-1.35}$, Nmai & Darwin (1984) and Current Study

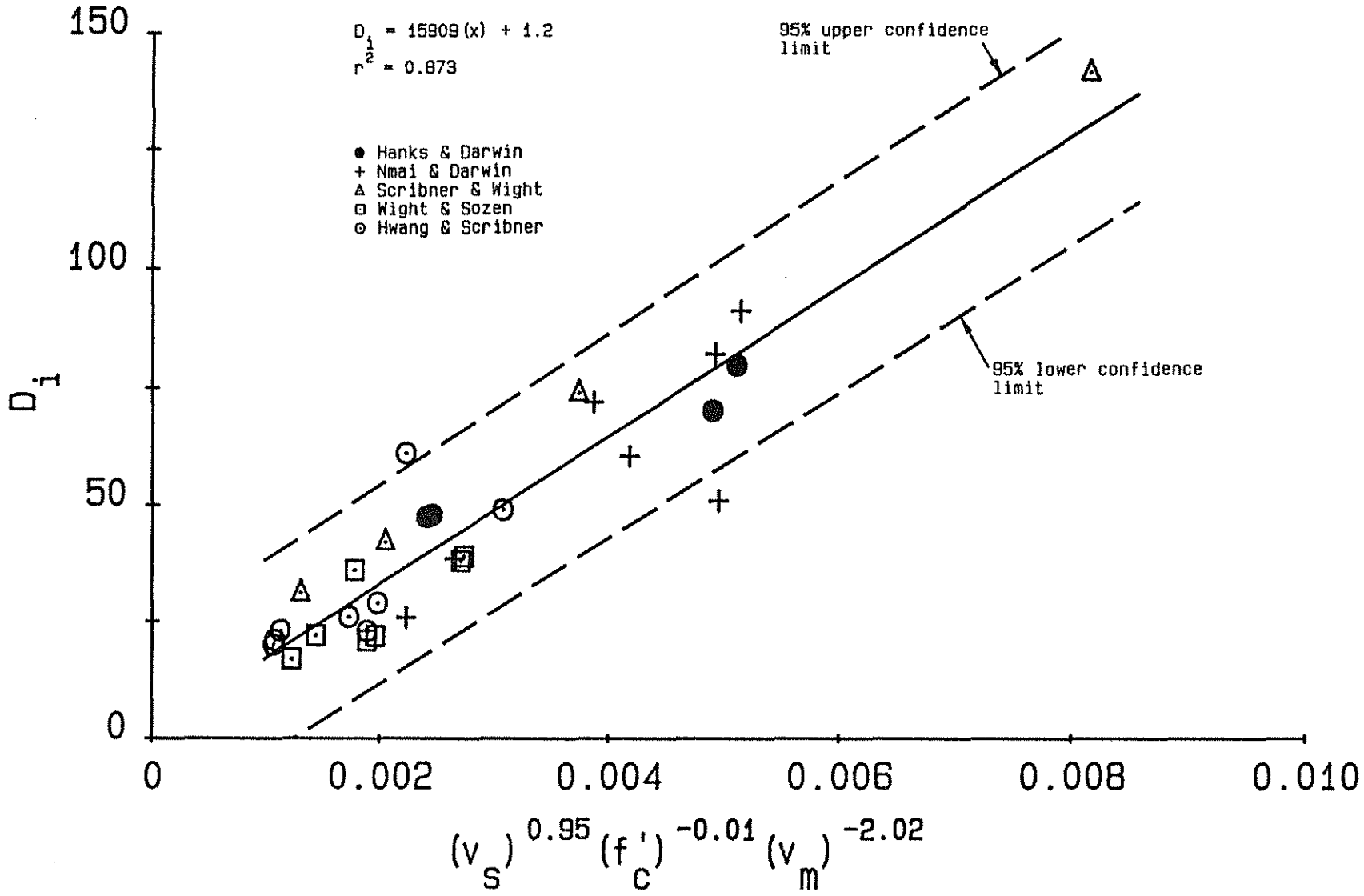

Fig. 3.7 D_i versus $(v_s)^{0.95}(f'_c)^{-0.01}(v_m)^{-2.02}$, Specimens Used in D_i Analysis

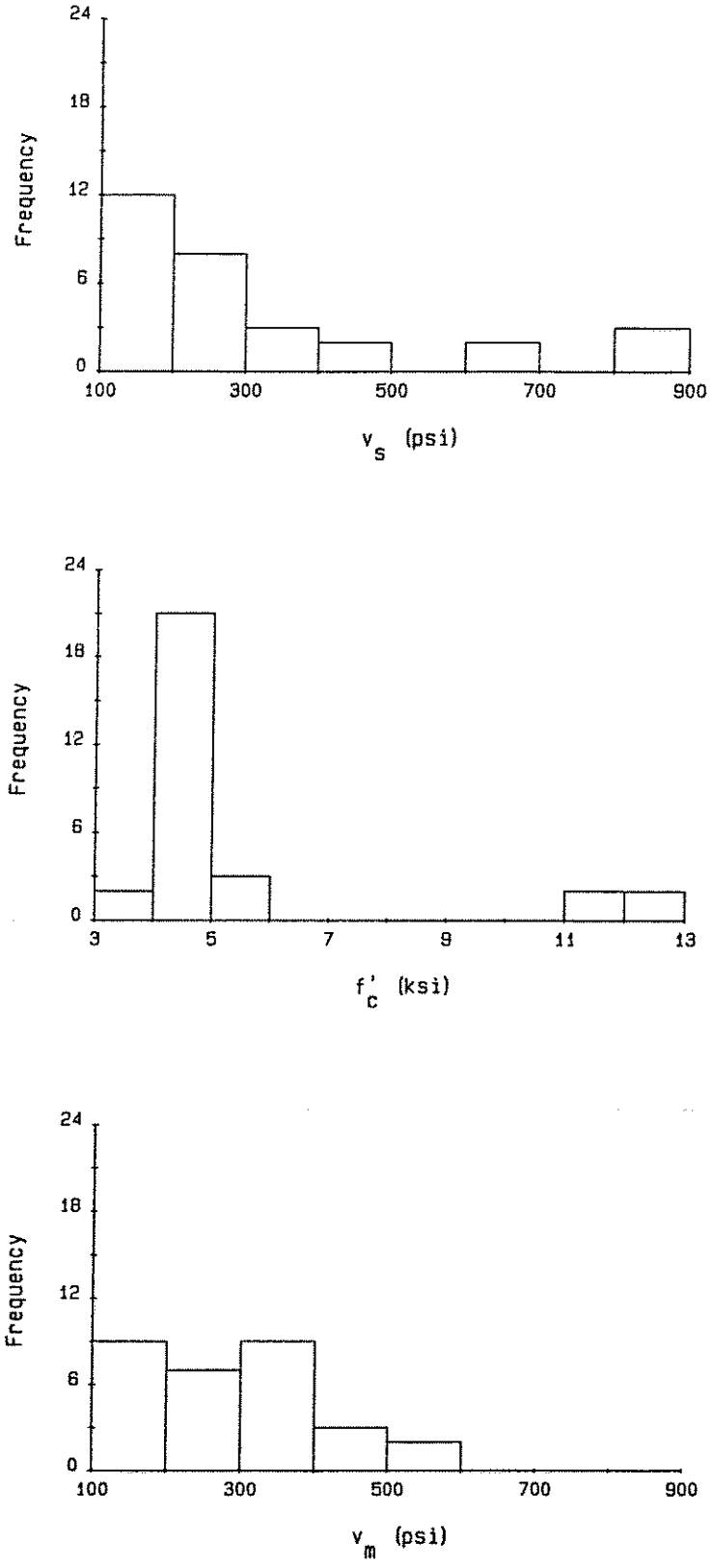

Fig. 3.8 Distribution of v_s, f'_c, and v_m, Specimens Used in D_i Analysis

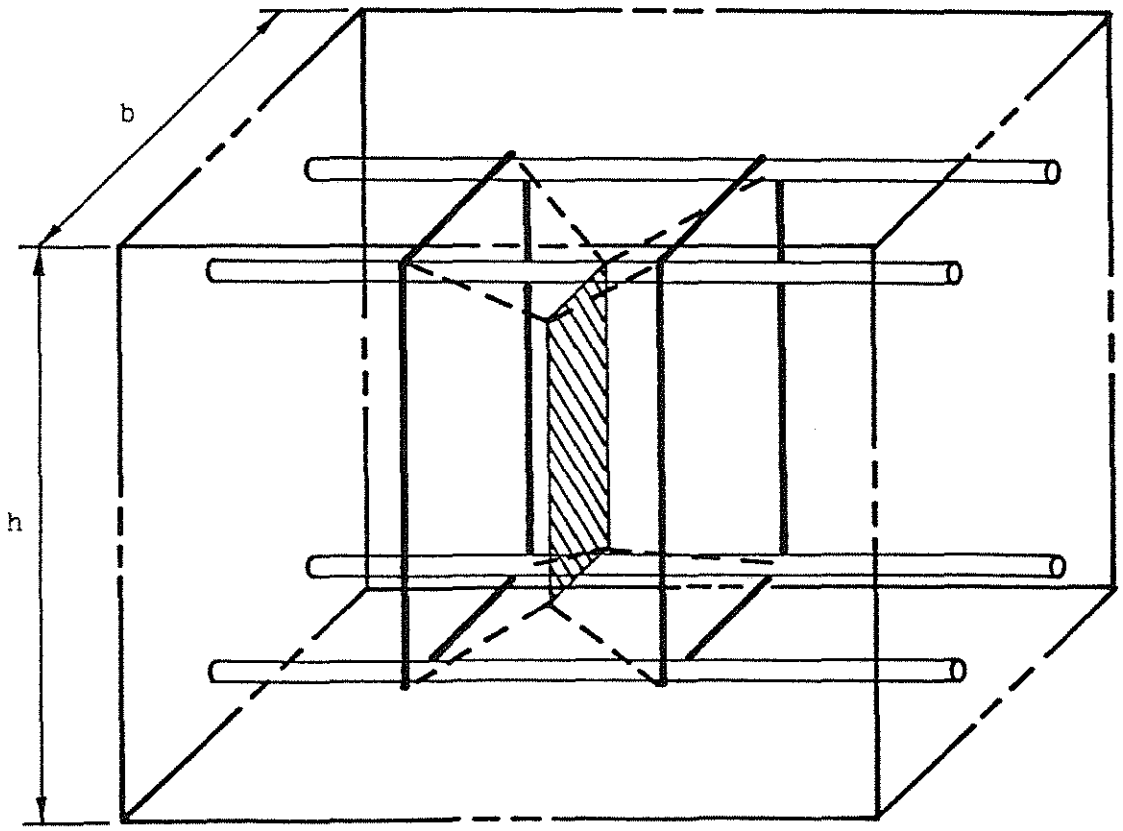

Fig. 3.9(a) Confined Concrete Volume

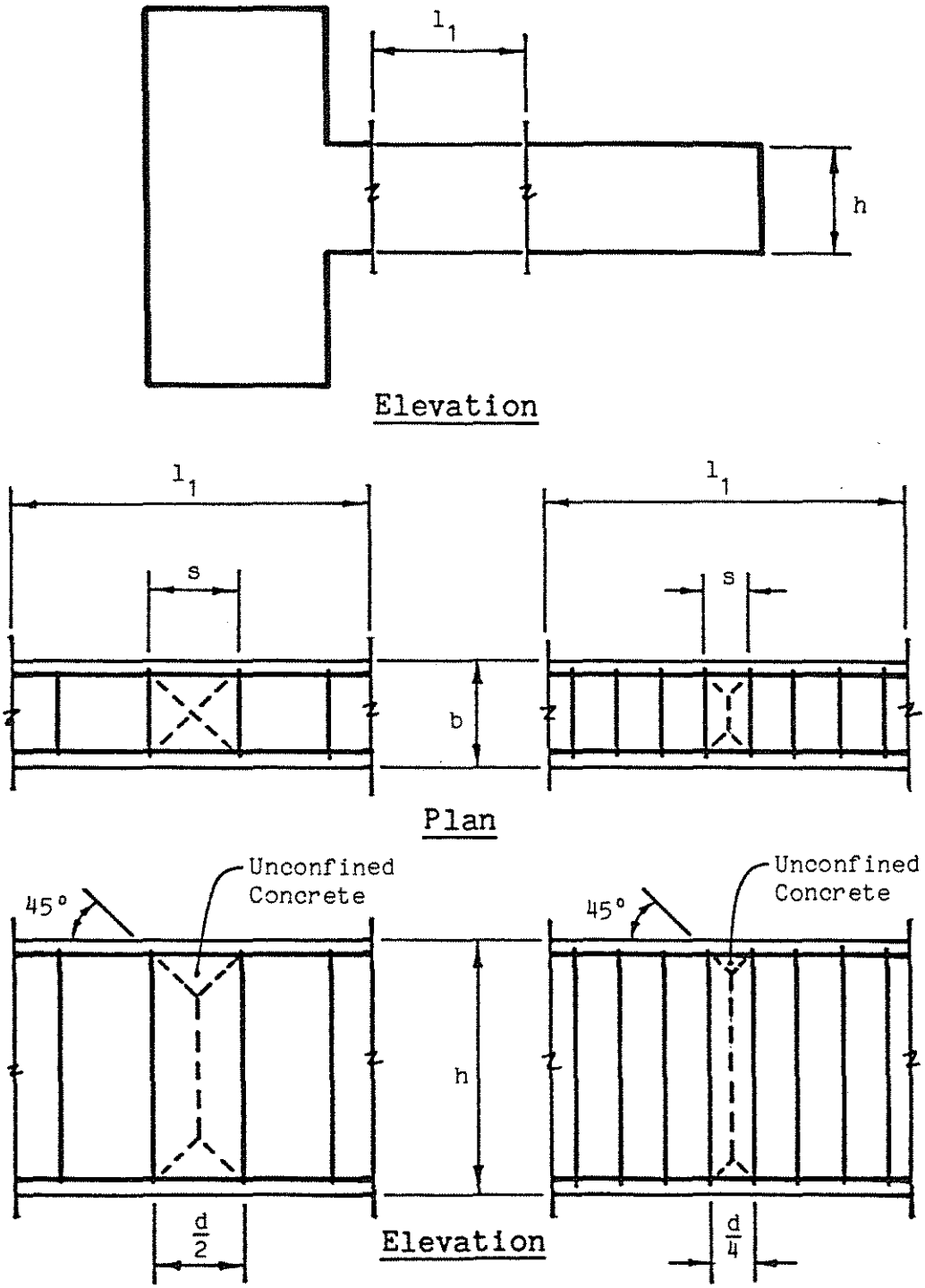

Fig. 3.9(b) Effect of Reduced Stirrup Spacing on Concrete Confinement

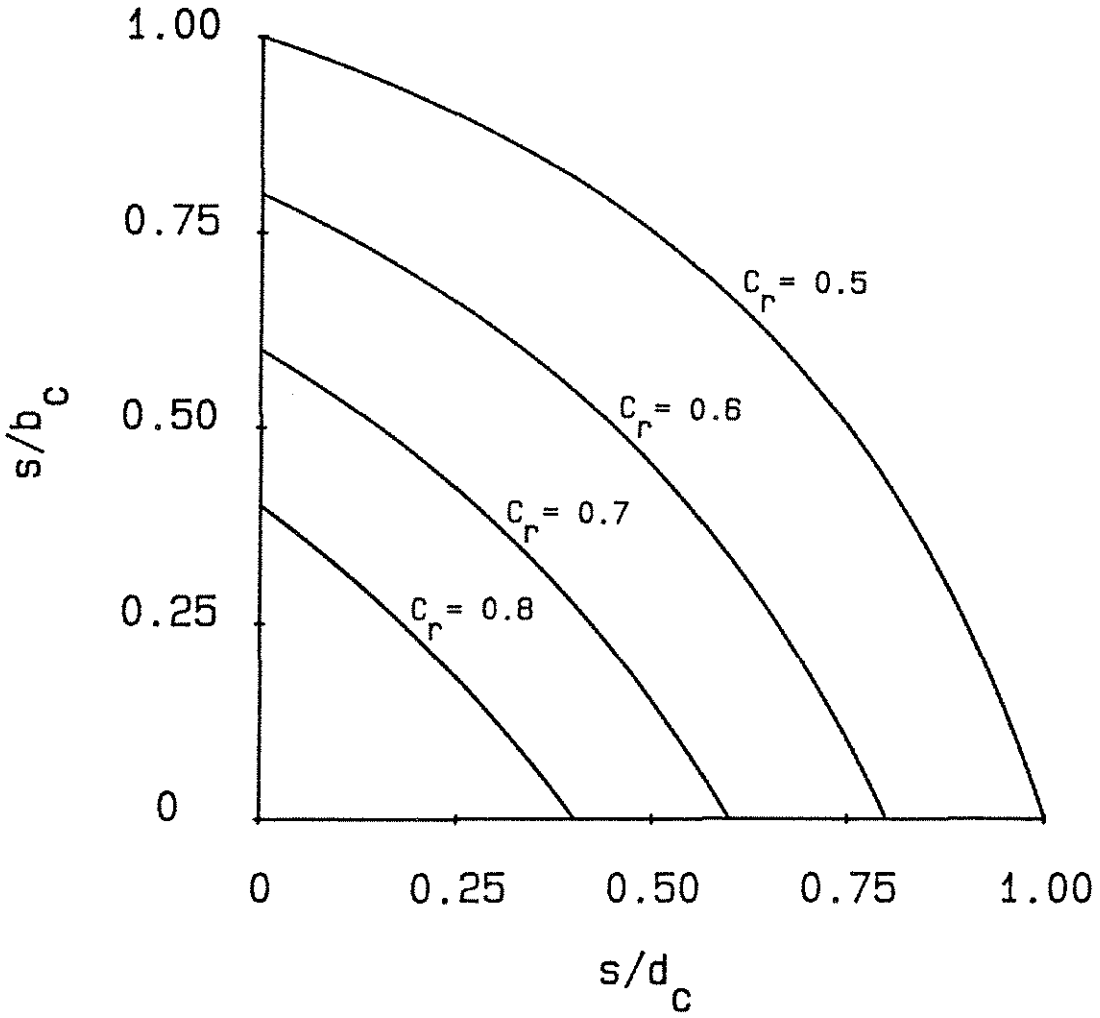

Fig. 3.10 Confinement Ratio, C_r, Isobars for s/d_c versus s/b_c

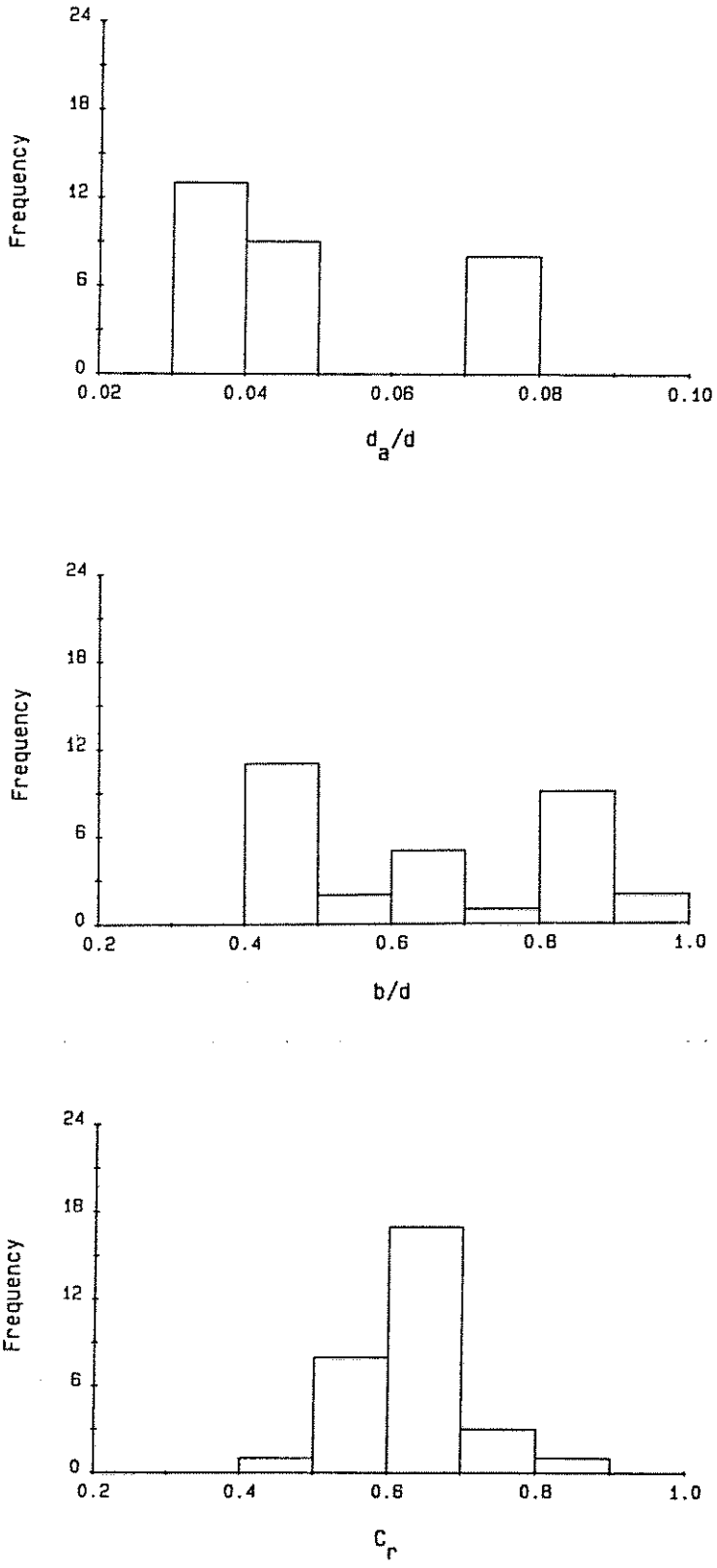

Fig. 3.11 Distribution of d_a/d, b/d, and C_r, Specimens Used in D_i Analysis

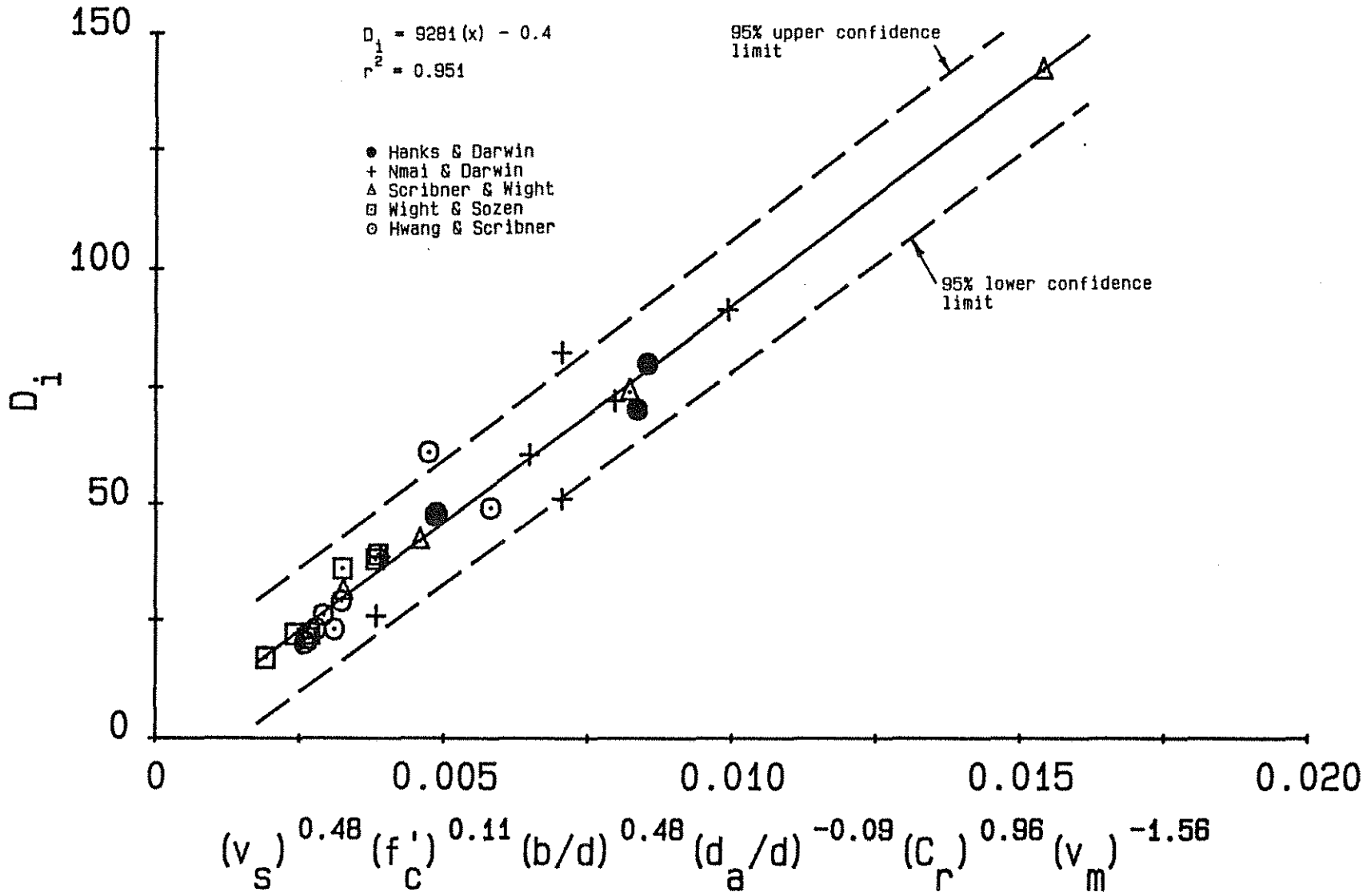

Fig. 3.12 D_i versus $(v_s)^{0.48}(f'_c)^{0.11}(b/d)^{0.48}(d_a/d)^{-0.09}(C_r)^{0.96}(v_m)^{-1.56}$, Specimens Used in D_i Analysis

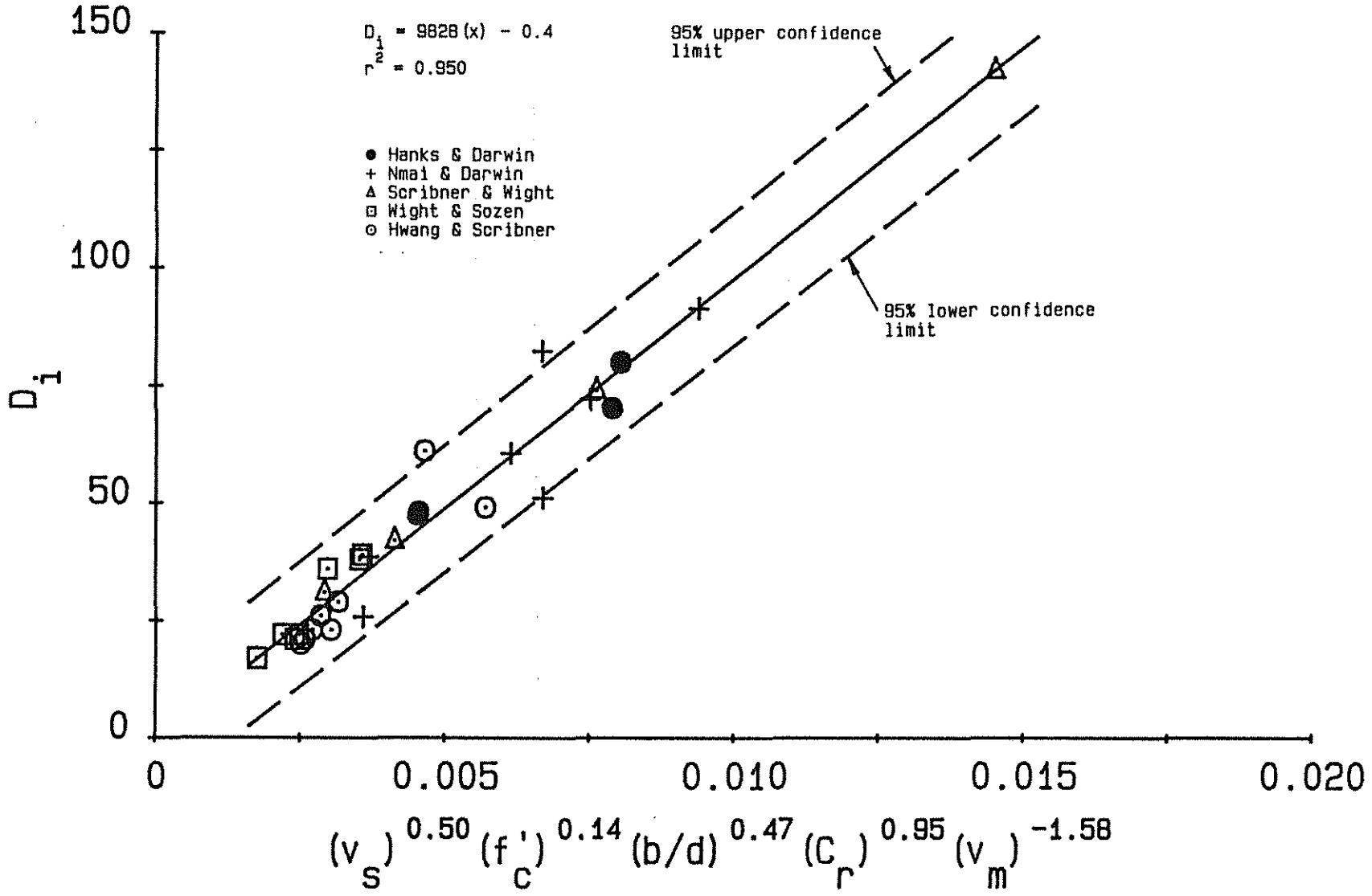

Fig. 3.13 D_i versus $(v_s)^{0.50}(f'_c)^{0.14}(b/d)^{0.47}(C_r)^{0.95}(v_m)^{-1.58}$, Specimens Used in D_i Analysis

APPENDIX A

NOTATION

a = shear span

A_{core} = area of core

A_g = gross area of section

A_i = area of intermediate beam reinforcement

A_s = area of top reinforcing steel

A'_s = area of bottom reinforcing steel

A_v = total cross-sectional area of shear reinforcement

b = width of beam section = b_w

b_c = width of concrete core measured to outside of stirrups

b_w = width of rectangular beam or web width of T-beam

c = exponential value used in regression analysis

C_r = confinement ratio

d = effective depth (distance from bottom of beam to centroid of top reinforcement)

d_1 = effective depth (distance from top of beam to centroid of bottom reinforcement)

d_a = coarse aggregate diameter

d_c = depth of concrete core measured to outside of stirrups

D = diagonal dimension of region spanned by each set of diagonal LVDTs

D_i = energy dissipation index = $E/0.5P_y\Delta_y[1 + (A_s'/A_s)^2]$

E = total energy dissipated for cycles in which $P_n \geq 0.75P_y$

f_c' = compressive strength of concrete from 6 x 12 in. cylinders

f_{vy} = yield strength of shear reinforcement

f_y = yield strength of flexural reinforcement

h = height of beam cross section

h_h = horizontal dimension of region spanned by diagonal LVDTs

h_v = vertical dimension of region spanned by diagonal LVDTs

I_w = $\sum P_n\Delta_n/P_y\Delta_y$

I_w' = $I_w(1 - d_c/a)(1 + 0.0005N/A_{core})$

k = constant used in regression analysis

l = span of beam

l_1 = partial span of beam

L = center to center length between two columns

M^+ = positive moment capacity at a column face

M^- = negative moment capacity at a column face

N = axial compression load

P_n = maximum beam load in nth cycle of loading

P_y = beam load at yielding of top flexural reinforcement

P_y' = beam load at yielding of bottom flexural reinforcement

r = correlation coefficient

r^2 = coefficient of determination

s = stirrup spacing

v_n = nominal shear stress = $V_n/(b_w d)$

v_m = maximum shear stress = $V_m/(b_w d)$

v_s = stirrup stress = $V_s/(b_w d)$

v_u = factored shear stress = $V_u/(b_w d)$

V = shear force due to lateral deformation = $(M^+ + M^-)/L$

V_c = nominal shear force carried by concrete

V_n = nominal shear force

V_m = maximum shear force

V_s = nominal stirrup shear capacity = $(A_v f_{vy} d)/s$

V_u = factored shear force

V_y = shear force at yielding of main flexural reinforcement

= P_y

x = predictor variable used in regression analysis

Y = response variable used in regression analysis

α = parameter used in regression analysis

β = coefficient used in regression analysis

γ = shear deformation = $(\gamma_1 + \gamma_2)/2$

γ_1 = first component of total shear deformation

= $\left[\sqrt{(D + \Delta_1)^2 - h_h^2} - h_v\right]/h_h$

γ_2 = second component of total shear deformation

= $\left[h_v - \sqrt{(D + \Delta_2)^2 - h_h^2}\right]/h_h$

Δ_b = change in length measured with LVDT #8

Δ_n = maximum load-point deflection in nth cycle of loading

Δ_t = change in length measured with LVDT #7

Δ_y = load-point deflection at yielding of top flexural reinforcement

Δ'_y = load-point deflection at yielding of bottom flexural reinforcement

Δ_1 = change in length of diagonal measured with LVDT #3 or #5

Δ_2 = change in length of diagonal measured with LVDT #4 or #6

θ = beam flexural rotation relative to column-stub

$= (\Delta_b + \Delta_t)/h_v$

μ = displacement ductility factor

ρ = flexural reinforcement ratio = $A_s/(b_w d)$

APPENDIX B

COMPUTATION OF SHEAR DEFORMATION AND BEAM FLEXURAL ROTATION RELATIVE TO COLUMN-STUB

B.1 COMPUTATION OF SHEAR DEFORMATION

The shear deformation, γ, was calculated based on measurements obtained from diagonally crossing LVDTs (Bertero et al. 1974). The total shear deformation consists of two components, γ_1 and γ_2 (Fig. B.1), given by

$$\gamma_1 = \left[\sqrt{(D + \Delta_1)^2 - h_h^2} - h_v\right]/h_h \qquad (B.1)$$

and

$$\gamma_2 = \left[h_v - \sqrt{(D + \Delta_2)^2 - h_h^2}\right]/h_h \qquad (B.2)$$

in which

γ_1 = first component of total shear deformation

γ_2 = second component of total shear deformation

D = diagonal dimension of region spanned by each set of diagonal LVDTs

h_h = horizontal dimension of region spanned by diagonal LVDTs = 15 in.

h_v = vertical dimension of region spanned by diagonal LVDTs = 12.75 in.

Δ_1 = change in length of diagonal measured with LVDT #3 or #5

Δ_2 = change in length of diagonal measured with LVDT #4 or #6

The shear deformation, γ, was then computed as follows:

$$\gamma = (\gamma_1 + \gamma_2)/2 \qquad (B.3)$$

B.2 COMPUTATION OF BEAM FLEXURAL ROTATION RELATIVE TO COLUMN-STUB

The flexural rotation of the beam relative to the column-stub, θ, was computed as follows (Nmai & Darwin 1984):

$$\theta = (\Delta_b + \Delta_t)/h_v \qquad (B.4)$$

in which

Δ_b = change in length measured with LVDT #8

Δ_t = change in length measured with LVDT #7

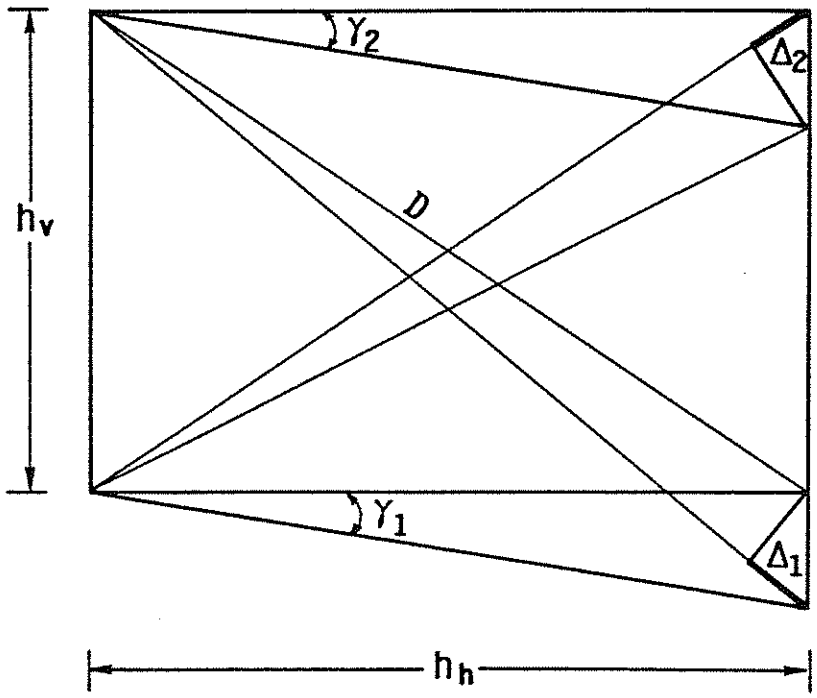

Fig. B.1 Shear Deformation Measurement (Nmai & Darwin 1984)

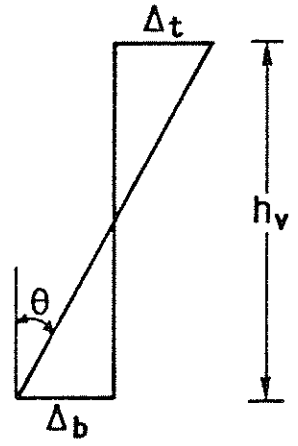

Fig. B.2 Relative Flexural Rotation Measurement (Nmai & Darwin 1984)

APPENDIX C

CONSTRAINED OPTIMIZATION OF A NONLINEAR FUNCTION

A straight line relationship between two variables may be readily obtained by using standard regression analysis techniques such as the least squares method. When one variable depends upon of several parameters, the method to obtain a "best fit" linear relationship becomes slightly more difficult. A generalized function representing the influence of multiple parameters on an observed or response variable, Y_i, may be expressed as

$$Y_i = \beta_1[(\alpha_{i1})^{c_1}(\alpha_{i2})^{c_2}\ldots(\alpha_{in})^{c_n}] + \beta_0 \qquad (C.1)$$

in which $\alpha_{i1},\alpha_{i2},\ldots,\alpha_{in}$ are the controlling parameters with exponential characteristics $c_1,c_2,\ldots,c_n$, respectively, and β_1 and β_0 are the regression coefficients representing the slope and intercept of the best fit line. The optimum correlation for all i observations is one in which the choice of regression coefficients and exponents provide a maximum correlation coefficient r or coefficient of determination r^2 (Neter & Wasserman 1974).

Optimization of the exponents for each parameter in Eq. C.1 is equivalent to minimizing the square of the difference between Y_i and $\beta_1[(\alpha_{i1})^{c_1}(\alpha_{i2})^{c_2}\ldots(\alpha_{in})^{c_n}] + \beta_0$. The function to be minimized can be expressed as

$$F = \sum_{i=1}^{q} \{[Y_i - k(\alpha_{i1})^{c_1}(\alpha_{i2})^{c_2}\ldots(\alpha_{in})^{c_n}]\}^2 \qquad (C.2)$$

in which k = constant and q = the total number of observations or data points. For this study IMSL (1985) routine ZXMWD, which uses a quasi-Newton technique for problem solution, minimizes the specified function, F.

Optimizing routines, including ZXMWD, frequently require a starting point or initial estimate of the problem unknowns to initiate solution. Initial estimates of the unknowns are available by expressing $[Y_i - k(\alpha_{i1})^{c_1}(\alpha_{i2})^{c_2}\ldots(\alpha_{in})^{c_n}]$ in a logarithmic form and using multiple regression analysis procedures (Burr 1974) to solve for k and each exponential value. This procedure was used by Zsutty (1968) to determine the exponents of multiple parameters in a predictor variable which estimated beam shear strength as a function of concrete strength, reinforcement ratio, and effective depth-to-shear span ratio.

An expression representing the linearized logarithmic transformation can be written as

$$\sum_{i=1}^{q} \{[\ln(Y_i) - c_0 - c_1\ln(\alpha_{i1}) - c_2\ln(\alpha_{i2}) - \ldots - c_n\ln(\alpha_{in})]\}^2 \qquad (C.3)$$

in which $c_0 = \ln(k)$. When Eq. C.3 is differentiated with respect to each b_i, the simultaneous solution of the resulting n + 1

linear equations provides initial estimates of k and c_1 thru c_n which are required to initiate the optimized solution of Eq. C.2. It should be noted that to ensure solution convergence of the nonlinear function represented by Eq. C.2, boundaries or constraints must be imposed upon the initial estimates of k and each exponent (i.e. constrained optimization).

Once the optimized exponents are obtained and substituted into Eq. C.1, application of the least squares method provides a solution for the regression coefficients β_0 and β_1.

The procedure for determining the values of β_0, β_1 and c_1 thru c_n is illustrated by substituting $(v_s)_i = \alpha_{i1}$, $(f'_c)_i = \alpha_{i2}$, $(v_m)_i = \alpha_{i3}$ and $(D_i)_i = Y_i$ into Eq. C.1. For the 30 applicable test results presented in Table 3.1 (i.e. q = 30), implementation of IMSL (1985) routine LEQIF, which uses a version of Gaussian elimination to solve the linear equations obtained by applying the least squares method to Eq. C.3, provides initial estimates of $k = 4594$, $c_1 = 0.7530$, $c_2 = 0.1106$ and $c_3 = -1.781$. Substitution of these values into Eq. C.2 permits optimization of c_1 thru c_n. The solution obtained from IMSL (1985) routine ZXMWD provides optimized exponents of $c_1 = 0.9547$, $c_2 = -0.0122$ and $c_3 = -2.021$ which are now substituted into Eq. C.1. Application of the least squares method to Eq. C.1 results in a best fit line of

$$D_i = 15909.0[(v_s)^{0.9547}(f'_c)^{-0.0122}(v_m)^{-2.021}] + 1.16 \qquad (C.4)$$

with $r^2 = 0.873$ (Fig. 3.7).